

Doctoral theses at NTNU, 2012:15

Lihao Zhao

Particles in wall turbulence

ISBN 978-82-471-3292-0 (printed ver.)
ISBN 978-82-471-3293-7 (electronic ver.)
ISSN 1503-8181

NTNU
Norwegian University of
Science and Technology
Thesis for the degree of
philosophiae doctor
Faculty of Engineering Science and Technology
Department of Energy and Process Engineering

Doctoral theses at NTNU, 2012:15

 **NTNU**
Norwegian University of
Science and Technology

 **NTNU**
Norwegian University of
Science and Technology

 NTNU

Lihao Zhao

Particles in wall turbulence

Thesis for the degree of philosophiae doctor

Trondheim, December 2011

Norwegian University of
Science and Technology
Faculty of Engineering Science and Technology
Department of Energy and Process Engineering



Norwegian University of
Science and Technology

NTNU

Norwegian University of Science and Technology

Thesis for the degree of philosophiae doctor

Faculty of Engineering Science and Technology
Department of Energy and Process Engineering

©Lihao Zhao

ISBN 978-82-471-3292-0 (printed ver.)

ISBN 978-82-471-3293-7 (electronic ver.)

ISSN 1503-8181

Doctoral Theses at NTNU, 2012:15

Printed by Tapir Uttrykk

Dedication

This work is proudly dedicated to:

My mother and my father.

Thank you for your unconditional love all the time!

Lihao Zhao
Trondheim 2011

Particles in wall turbulence

Lihao Zhao 2011

Fluids Engineering Division, EPT-NTNU
NO-7491 Trondheim, Norway.

Abstract

The overall objective of this doctoral thesis is to investigate how tiny particles are dispersed in a turbulent channel flow and how the fluid turbulence is modulated due to the presence of particles. Both spherical and prolate spheroidal particles are considered in present work and their translational and rotational motions are described in a Lagrangian framework using point-particle approximation. The turbulence of the fluid phase is obtained by means of direct numerical simulation (DNS). Accounting for the feed-backs from the particles onto the flow field, a novel scheme of torque-coupling has been developed and implemented together with the more conventional force-coupling in current program. In the case of spherical particle Reynolds number effect on particle velocity statistics and Stokes number effect on the particle slip velocity have been explored in dilute suspension flow with one-way coupling approach. The study on turbulence modulations by spherical particles has been carried out in two-way coupled simulations. The effects of Stokes number and particle volume fraction have been mainly investigated and the mechanisms of particle-turbulence interaction were elucidated by kinetic energy transfer and particle induced dissipation between particle phase and local fluid phase. In the case of prolate spheroidal particle both torque-coupling and force-coupling has been applied in the simulations of particle suspension turbulent shear flow in which the turbulence modulations and particle orientations and spins have been examined. Some results on the comparison of Lagrangian approach and statistical approach in simulating the particle suspensions were presented.

Descriptors: Direct numerical simulations, wall turbulence, spherical particle, prolate spheroidal particle, turbulence modulation, particle dissipation, two-way coupling, torque-coupling.

Contents

Abstract	v
Preface	1
List of articles	3
Part 1. Summary	5
Chapter 1. Introduction	7
1.1. Turbulence	7
1.2. Dispersed multiphase flow	7
1.3. Objectives	9
Chapter 2. Governing equations and numerical methods	11
2.1. Channel flow	11
2.1.1. Governing equations	11
2.1.2. Numerical methods	12
2.2. Particle dynamics	14
2.2.1. Spherical particle	14
2.2.2. Prolate spheroidal particle	16
2.3. Coupling methods	19
2.3.1. Force-coupling	20
2.3.2. Torque-coupling	20
2.3.3. Parallelization in computation	23
Chapter 3. Summary of articles	25
3.1. One-way coupled simulations of spherical particle suspensions	25
3.2. Two-way coupled simulations of spherical particle suspensions	26
3.3. One-way coupled simulations of prolate spheroid suspensions	28
3.4. Two-way coupled simulations of prolate spheroid suspensions	29
3.5. Appendixes	29
Bibliography	31
Part 2. Articles	35

Preface

This thesis represents the culmination of learning and research work that have been performed at the Department of Energy and Process Engineering of the Norwegian University of Science and Technology (NTNU) during a period from August 2008 to January 2012 in Trondheim, Norway. Parts of study have been carried out at Delft University of Technology (TU Delft) in 2008 autumn. The PhD fellowship has been funded by A/S Norske Shell, which is gratefully acknowledged.

This thesis would not have been possible without the continuous support and help of many kind people. First and foremost I want to sincerely express my deeply-felt thanks to my advisor Professor Helge I. Andersson for his persistent support and thoughtful guidance. His enthusiasm, inspiration and unsurpassed knowledge of turbulent flow and particle suspensions always motivate and lead me forward on both an academic and a personal level throughout the past three years. I will always be indebted to him.

I would like to also warmly thank Professor Bendiks J. Boersma at TU Delft for the helpful discussions and the opportunity of DNS code learning in TU Delft. I am especially grateful to Dr. Jurriaan J. J. Gillissen at TU Delft. The gratitude is for his help with the code training, programming problem solving, many interesting discussions and invaluable suggestions in the phone meetings. I wish to express my appreciation to Dr. Cristian Marchioli at University of Udine for the numerous stimulating discussions and helps.

Special thanks goes to my colleagues at the Department of Energy and Process Engineering of NTNU. The pleasant discussions and cooperations with Dr. Mustafa Barri will not be forgotten. I want to thank Hatef Khaledi, Afshin Abbasi-Hoseini, Dr. Vagesh Narasimhamurthy, and Christopher Nilsen for the good time passed together in our group.

I am very thankful to my kind Chinese friends in Trondheim, Zhao Pei, Zhao Wei, Pan Qingqing, Han Fenglin, Fu Chao, Chao Zhongxi, Yan Tianjiao, Xie Lang, Lv Wenjun, Gao Yuehong and so on. Thank you all very much to accompany me and the colorful memories of the good time here we had will never be faded.

My girlfriend, Liu Tianshu, deserves the special mention and gratitude for her love and being always there with me.

Finally, words fail me to express my appreciation to my parents and my younger sister Yuanyuan for the love and courage they gave me. I will always be indebted to them.

List of articles

The thesis is based on and contains the following articles.

Article 1. Andersson, H. I. & **Zhao, Lihao** 2010 Computation of particle-laden turbulent flows. *The 23rd Nordic Seminar on Computational Mechanics*, Stockholm, Sweden.

Article 2. **Zhao, Lihao** & Andersson, H. I. 2012 Statistics of particle suspensions in turbulent channel flow. *Communications in Computational Physics*, **11**, 1311-1322.

Article 3. **Zhao, Lihao**, Marchioli C. & Andersson, H. I. 2011 Stokes number effects on particle slip velocity in wall-bounded turbulence and implications for dispersion models. *Physics of Fluids*, accepted for publication.

Article 4. **Zhao, Lihao**, Andersson, H. I. & Gillissen J.J.J. 2010 Turbulence modulation and drag reduction by spherical particles. *Physics of Fluids*, **22**, 081702.

Article 5. **Zhao, Lihao** & Andersson, H. I. 2011 On particle spin in a two-way coupled turbulent channel flow simulation. *Physics of Fluids*, **23**, 093302.

Article 6. **Zhao, Lihao** & Andersson, H. I. 2011 Two-way coupled simulations of particle-laden wall turbulence. *Particles in turbulence 2011 - International Conference on Fundamentals, Experiments, Numeric and Applications*, Potsdam, Germany.

Article 7. **Zhao, Lihao** & Andersson, H. I. 2011 On particle stress in gas-solid channel flows. In preparation for submission.

Article 8. **Zhao, Lihao**, Andersson, H. I. & Gillissen J.J.J. 2011 Interphasial energy transfer and particle dissipation in particle-laden wall turbulence. Submitted to *Journal of Fluid Mechanics*.

Article 9. Andersson, H. I. & **Zhao, Lihao** 2010 DNS of non-spherical particles in turbulent flows. *ERCOTAC bulletin*, **84**, 4-8.

Article 10. **Zhao, Lihao**, Andersson, H. I. & Gillissen J.J.J. 2011 Comparison of Lagrangian approach and statistical approach in simulation of fiber suspension turbulent channel flow. *manuscript*.

Article 11. Andersson, H. I., **Zhao, Lihao** & Barri M. 2011 Torque-coupling and fiber-turbulence interactions. *Journal of Fluid Mechanics*, accepted for publication.

Appendix 1. **Zhao, Lihao** 2011 Modulations on turbulence with the presence of particle $St=200$. *Appendix* .

Appendix 2. **Zhao, Lihao** 2011 Two-way coupled simulation of particle laden channel flow at $Re_\tau = 790$. *Appendix* .

Appendix 3. **Zhao, Lihao** 2011 H. I. 2011 Two-way coupled simulation of fiber suspension turbulent channel flow. *Appendix*.

The following relevant conference papers are listed below as a part of the PhD work but not included in present thesis.

Article 1. **Zhao, Lihao**, Andersson, H. I., Gillissen J.J.J. & Boersma, B.J. 2009 Simulation of Fibre Suspension Flow by an Eulerian-Lagrangian Approach. *Mek-IT09: 5th National Conference on Computational Mechanics*, Trondheim, Norway.

Article 2. **Zhao, Lihao**, Andersson, H. I., Gillissen J.J.J. & Boersma, B.J. 2009 Simulating fibre suspensions: Lagrangian versus statistical approach. *12th EUROMECH European Turbulence Conference*, Marburg, Germany.

Article 3. Andersson, H. I., Mortensen, P. H., Gillissen J.J.J., **Zhao, Lihao**, & Boersma, B.J. 2009 How to discriminate between light and heavy particles in turbulence. *12th EUROMECH European Turbulence Conference*, Marburg, Germany.

Article 4. **Zhao, Lihao** & Andersson, H. I. 2010 Statistics of particle suspensions in turbulent channel flow. *The 8th Asian Computational Fluid Dynamics Conference*, Hongkong, China.

Article 5. **Zhao, Lihao** & Andersson, H. I. 2011 Two-way coupled simulations of ellipsoidal particles suspended in a turbulent channel flow. *EUROMECH Colloquium 513 on Non-Spherical Particles in Fluid Turbulence*, Udine, Italy.

Article 6. Andersson, H. I., **Zhao, Lihao** & Barri M. 2011 New scheme for torque coupling. *EUROMECH Colloquium 513 on Non-Spherical Particles in Fluid Turbulence*, Udine, Italy.

Article 7. **Zhao, Lihao**, Andersson, H. I. & Gillissen J.J.J. 2011 Turbulence modulation in particle-laden channel flow. *7th International Symposium on Turbulence and Shear Flow Phenomena*, Ottawa, Canada.

Part 1

Summary

CHAPTER 1

Introduction

”Stars suspend in the vastness of the plain,
the moon is swinging in the river.”
<A night abroad>
- Du Fu, China, A.D. 756.

In everyday life we may meet various flow phenomena, the smoke rising from a cigarette, the wind in the wild or the water flowing from a tap. With our intuitive knowledge a fluid is easily deformed and soft compared with a solid. While in a scientific point of view a fluid, such as gas or liquid, is defined as a substance that continually deforms (flows) under an applied shear stress. With the adoption of Newton’s second law the Navier-Stokes equations (1845) constitute a complete mathematical model for describing the motion of fluid substances.

1.1. Turbulence

Most flows commonly occur in nature and in industry are turbulent. Turbulence is a three-dimensional, time-dependent flow phenomenon at large Reynolds number and is characterized by chaotic, stochastic, diffusive, dissipative properties and its physics is still not fully comprehended. Another character of turbulence is that the eddies comprise of a wide range of length and time scales. The length scale varies from the smallest dissipative Kolmogorov scale to the integral scale. The eddies in the integral scale with low frequency mainly obtain energy from the mean flow and contain the most of the turbulent energy. In the Komogorov scale the kinetic energy of the smallest eddies are dissipated into thermal energy due to the viscosity. The concept of *energy cascade* is normally used to describe the energy transfer from large scales down to smaller and smaller scales. The turbulent flows can be described by the Navier-Stokes equations. However, there is no general solution to the Navier-Stokes equations due to the nonlinearity. Consequently, no general solutions are available to turbulent flows until now. More detailed discussions of turbulent flows can be found in the text books (Tennekes and Lumley 1972, Pope 1972, Lesieur 1987 and Davidson 2004).

1.2. Dispersed multiphase flow

Dispersed multiphase flow is characterized by the flow where one phase constituted by solid particles, bubbles or droplets, dispersed in the other continuous fluid phase, liquid or gas. The present thesis mainly investigates the flow of solid particles dispersed in the fluid phase. These gas-solid or liquid-solid flows are commonly encountered both in many engineering and environmental applications. In chemical



FIGURE 1.1. Left: Sand storm over Khartoum (photo by Dijana Kostovic-Vlahovic); right: Blurred sky in Beijing by polluted gas with PM2.5 (photo by NRDC, Engadget)

industry the knowledge of particle suspensions in a fluidize bed is important. The study of the flow of pollutant gas with tiny particles from the power plant and cars by burning of fossil fuels, is meaningful for public heath concern. Since the fine particles, e.g particle size smaller than 2.5 micrometer (PM 2.5) shown in Figure 1.1, can be inhaled into and accumulate in the respiratory system which poses the great health risks of different respiratory diseases. Particulate pollution is estimated to cause 20 000 - 50 000 deaths per year only in the United States (Mokdad et al. 2004). In nature, we can also see these kind of flows in the sand storm, sedimentation in rivers and the volcanic ashes transport in atmosphere like the one from Eyjafjallajökull at Iceland in 2010 . In many cases of particulate flows, the shape of particles is not only spherical, elongated non-spherical particles are also very common. Suspensions of cellulose fibers in water represent a major challenge in the pulp and paper industry. Carbon nanotubes (CNTs) have received immense attention in recent years due to their novel and useful properties. The cylinder-shaped CNT typically has a diameter of a few nm and a length of say 10 μm . CNTs are so small that they can be inhaled deep into the lungs. Recently, potential hazards associated also with the foreseen extensive use of CNTs have been addressed for instance by Donaldson et al. (2006). The dynamical behaviour of micro-organisms in the sea can be considered as a dilute particle suspension. Photosynthesizing microscopic organisms inhabit the euphotic upper layer of the ocean. The phytoplankton is an essential ingredient in aquatic ecosystems and their motions and orientations in the turbulent environment affect for instance their feeding abilities (Mann et al. 2006) and in turn the potential for their blooming (Ghosal and Mandre 2003).

In past several decades the vast majority of investigations have naturally focused on the behavior of spherical particles in a fluid flow and occasionally also on how the flow field is affected by the presence of the particles. The recent review article by Balachandar and Eaton (2010) provides a useful introduction to the state-of-the-art in this vast area of research. The current understanding of the complex behaviour of inertial spherical particles in turbulent wall flows was conducted. Several investigations have focused on the particle deposition and particle preferential concentration in wall turbulence or homogenous turbulence, see

for instance Pedinotti et al. (1992), Soltani and Ahmadi (1995), Marchioli and Soldati (2002), Narayanan et al. (2003) and Picciotto et al. (2005). To obtain better understanding of particle transport and particle velocity statistics, several studies were reported by Marchioli and Soldati (2002), Kulick et al. (1994) and Geashchenko et al. (2008). Some experiments were done on the study of turbulence modulations with presence of particles, such as Rashidi et al. (1990), Kulick et al. (1994) and Hussainov et al. (2000). Several numerical simulations on the turbulence modulations can be found as, Squires and Eaton (1990), Elghobashi and Truesdell (1993), Truesdell and Elghobashi (1994), Pan and Banerjee (1996), Yamamoto et al. (2001), Li et al. (2001), Vreman (2007), Dritselis and Vlachos (2008, 2009) and Bijlard et al. (2010).

The non-spherical shape of particle makes the numerical study become more complicated. This is known as the Euler-Lagrangian approach and has already been used to study motions of elongated fiber-like particles in laminar flows by for instance Högberg et al. (2008) and Lundell and Carlsson (2010) and in turbulent flows by Zhang et al. (2001), Mortensen et al. (2008a, 2008b) and Marchioli et al. (2010). The last-mentioned investigations follow the same basic modeling principles as in the pioneering study by Zhang et al. (2001) and our current work aims to extend this approach in some different directions with the view to improve the physical realism of the computational modelling.

1.3. Objectives

The overall objective of this generic PhD project is to explore by means of computer experiments (DNS) how spherical and elongated non-spherical particles are dispersed in a turbulent channel flow and how the fluid turbulence is modulated by spherical and elongated non-spherical particles.

CHAPTER 2

Governing equations and numerical methods

This chapter presents the mathematical equations of turbulent flow, particle dynamics, force- and torque-coupling approaches, and also the numerical methods. The flow field is obtained directly from the Navier-Stokes equations in a direct numerical simulation (DNS) while tiny particles are represented by Lagrangian point-particle approach. In present work two types of particle, spherical and prolate ellipsoidal particles, are investigated. To account for the effect of particle on the carrier flow, a novel scheme for the torque coupling between inertial particles phase and a continuous Eulerian fluid phase has been developed and implemented together with the more conventional force-coupling in present program.

2.1. Channel Flow

2.1.1. Governing equations

The fully-developed turbulent flow in a plane channel is considered as a prototype of wall-bounded shear flow. The motion of the incompressible Newtonian fluid including the feedback of inertial particle is governed by the continuity and momentum conservation equations,

$$\nabla \cdot \vec{u} = 0 \tag{2.1}$$

$$\rho \left[\frac{\partial \vec{u}}{\partial t} + (\vec{u} \cdot \nabla) \vec{u} \right] = -\nabla p + \mu \nabla^2 \vec{u} + \vec{f}^P + \nabla \cdot \vec{T}^P \tag{2.2}$$

Here, \vec{u} and ∇p are the instantaneous fluid velocity vector and pressure gradient, respectively. ρ and μ are the density and the dynamic viscosity of the carrier fluid. \vec{f}^P denotes the force per unit volume from the particles. \vec{T}^P is a anti-symmetric stress tensor to account for the effect of torques on the fluid motion due to the particle rotation. The details of \vec{f}^P and \vec{T}^P will be introduced in Section (2.3).

The governing equations (2.1) and (2.2) of particle-laden flow can be written in non-dimensional form. The characteristic length scale L and a velocity scale U can be introduced and the dimensionless variables with the superscript "+" are defined as:

$$\begin{aligned} \vec{x}^+ &= \vec{x}/L, \\ \vec{u}^+ &= \vec{u}/U, \\ t^+ &= tU/L, \\ p^+ &= p/\rho U^2, \\ \vec{f}^{P+} &= \vec{f}^P L/\rho U^2, \\ \vec{T}^{P+} &= \vec{T}^P/\rho U^2. \end{aligned} \tag{2.3}$$

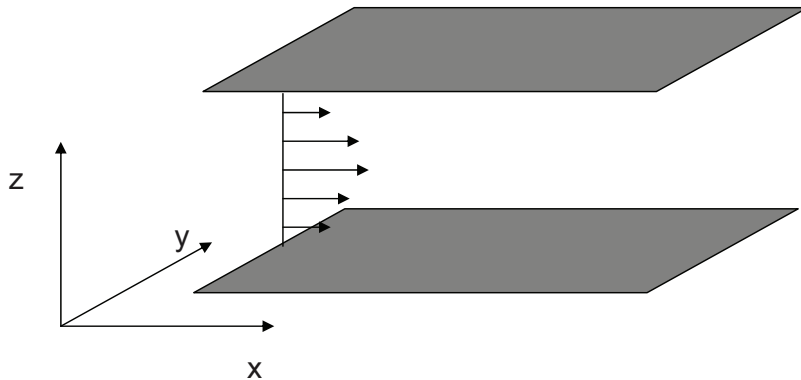


FIGURE 2.1. The geometry of the channel.

Substituting the variables of equation (2.3) into the fluid mass and momentum equations (2.1) and (2.2),

$$\nabla \cdot \vec{u}^+ = 0 \quad (2.4)$$

$$\rho \left[\frac{\partial \vec{u}^+}{\partial t} + (\vec{u}^+ \cdot \nabla) \vec{u}^+ \right] = -\nabla p^+ + Re^{-1} \nabla^2 \vec{u}^+ + \vec{f}^{P+} + \nabla \cdot \vec{T}^{P+} \quad (2.5)$$

Here Re is the Reynolds number defined as $Re = UL/\nu$, where ν is the kinematic viscosity of the carrier fluid. Reynolds number is an important parameter to represent the ratio of fluid inertial force to viscous force and turbulence generally happens at larger Reynolds number. Commonly Reynolds number in the channel flow can be expressed as friction Reynolds number, i.e. $Re_\tau = U_\tau L/\nu$, according to the frictional velocity U_τ , which is defined as,

$$U_\tau = \sqrt{\tau_{wall}/\rho} \quad (2.6)$$

where τ_{wall} is the wall shear stress.

2.1.2. Numerical methods

In general, there are mainly three Computational Fluid Dynamics (CFD) methods available to solve the turbulent flow numerically. The most conventional numerical technique is the Reynolds-Averaged Navier-Stokes (RANS) simulation where the turbulent Reynolds stress has to be modeled. RANS method is widely used in solving industry problems with its fast and economic characteristics but the accuracy of results is usually not guaranteed. The Large Eddy Simulation (LES) technique can directly compute the large scales of turbulent flow while small scales are modeled with subgrid models. The LES can acquire the main feature of the turbulence to achieve higher accuracy than RANS simulation. The last one solving the Navier-Stokes equations from the first principles without any model is called direct numerical simulation (DNS). DNS resolves all relevant scales from the smallest dissipative Kolmogorove scale to the integral scale, which makes the physics of turbulence available in great details. To capture the smallest eddy DNS needs high resolution computational mesh and time step which leads a huge consumption of

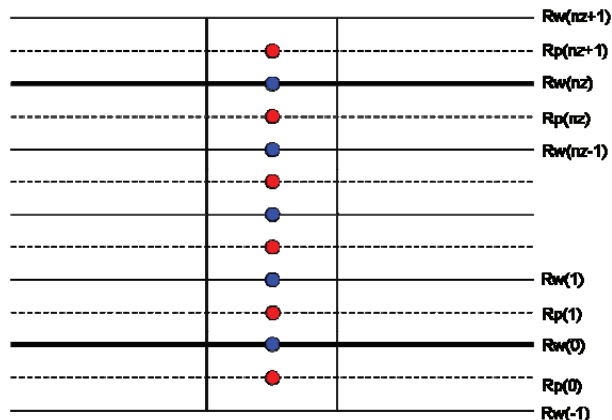


FIGURE 2.2. Computational grid in wall-normal direction. Red and blue circles represent the cell-centers and cell-faces, respectively.

memory and CPU hours. Moreover, Kolmogorov scale is becoming much smaller with increasing of Reynolds number. In the computation domain the number of grid points increases at the power of $Re^{9/4}$ and time step resolution is determined by the Komogorov time-scale as $Re^{1/2}$. Consequently, the computation cost of DNS is nearly proportional to $Re^{11/4}$. In general DNS as a numerical experiment is quit expensive and only restricted in the relatively low Reynolds number flows. The earliest DNS computations were described by Fox and Lily (1972). In 1987 Kim *et al.* firstly performed DNS of the turbulent channel flow which is still regarded as a standard reference for wall-bounded turbulent flow until now. A well arranged review on DNS of turbulent flow can be found in Moin and Mahesh (1998).

In present work we used a pseudo-spectral DNS code to compute the turbulent particle suspension channel flow. The code is written in Fortran language and was originally provided by Prof. Boersma and Dr. Gillissen in TU Delft and later developed by Dr. Mortensen and Zhao Lihao in NTNU. The DNS-solver is the same as that employed by Gillissen *et al.* (2008) and Mortensen *et al.* (2008a, 2008b).

The reference geometry of the channel flow is shown in Figure 2.1 and consists of two infinite flat parallel walls with a distance h . The coordinate axes are referred as streamwise x , spanwise y and wall-normal z . Periodic boundary conditions are used in the homogenous directions (x and y) and no-slip boundary conditions are imposed at the channel walls ($z=0$ and h). The friction Reynolds number is defined as $Re_\tau = u_\tau h/\nu$. The flow is driven by means of a constant pressure gradient ∇p in streamwise. The dimensionless equations (2.4) and (2.5) are discretized with a three dimensional Cartesian grid.

In the homogeneous directions, streamwise and spanwise, the grid is uniform and spatial derivatives are computed with a pseudo-spectral method. The derivatives are transformed into Fourier space by using Fast Fourier Transformation (FFT), for example, the velocity vector \vec{u} can be expanded as, $\vec{u}(\vec{x}, t) = \sum_k \vec{u}_k(t)e^{ik\vec{x}}$, where \vec{x} is the position vector in physical space and k is the wave number in spectra space. After the derivatives are determined in spectra space by

using inverse FFT, the Fourier component is multiplied by its wavenumber and the Fourier sequence is transformed back to physical space.

In the wall-normal direction the derivatives are computed by a second-order, central finite difference method. The grid in wall-normal direction is staggered and non-uniform that the grid-spacing is increasing away from both walls (Figure 2.2). The velocity components u_x and u_y , pressure p and force terms f_x^P and f_y^P are imposed in the grid-cell centers and the velocity component u_z and force terms f_z^P are defined on the grid-face centers.

The time advancement is carried out with a second-order explicit Adams-Bashforth scheme in the integration of the Navier-Stokes equations. Mass conservation is assured by means of a standard projection method and the resulting Poisson equation is transformed to Fourier space in the homogeneous directions.

2.2. Particle dynamics

In this section the dynamics and numerical methods of particles in turbulent channel flow are briefly presented. Current work focuses two types of particles with different geometries, spherical and prolate spheroidal particles. Both types of particles are represented by means of Lagrangian point-particle approach, each individual particle is tracked at every time-step. The point-particle method can be illustrated as the size of the particles is smaller than the Komogorove length scale in the flow such that the force on the particle can be treated as a point force and the neighboring flow can be considered as Stokesian flow or creeping flow. Consequently, the particle Reynolds number $Re_p = 2a(\bar{u}(\vec{x}_p) - \bar{v})/\nu$, based on the particle diameter $2a$ and the slip velocity between the local fluid and particle, should be smaller than unity to satisfy the criteria of Stokes flow in the particle vicinity. In the Stokes flow the nonlinear convective inertia term in the Navier-Stokes equation is neglected and the analytical expressions for forces and torques acting on particles are available. Both translational and rotational motions of particles can be computed in present work.

2.2.1. Spherical particle

Suspensions of spherical particles in turbulent pipe and channel flows have been extensively studied during the years with the view to better understand the particle transport, dispersion, and segregation in wall-turbulence and also the influence of the presence of the solid spheres on the turbulence of the carrier fluid. The current understanding of the complex behaviour of inertial spherical particles in turbulent wall flows was summarized in a keynote lecture by Soldati (2005). The survey of experimental studies and two-way coupled computer simulations by Balachandar and Eaton (2010) furthermore addressed the turbulence modulation observed in the presence of inertial particles. There are several common forces acting on the spherical particle in the Stokes flow,

- I. Steady drag force: local pressure and shear forces on the particle surface.
- II. Basset force and virtual mass force: acceleration of the particle with respect to the uniform flow field.

III. External pressure force: a particle in a fluid with a global pressure gradient.

IV. Lift force: there is asymmetry in the flow field or particle is rotating.

V. Gravity and buoyancy force: in the gravitational field and with hydrostatic pressure variation.

Forces listed above other than Stokes drag will not be taken into account in the present study, since other forces, like buoyancy and Basset forces, are negligibly small when the spherical particles are much heavier than the fluid, i.e. $\rho_p/\rho \gg 1$ (Elghobashi & Truesdell 1992). Wang *et al.* (1997) showed that the particle deposition rate was only marginally reduced when lift forces were neglected, whereas Pan *et al.* (2001) retained a lift force in their DNS study and found only a modest influence as compared with the drag force. Arcen *et al.* (2006) demonstrated that the wall-corrections of the drag force and the optimum lift force as defined by Wang *et al.* (1997), have a negligible effect on particle response times of the same order as those in the present study. The gravity can induce large particle slip velocity and this can be the main mechanism in many real situations, however, it is ignored in present work to isolate the turbulence-particle interaction.

Let us consider the motion of spherical particles with radius a , mass m , and moment of inertia $I = 2ma^2/5$. The equations governing the translational and rotational motion of one single particle are Newton's 2nd law of motion,

$$m \frac{d\vec{v}}{dt} = \vec{F}, \quad (2.7)$$

and Euler's equation:

$$I \frac{d\vec{\omega}}{dt} = \vec{N}. \quad (2.8)$$

Here, \vec{v} and $\vec{\omega}$ are the translational and the angular velocity of the particle, respectively. In the Stokesian flow the drag force \vec{F} and torque \vec{N} acting on the particle by the surrounding fluid can be expressed as,

$$\vec{F} = 6\pi\mu a[\vec{u}(\vec{x}_p, t) - \vec{v}(t)], \quad (2.9)$$

and

$$\vec{N} = 8\pi\mu a^3[\vec{\Omega}(\vec{x}_p, t) - \vec{\omega}(t)]. \quad (2.10)$$

Here $\vec{u}(\vec{x}_p, t)$ is the fluid velocity at the particle position \vec{x}_p at time t and $\vec{\Omega}(\vec{x}_p, t) = 1/2\nabla \times \vec{u}(\vec{x}_p, t)$ is thus the fluid angular velocity at the particle position. If the particle Reynolds number Re_p is larger than one, the drag force should include a non-linear correction as,

$$\vec{F} = 6\pi\mu a[\vec{u}(\vec{x}_p, t) - \vec{v}(t)](1 + 0.15Re_p^{0.687}), \quad (2.11)$$

Therefore the equations governing the translational and rotational motion of, with the force \vec{F} given in equation(2.9) and the torque \vec{N} as in equation(2.10), can be written as:

$$\frac{d\vec{v}}{dt} = \frac{1}{\tau_t}(\vec{u}(\vec{x}_p, t) - \vec{v}(t)), \quad \text{where} \quad \tau_t = \frac{2Da^2}{9\nu} \quad (2.12)$$

$$\frac{d\vec{\omega}}{dt} = \frac{1}{\tau_r}(\vec{\Omega}(\vec{x}_p, t) - \vec{\omega}(t)), \quad \text{where} \quad \tau_r = \frac{Da^2}{15\nu} \quad (2.13)$$

Here D is the ratio between the particle density ρ_p and the fluid density ρ . The response time τ is the time particle needs to adjust its motions when local flow field changes. Both translational and rotational response times are sensitive to the density ratio and particle size. The rotational response time τ_r is exactly 3/10 of the translational response time τ_t which implies that particle spin adjusts about 3 times faster to the fluid spin than the particle velocity adjusts to the fluid velocity. The Stokes number St , as an important non-dimensional parameter, is defined as the ratio between the particle response time and the viscous time scale. The large Stokes number indicates the slowly respond to the local fluid, for instance a bullet through the air; in contrast with small Stokes number the particle can adjust fast and follow the flow passively, e.g. the tracer particle in the particle image velocimetry (PIV) experiment.

The governing equations (2.12) and (2.13) of particle dynamics are scaled with channel height h and frictional velocity u_τ and integrated forward in time by using an explicit second-order Adams-Bashforth scheme along with the Eulerian fluid equations (2.4) and (2.5) for the fluid motion.

$$\vec{v}^{n+1} = \vec{v}^n + \frac{\Delta t}{\tau_t^+} \left[\frac{3}{2}(\vec{u}^n - \vec{v}^n) - \frac{1}{2}(\vec{u}^{n-1} - \vec{v}^{n-1}) \right], \quad (2.14)$$

$$\vec{\omega}^{n+1} = \vec{\omega}^n + \frac{\Delta t}{\tau_r^+} \left[\frac{3}{2}(\vec{\Omega}^n - \vec{\omega}^n) - \frac{1}{2}(\vec{\Omega}^{n-1} - \vec{\omega}^{n-1}) \right]. \quad (2.15)$$

$$\vec{x}_p^{n+1} = \vec{x}_p^n + \Delta t \left[\frac{3}{2}\vec{x}_p^{n+1} - \frac{1}{2}\vec{x}_p^n \right], \quad (2.16)$$

The fluid variables in equation (2.14) and (2.15) are interpolated at particle location every time-step by using a quadratic interpolation scheme which uses the information from 27 closest grid-points (van Haarlem 2000). The position of particle at a new time-step can be updated in equation (2.16). Periodic boundary conditions are used in the homogenous directions and fully elastic collision model is employed when particle hits the walls, i.e. a particle which happens to hit a wall bounces elastically back while retaining its previous velocity and spin, besides that the wall-normal velocity component changes sign.

2.2.2. Prolate spheroidal particle

One of our primary objective is to study the motion and influence of non-spherical particles in turbulent flows. As a representative model of non-spherical particles we consider ellipsoidal particles used as a prototype of elongated fiber-like particles (Figure 2.3). More specifically, the prolate spheroids are with mass m and aspect ratio $\lambda = b/a$ where a and b are radius in the semi-minor and semi-major axes,

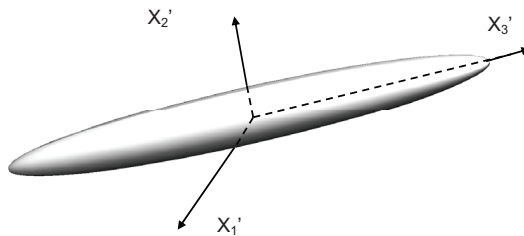


FIGURE 2.3. A schematic of a prolate spheroid with an aspect ratio of about to 5. The major or polar axis is aligned with the x'_3 -direction in the particle coordinate system which has its origin in the center of the spheroidal particle.

respectively. Such spheroids can be either oblate if $b < a$ or prolate when $b > a$. When $b/a \gg 1$ the spheroids mimic elongated particles and when $b/a \ll 1$ the spheroids resemble disks. The special case $b/a = 1$ corresponds to the more trivial case of spherical particles. The mathematical modeling of the ellipsoidal point-particles follows the methodology outlined by Zhang et al. (2001) and subsequently adopted by Mortensen et al. (2008) and Marchioli et al. (2010)

The translational and rotational motion of one single particle is governed by:

$$m \frac{dv_i}{dt} = F_i, \quad (2.17)$$

$$I'_{ij} \frac{d\omega'_j}{dt} + \epsilon_{ijk} \omega'_j I'_{kl} \omega'_l = N'_i \quad (2.18)$$

respectively, where ϵ_{ijk} is the Levi-Civita alternating or permutation tensor. Two different Cartesian frames of reference are used. Newton's 2^{nd} law of motion (2.17) is expressed in an *inertial frame* $x_i = \langle x_1, x_2, x_3 \rangle$ and Euler's equation (2.18) is formulated in the *particle frame* $x'_i = \langle x'_1, x'_2, x'_3 \rangle$ with its origin at the particle mass center and the coordinate axes aligned with the principal directions of inertia. Thus, $v_i = dx_i/dt$ denotes the translational particle velocity in the inertial frame whereas ω'_i is the particle angular velocity in the particle frame and I'_{ij} is the moment of inertia tensor for the elongated particles.

If the particles are sufficiently small so that the neighboring flow can be considered as Stokesian, the force F_i acting on a particle from the surrounding fluid can be expressed as:

$$F_i = D_{ij}(u_j - v_j) + \frac{Re_\kappa^{1/2}}{\mu a} D_{ij} L_{jk} D_{kl}(u_l - v_l), \quad D_{ij} = \pi \mu a K_{ij} \quad (2.19)$$

where u_i is the fluid velocity at the particle position and $Re_\kappa = \rho \kappa a^2 / \mu$ is a shear Reynolds number based on the modulus κ of the velocity gradient tensor. Here, L_{ij} is the lift tensor and the resistance tensor K_{ij} in the inertial frame is related to the resistance tensor K'_{ij} in the particle frame as $K_{ij} = A_{ik}^t K'_{kl} A_{lj}$ where A_{ij} denotes the orthogonal transformation matrix which relates the same vector

in the two different frames through the linear transformation $x_i = A_{ij}x'_j$. The expressions for the hydrodynamic drag and lift forces on a non-spherical particle were derived by Brenner (1964) and Harper & Chang (1968), respectively. According to equation (2.19) the force acting on the particle is therefore linearly dependent on the difference in translational velocity between the fluid and the particle.

Similarly, the torque N'_i is linearly dependent on the difference in angular velocity between the fluid and the particle, i.e.

$$\begin{aligned} N'_1 &= \frac{16\pi\mu a^3\lambda}{3(\beta_0+\lambda^2\gamma_0)}[(1-\lambda^2)S'_{23} + (1+\lambda^2)(\Omega'_1 - \omega'_1)] \\ N'_2 &= \frac{16\pi\mu a^3\lambda}{3(\alpha_0+\lambda^2\gamma_0)}[(\lambda^2-1)S'_{13} + (1+\lambda^2)(\Omega'_2 - \omega'_2)] \\ N'_3 &= \frac{32\pi\mu a^3\lambda}{3(\alpha_0+\beta_0)}(\Omega'_3 - \omega'_3) \end{aligned} \quad (2.20)$$

respectively. The parameters α_0 , β_0 and γ_0 depend on the particle aspect ratio λ . These expressions were first derived by Jeffery (1922) for an ellipsoidal particle in creeping motion. Here, S'_{ij} and Ω'_i denote the fluid rate-of-strain tensor and rate-of-rotation vector, respectively. The vorticity of the fluid flow field is thus $2\Omega'_i$.

The shape of a prolate spheroid is characterized by the particle aspect ratio λ , whereas the ability of the particle to adjust to the ambient flow field can be estimated in terms of the particle response time:

$$\tau = \frac{2\lambda\rho_p a^2 \ln(\lambda + \sqrt{\lambda^2 - 1})}{9\mu \sqrt{\lambda^2 - 1}} \quad (2.21)$$

To represent the particle orientation the Euler parameters, e_1 , e_2 , e_3 and e_4 , are used and must satisfy the constraint,

$$e_0^2 + e_1^2 + e_2^2 + e_3^2 = 1 \quad (2.22)$$

The orthogonal transformation matrix A_{ij} can be expressed by the Euler parameters,

$$\begin{aligned} A_{11} &= e_0^2 + e_1^2 - e_2^2 - e_3^2 \\ A_{12} &= 2(e_1e_2 + e_0e_3) \\ A_{13} &= 2(e_1e_3 - e_0e_2) \\ A_{21} &= 2(e_1e_2 - e_0e_3) \\ A_{22} &= e_0^2 - e_1^2 + e_2^2 - e_3^2 \\ A_{23} &= 2(e_2e_3 + e_0e_1) \\ A_{31} &= 2(e_1e_3 + e_0e_2) \\ A_{32} &= 2(e_2e_3 - e_0e_1) \\ A_{33} &= e_0^2 - e_1^2 - e_2^2 + e_3^2 \end{aligned} \quad (2.23)$$

The time evolution of these Euler parameters can be obtained by using the particle spins as,

$$\begin{pmatrix} \dot{e}_0 \\ \dot{e}_1 \\ \dot{e}_2 \\ \dot{e}_3 \end{pmatrix} = 1/2 \begin{pmatrix} e_0 & -e_1 & -e_2 & -e_3 \\ e_1 & e_0 & -e_3 & e_2 \\ e_2 & e_3 & e_0 & -e_1 \\ e_3 & -e_2 & e_1 & e_0 \end{pmatrix} \begin{pmatrix} 0 \\ \omega'_x \\ \omega'_y \\ \omega'_z \end{pmatrix} \quad (2.24)$$

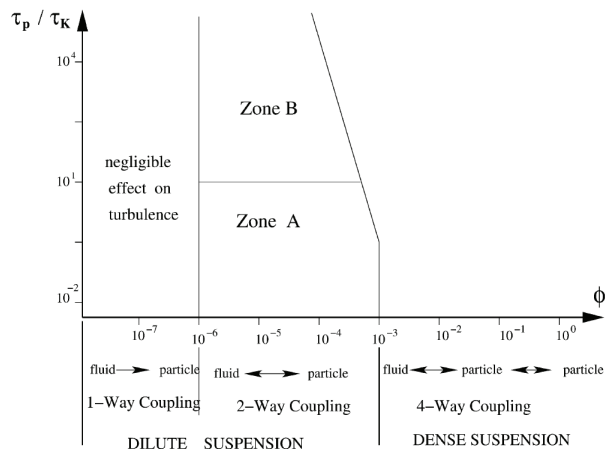


FIGURE 2.4. The map of different coupling regimes based upon volume fraction Φ from Elghobashi (2006). τ_p is the particle response time and τ_k is the Komogorov time-scale.

In the simulation, the translational and rotational equations (2.17) and (2.18) of the particles are integrated in time with a semi-implicit method (Fan and Ahmadi 1995). Time integrations of particle updated positions and orientations are using a second order Adams-Bashforth scheme. The size of time-step in the integration is the same with that used in Navier-Stokes equations. The fluid variables at particle location are interpolated by means of a quadratic interpolation scheme, as was used for spherical particle. The boundary conditions are periodic in the streamwise and spanwise directions, and fully elastic collision model is used at the walls.

2.3. Coupling methods

The main objective of this PhD work is to investigate the physics of particle-turbulence interaction. In the numerical simulation of particle-laden flow there are different coupling approaches between the Eulerian fluid phase and particle phase depending on the particle volume fraction Φ (Elghobashi 1994, 2006) as shown in Figure 2.4. With the simplest coupling, *one-way* coupling, e.g. Marchioli and Soldati (2002), Picciotto *et al.*(2005), the particles are driven by the local flow, but there is negligible effect from particles on the fluid and also the particle-particle interaction can be neglected. This approach is suitable for sufficiently dilute suspension flows when the particle volume fraction is small. *Two-way* coupling includes interactions between the particle phase and the fluid phase, while *four-way* coupling not only considers the interaction between particles and fluid, but also includes the effect of inter-collisions among the particles themselves.

In this section we mainly focus on the two-way coupling schemes. The conventional two-way coupling method indicates only the force-coupling based on Newton's third law. However, the influence of particle torque components on turbulence are of similar importance as the force components especially when the particles are non-spherical. Consequently, a full mechanical coupling can only be achieved if torque-coupling is applied along with the more conventional force-coupling. Results in present work indicate the effect of torque-coupling is negligible in spherical

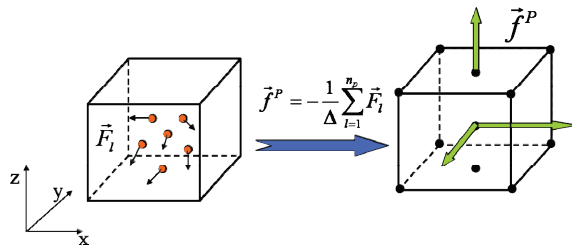


FIGURE 2.5. Illustration of point-particle forces \vec{F}_l transferred into volume force \vec{f}^P of fluid on the grid-nodes.

particle case but can be clearly observed in prolate spheroidal particle case. Additionally, the stress-coupling between elongated fiber-like particle phase and fluid phase is another approach of two-way coupling. The stress-coupling has been used to explore the fiber-turbulence interaction and also the mechanism of drag reduction in the wall turbulence (Gillissen *et al.* 2008). The author believe the fully two-way coupling scheme should include three terms, I. force-coupling, II. torque-coupling, and III. stress-coupling. However, stress-coupling is not considered in present work but has been planned to be explored in future.

2.3.1. Force-coupling

The point-force from a individual particle on the fluid is equal to $-\vec{F}$ according to Newton's 3rd law 'actio equals reactio'. As shown in Figure (2.5) the feedback from n_p particles within a given volume, e.g. a cell-volume, adds up to:

$$\vec{f}^P = -\frac{1}{\Delta} \sum_{l=1}^{n_p} \vec{F}_l \quad (2.25)$$

where \vec{F} is given by equation (2.11) and (2.19). This force per unit volume can be included in the linear momentum equation (2.5) to account for the effect of the solid particles on the fluid motion. This is known as the *point-force approximation* to two-way coupling. This approach was probably first introduced by Squires and Eaton (1990) in order to study the modulation of isotropic turbulence by spherical particles.

2.3.2. Torque-coupling

Compared with force-coupling, torque-coupling can be achieved as the torque vector acting from the particles on the fluid expressed in terms of a new anti-symmetric particle stress tensor which adds to the Newtonian stress tensor.

Firstly Cauchy's equation of motion, i.e. the principle of conservation of linear momentum, can be expressed in Cartesian tensor notation as:

$$\rho \frac{Du_i}{Dt} = \frac{\partial T_{ji}}{\partial x_j} + \rho f_i \quad (2.26)$$

where T_{ji} is a stress tensor and f_i is a body force. For a Newtonian fluid the stress tensor is:

$$T_{ji} = T_{ij} = -p\delta_{ij} + \mu\left(\frac{\partial u_i}{\partial x_j} + \frac{\partial u_j}{\partial x_i}\right) \quad (2.27)$$

and when this symmetric stress tensor is inserted in the Cauchy equation (2.26) we arrive at the celebrated Navier-Stokes equations.

For micropolar fluids Eringen (1966) suggested that Stokes' stress tensor (2.27) should be replaced by:

$$T_{ij} = -p\delta_{ij} + \mu\left(\frac{\partial u_i}{\partial x_j} + \frac{\partial u_j}{\partial x_i}\right) + \mu_r\left(\frac{\partial u_j}{\partial x_i} - \frac{\partial u_i}{\partial x_j}\right) - 2\mu_r\varepsilon_{mij}\omega_m \quad (2.28)$$

The positive constant μ_r is called the dynamic *microrotation viscosity* and this new viscosity coefficient is understood to be a fluid property which is characteristic for the fluid-particle suspension. A comprehensive account of the theory of micropolar fluids has been provided by Lukaszewicz (1999).

The expression within the second parenthesis in (2.28) is directly related to the angular velocity of the fluid as:

$$\left(\frac{\partial u_j}{\partial x_i} - \frac{\partial u_i}{\partial x_j}\right) = 2\Omega_m\varepsilon_{mij} \quad (2.29)$$

since components of the fluid angular velocity vector can be written as $\Omega_m = (1/2)\varepsilon_{mji}\partial u_i/\partial x_j$ and use has been made of the identity $\varepsilon_{ijk}\varepsilon_{rsk} = \delta_{ir}\delta_{js} - \delta_{is}\delta_{jr}$. Eringen's expression (2.28) for the stress tensor in a micropolar fluid can now be rewritten as:

$$T_{ij} = -p\delta_{ij} + \mu\left(\frac{\partial u_i}{\partial x_j} + \frac{\partial u_j}{\partial x_i}\right) + \underbrace{2\mu_r\varepsilon_{mij}(\Omega_m - \omega_m)}_{T_{ij}^P} \quad (2.30)$$

where the last term is considered to represent the effect of the particles on the motion of the fluid-particle mixture. The vector field ω_i is called the field of *microrotation* and represents the angular velocity of the rotation of the solid particles. In the theory for micropolar fluids ω_i is obtained from a transport equation for angular momentum; see Eringen (1966) and Lukaszewicz (1999). In the present context, however, the expression (2.26) replaces the modelling of T_{ij}^P (2.30) used in the continuum mechanics approach by Eringen (1966). The concept of microrotation viscosity μ_r is therefore avoided since the particle stress tensor is computed directly from the individual point particles inside a fluid volume (or grid cell) in accordance with (2.26).

Similar with the force-coupling, the torque from a single particle on the fluid is $-N_i$ where N_i is given in equation (2.20). It is known from tensor analysis that to any vector $-N_i$ corresponds an anti-symmetric tensor of 2^{nd} -order that contains the same information as the vector; see e.g. Irgens (2008). The torque vector $-N_i$ can thus be obtained from a *particle stress tensor* T_{ij}^P according to:

$$-N_m = -\frac{1}{2}\varepsilon_{mij}T_{ij}^P \Delta \quad (2.31)$$

In practice, the torque should be the sum of torques over all particles inside the grid cell under consideration. We furthermore assume that $T_{ij}^P = -T_{ji}^P$, i.e. we impose an anti-symmetry on T_{ij}^P . From equation (2.31) we thus arrive at the following expression for the anti-symmetric particle stress tensor:

$$T_{ij}^P = \frac{1}{\Delta} \sum_{l=1}^{n_p} \epsilon_{mij} N_m = \frac{1}{\Delta} \sum_{l=1}^{n_p} \begin{bmatrix} 0 & +N_3 & -N_2 \\ -N_3 & 0 & +N_1 \\ +N_2 & -N_1 & 0 \end{bmatrix} \quad (2.32)$$

where the summation is carried out over all particles in the volume Δ .

When the new stress tensor (2.32) is introduced in the Cauchy equation (2.26) together with the familiar Stokes stress tensor (2.27), the torques exerted by the particles on the fluid give rise to the additional term:

$$\frac{\partial T_{ji}^P}{\partial x_j} = -\frac{\partial T_{ij}^P}{\partial x_j} = -\frac{1}{\Delta} \epsilon_{mij} \frac{\partial}{\partial x_j} \sum_{l=1}^{n_p} N_m \quad (2.33)$$

to be added to the x_i -component of the Navier-Stokes equation. If Δ is the volume of a computational grid-cell, this accounts for the feedback on the fluid of the total torque from the n_p particles inside the cell. This is a *point-torque approximation* analogous to the point-force approximation (2.25) commonly employed in two-way coupled simulations.

In the simulation, we can define the volume torque components as we did for the volume forces as,

$$n_i = -\frac{1}{\Delta} \sum_{l=1}^{n_p} N_i \quad (2.34)$$

Then the terms to be added into x_i -component of Navier-Stokes equation (2.5) can be expressed as,

$$x_1 : \quad \frac{\partial n_3}{\partial x_2} - \frac{\partial n_2}{\partial x_3} \quad (2.35)$$

$$x_2 : \quad \frac{\partial n_1}{\partial x_3} - \frac{\partial n_3}{\partial x_1} \quad (2.36)$$

$$x_3 : \quad \frac{\partial n_2}{\partial x_1} - \frac{\partial n_1}{\partial x_2} \quad (2.37)$$

As shown in Figure (2.2) x_1 and x_2 components in the Navier-Stokes equation should be imposed on the pressure point *Rp*. x_3 component should be input on the wall point *Rw*. n_1 and n_2 are computed at wall points but n_3 is at pressure point. In homogeneous directions, i.e. streamwise and spanwise, to solve equation (2.35) and (2.36) a central difference scheme is used,

$$\frac{\partial n_3}{\partial x_2} = \frac{n_3(i, j+1, k) - n_3(i, j-1, k)}{2\Delta y} \quad (2.38)$$

$$\frac{\partial n_3}{\partial x_1} = \frac{n_3(i+1, j, k) - n_3(i-1, j, k)}{2\Delta x} \quad (2.39)$$

$$\frac{\partial n_2}{\partial x_1} = \frac{n_2(i+1, j, k) - n_2(i-1, j, k)}{2\Delta x} \quad (2.40)$$

$$\frac{\partial n_1}{\partial x_2} = \frac{n_1(i, j + 1, k) - n_1(i, j - 1, k)}{2\Delta y} \quad (2.41)$$

and backward difference in wall-normal direction (2.37),

$$\frac{\partial n_2}{\partial x_3} = \frac{n_2(i, j, k) - n_2(i, j, k - 1)}{Rw(k) - Rw(k - 1)} \quad (2.42)$$

$$\frac{\partial n_1}{\partial x_3} = \frac{n_1(i, j, k) - n_1(i, j, k - 1)}{Rw(k) - Rw(k - 1)} \quad (2.43)$$

2.3.3. Parallelization in computation

Current code is parallelized by using the Message Passing Interface (MPI). In the wall-normal direction the computation domain is divided into slices and the wall-normal derivatives communicates to the adjacent slices. In the streamwise the computation domain is also divided into slices in solving the Fourier transformed Poisson equation. The particles are divided into groups and the group number equals the processor number, i.e. each processor computes the same amount of particles. In two-way coupled simulation, the communication between particles and fluid is achieved by using a standard MPI routines called "MPI_ALLTOALL".

CHAPTER 3

Summary of articles

In this chapter a brief summary constituted by eleven articles and three appendixes is presented. The articles are sorted into the four categories (Section 3.1-3.4) according to the coupling methods and the types of particles. First, the PhD work started with the study on spherical particle suspensions with different relaxation times and Reynolds numbers by means of one-way coupling (article 1-3). Secondly, the spherical particle-turbulence interaction, as one of main objectives in present work, are investigated after two-way coupling method implemented by present author (article 4-8). Furthermore, the two-way force coupling scheme is applied in the prolate spheroids suspension (appendix 3) afterwards a novel scheme for torque-coupling was developed and employed accompanying with the conventional force-coupling approach (article 11). Additionally some study on the comparison between current Lagrangian approach and statistical approach was conducted in the simulation of fiber suspensions in the channel flow (article 10).

3.1. One-way coupled simulations of spherical particle suspensions

Article 1

Computation of particle-laden turbulent flows.

H.I. ANDERSSON & LIHAO ZHAO

This short article summarized the outlines of the mixed Eulerian-Lagrangian approach in simulations of dilute suspensions of spherical particles in turbulent fluid flows. It generally introduces both one-way coupling and two-way coupling schemes. An extension to non-spherical particles is also addressed. This article with a general scope of current work is firstly shown in the paper list as a starting point.

Article 2

Statistics of particle suspensions in turbulent channel flow.

LIHAO ZHAO & H.I. ANDERSSON

This work was completed in the early stage of the present PhD study. The DNS simulation of particles in wall-bounded turbulence is performed with one-way coupling. The main objectives of this article are exploring the effect of Reynolds number and particle concentration on the particle velocity statistics in the dilute suspensions. Four different particle response times τ_p in the range $1 < \tau_p < 100$ are examined for three different Reynolds numbers, $Re_\tau = 200, 360, 790$ (based on channel height

and friction velocity). The vast majority of DNS of dilute particle suspensions are performed at the fairly low Reynolds number of 300, in this work we performed simulations at a higher Reynolds number 790. The particle concentration evolves with time and statistics obtained during three different sampling periods might be distinctly different. The mean and fluctuating particle velocities are substantially affected both by the particle response time and by the Reynolds number of the flow.

Article 3

Particle slip velocity in wall-bounded turbulence and implications for dispersion models.

LIHAO ZHAO, C. MARCHIOLI & H.I. ANDERSSON

The idea of this article is generated during the cooperation with Dr. Marchioli this year. The particle slip velocity is found out to be an interesting topic to further investigate on when we examined the data in Article 2 and in iCFD database (<http://cfd.cineca.it>). In the results the statistical moments of the slip velocity are evaluated considering particles with Stokes number, defined as the ratio between the particle response time and the viscous time scale, in the range $1 < St < 100$. The slip velocity fluctuations exhibit a monotonic increase with increasing particle inertia, whereas the fluid-particle velocity covariance is gradually reduced for $St \geq 5$. Even if this covariance equals the particle turbulence intensity, a substantial amount of particle slip may occur. Relevant to two-fluid modeling of particle-laden flows is the finding that the standard deviation of the slip velocity fluctuations is significantly larger than the corresponding mean slip velocity.

3.2. Two-way coupled simulations of spherical particle suspensions

Article 4

Turbulence modulation and drag reduction by spherical particles.

LIHAO ZHAO, H.I. ANDERSSON & J.J.J. GILLISSEN

This is the first paper on the study of turbulence-particle interaction. We performed the two-way coupled DNS simulation of particle-laden channel flow. Millions of tiny inertial particles interacting with the fluid leads the pronounced turbulence modulations, i.e. augmentation in streamwise turbulence intensity and attenuations in spanwise and wall-normal directions, and the accompanying drag reduction, an increase of bulk velocity of the flow with constant pressure gradient. The present results support the view that drag reduction can be achieved not only by means of polymeric or fiber additives, but also with spherical particles.

*Article 5***On particle spin in a two-way coupled turbulent channel flow simulation.**

LIHAO ZHAO & H.I. ANDERSSON

With the same two-way coupled approach in Article 4, the present article investigates further on the modulations of particle spins and also fluid vorticities due to the presence of inertial particles. This work is a continuation of the paper by Mortensen *et al.* (2007) which focused on particle spin but only in one-way coupled simulation. In current work particles with three different response times are considered at Reynolds number 360. The lightest particles with rotational response time 0.3 times the viscous time scale exhibited preferential concentration in areas with low streamwise vorticity but rotated passively along with the local fluid. The heaviest particles with a thirty times longer response time spun strikingly different from the particle spin observed in a one-way coupled simulation. This phenomenon can be ascribed primarily to the substantial modulation of the carrier-phase turbulence caused by the feed-back from the particles in the two-way coupled approach. Due to their higher rotational inertia, these particles did not even adjust to the rotational motion of the local fluid.

*Article 6***Two-way coupled simulations of particle-laden wall turbulence.**

LIHAO ZHAO & H.I. ANDERSSON

The present paper here is a step forward based on Article 4. We considered the effect of volume fraction on the turbulence modulations due to the particles. In the article two cases with different particle volume fractions are designed in the simulations and particle response time and radius are the same as used in Article 4. Comparisons between the particle-laden flows and an unladen channel flow are made. The results represent similar observations as shown Article 4 with high volume fraction (10^{-3}) but the modulations are negligible when the volume fraction reduced to 10^{-5} .

*Article 7***On particle stress in gas-solid channel flows.**

LIHAO ZHAO & H.I. ANDERSSON

The role of the particle stress and the accompanying particle viscosity in two-way coupled simulations of fully-developed turbulent channel flows is considered in present article. The particle stress arises due to the reaction force from the inertial point-particles and assists the viscous and turbulent shear stresses to balance the driving pressure gradient. Simulation results for particles with a response time 30 viscous time units show that the particle stress distribution exhibits a distinct peak about 18 viscous length units away from the wall, whereas the particle viscosity remains fairly constant and roughly equal to the molecular fluid viscosity over the entire logarithmic layer. The particle viscosity tends to increase the total viscosity, but the turbulent eddy viscosity is nevertheless reduced. The effect of particle additives is therefore twofold: they alter the apparent viscosity of the suspension and

modulate the turbulent flow field.

Article 8

Interphasial energy transfer and particle dissipation in particle-laden wall turbulence

LIHAO ZHAO H.I. ANDERSSON & J.J.J. GILLISSEN

The current article is the core article in the section of two-way coupled simulation. Most of the two-way coupled results are included and the major findings are presented. Transfer of mechanical energy between particle additives and a carrier fluid has been explored. Three different particle suspensions were simulated in order to examine the effect of particle loading on channel-flow turbulence and it was observed that the modulation of the turbulence field increased non-linearly with the number of particles. The physical mechanisms involved in the particle-fluid interactions were analyzed in detail for one of the particle classes. It was observed that the fluid transferred energy to the particles in the core region of the channel whereas the fluid received kinetic energy from the particles in the wall region. Locally an imbalance in the work performed by the particles on the fluid and the work exerted by the fluid on the particles was observed. This imbalance gave rise to a particle-induced energy dissipation which represents a loss of mechanical energy from the fluid-particle suspension. An independent examination of work associated with the different directional components of the Stokes force revealed that the dominating energy transfer was associated with the streamwise component. The streamwise turbulence intensity was enhanced in the buffer region due to work performed by the particles on the local fluid. Both the mean and fluctuating parts of the Stokes force promoted streamwise fluctuations in the near-wall region. The kinetic energy of the flow field in a cross-sectional plane was damped due to work done by the particles, and the energy was dissipated rather than recovered as particle kinetic energy. This explained the significant damping of the cross-plane velocity components. Novel component-wise scatter plots of instantaneous velocity versus instantaneous slip velocity provided further insight into the energy transfer mechanism beyond that of the statistical data. The observed modulations of the turbulence field could be thereby completely understood.

3.3. One-way coupled simulations of prolate spheroid suspensions

Article 9

DNS of non-spherical particles in turbulent flows.

H.I. ANDERSSON & LIHAO ZHAO

In this Bulletin paper, the general introduction and some literature review of the study on the dilute suspensions of elongated solid particles in turbulent gas or liquid flow are presented. An overview of fiber dynamics and the Eulerian-Lagrangian simulation approach are also given. This article is used as an introductory material here when the topic is shifted into the prolate spheroid suspensions.

Article 10

Comparison of Lagrangian approach and statistical approach in simulation of fiber suspension turbulent channel flow.

LIHAO ZHAO H.I. ANDERSSON & J.J.J. GILLISSEN

The main aim of this paper is focused on the comparison of current Lagrangian approach and statistical approach (Gillissen *et al.* 2008) in the simulation of fiber suspensions in a turbulent channel flow. The frictional Reynolds number is 360 based on the walls distance of the channel. The aspect ratio of fibers is 100 and the number of fibers is 10^5 . Three different particle response times are tested by using current Lagrangian approach. The effect of particle response time on the fiber orientations is also shown and discussed. The mean fiber stresses are obtained by Lagrangian approach and then compared with results by statistical method (Gillissen *et al.* 2008). Comparison shows good agreement with each other, the linkage of two different methods is discussed at last.

3.4. Two-way coupled simulations of prolate spheroid suspensions

Article 11

Torque-coupling and fiber-turbulence interactions.

H.I. ANDERSSON LIHAO ZHAO & M. BARRI

In current paper the main contribution is developing the novel scheme of torque-coupling. The scheme is applied along with the more conventional force-coupling. The torque vector acting from the particles on the fluid is expressed in terms of a new anti-symmetric particle stress tensor which adds to the Newtonian stress tensor. A fully-coupled simulation of a turbulent channel flow laden with prolate spheroidal particles with aspect ratio 5:1 demonstrated demonstrated that the inclusion of torque-coupling reduced the modulation of the turbulent flow field observed in a two-way coupled simulation. The spin and orientation of the spheroids were significantly affected.

3.5. Appendix

Appendix 1

Modulations on turbulence with the presence of particle $St=200$.

In this appendix, the main purpose is to verify the performance of present code implemented with two-way coupling scheme. The author performed a simulation with the same Reynolds number of flow and also the same type and number of particles as in the published article by Dritselis and Vlachos (2008). The modified mean velocity profile and also the turbulence intensities are compared and the results are identical with each other.

Appendix 2

Two-way coupled simulation of particle laden channel flow at $Re_\tau = 790$

Similar with Article 2, the Reynolds effect in the two-way coupled simulation is always planned to investigate. In recent the author have completed a two-way coupled simulation with a high Reynolds number at $Re_\tau = 790$ which costs a huge amount of CPU-hours. Four million particles are released in the fully developed turbulence and the mesh size is 394^3 , despite of the large mesh number, the interpolation of the millions particles consumes more computing time. The modified turbulence intensities and also the bulk velocity profiles are shown.

*Appendix 3***Two-way coupled simulation of fiber suspension turbulent channel flow.**

Compared with Article 11, in present paper only the conventional force-coupling method is adopted in the simulation of fiber suspensions in a channel flow. The effect of particle aspect ratio and lift force on the turbulence modulations is mainly investigated. The statistical results of the feedback forces acting on the fluid from the particles are plotted along the wall-normal direction. The results of particle with aspect ratio 10 are compared with the particle with aspect ratio 1 in the condition of the same mass loading and then compared in the condition of the same volume fraction.

Bibliography

- B. ARCEN, A. TANIÈRE, AND B. OESTERLÉ 2010 On the influence of near-wall forces in particle-laden channel flows. *Int. J. Multiphase Flow* **32**, 1326-1339.
- BALACHANDAR, S. & EATON, J. K. 2010 Turbulent Dispersed Multiphase Flow. *Annu. Rev. Fluid Mech.* **42**, 111-133.
- BIJLARD, M. J., OLIEMANS, R. V. A., PORTELA, L. M., & OOMS, G. 2010 Direct numerical simulation analysis of local flow topology in a particle-laden turbulent channel flow. *J. Fluid Mech.* **653**, 35-56.
- BRENNER, H. 1964 The Stokes resistance of an arbitrary particle IV. Arbitrary fields of flow. *Chem. Engng Sci.* **19**, 703-727.
- DAVIDSON, P. A. 2004 Turbulence - An introduction for scientists and engineers. *Oxford University Press*.
- DONALDSON, K., AITKEN, R., TRAN, L., STONE, V., DUFFIN, R., FORREST G. & ALEXANDER, A. 2006 Carbon nanotubes: a review of their properties in relation to pulmonary toxicology and workplace safety. *Toxicological Sciences* **92**, 5-22.
- DRITSELIS, C.D. & VLACHOS, N.S. 2008 Numerical study of educed coherent structures in the near-wall region of a particle-laden channel flow. *Phys. Fluids* **20**, 055103.
- DRITSELIS, C.D. & VLACHOS, N.S. 2008 Direct numerical simulation of particle interaction with coherent structures in a turbulent channel flow. *Progress in Turbulence III* Springer.
- ELGHOBASHI, S. & TRUESDELL, G. C. 1992 Direct simulation of particle dispersion in a decaying isotropic turbulence. *J. Fluid Mech.* **242**, 655-700.
- ELGHOBASHI, S. & TRUESDELL, G. C. 1993 Homogeneous turbulence and dispersed solid particles. I: turbulence modification. *Physics of Fluids A: Fluid Dynamics* **5**, 1790-1801.
- ELGHOBASHI, S. 1994 On predicting particle-laden turbulent flows. *Appl. Sci. Res.* **52**, 309-329.
- ELGHOBASHI, S. 2006 An updated classification map of particle-laden turbulent flows. *IUTAM Symposium on computational approaches to multiphase flow*, 3-10.
- ERINGEN, A.C. 1966 Theory of micropolar fluids. *J. Math. Mech.* **16**, 1-18.
- FAN, F-G. & AHMADI, G. 1995 A sublayer model for wall deposition of ellipsoidal particles in turbulent streams. *J. Aerosol Sci.* **26**, 813-840.
- FOX, D. G. & LILY, D. K. 1972 Numerical simulation of turbulent flows. *Rev. Geophysics* **10**, 51-72.
- GEASHCHENKO, S., SHARP, N., NEUSCAMMAN, S. & WARHAFT, Z. 2008 Lagrangian measurements of inertial particle accelerations in a turbulent boundary layer. *J. Fluid Mech.* **617**, 255-281.
- GHOSAL, S. & MANDRE, S. 2003 A simple model illustrating the role of turbulence on phytoplankton blooms. *Journal of Mathematical Biology* **46**, 333-346.

- GILLISSEN, J.J.J., BOERSMA, B.J., MORTENSEN, P.H. & ANDERSSON, H.I. 2008 Fibre-induced drag reduction. *J. Fluid Mech.* **602**, 209-218.
- HARPER, E.Y. & CHANG, I.-D. 1968 Maximum dissipation resulting from lift in a slow viscous shear flow. *J. Fluid Mech.* **33**, 209-225.
- HUSSAINOV, M., KARTUSHINSKY, A., RUDI, SHCHEGLOV, I., KOHNEN, G., & SOMMERFELD, M. 2000 Experimental investigation of turbulence modulation by solid particles in a grid-generated vertical flow. *Int. J. Heat Fluid Fl.* **21**, 365-373.
- HÖGBERG, S.M., ÅKERSTEDT, H.O., LUNDSTRÖM T.S. & FREUND J.B. 2008 Numerical model for fiber transport in the respiratory airways. *Proc. 19th International Symposium on Transport Phenomena* Reykjavik, Iceland.
- IRGENS, F. 2008. Continuum mechanics. *Springer Verlag*.
- JEFFERY, G. B. 1922 The motion of ellipsoidal particles immersed in a viscous fluid. *Proc. Roy. Soc. A* **102**, 161-179.
- KIM, J., MOIN, P. & MOSER, R. 1987 Turbulence statistics in fully developed channel flow at low Reynolds number. *J. Fluid Mech.* **177**, 133-166.
- KULICK, J. D., FESSLER, J. R. & EATON, J. K. 1994 Particle response and turbulence modification in fully developed channel flow. *J. Fluid Mech.* **277**, 109-134.
- LESIEUR, M. 1987 Turbulence in fluids. *Kluwer Academic publishers*.
- LI, Y., MCLAUGHLIN, J. B., KONTOMARIS, K. & PORTELA, L. 2001 Numerical simulation of particle-laden turbulent channel flow. *Phys. Fluids* **13**, 2957.
- LUKASZEWICZ, G. 1999 Micropolar fluids - theory and applications. *Birkhäuser Verlag*.
- LUNDELL, F. & CARLSSON, A. 2010 Heavy ellipsoids in creeping shear flow: transitions of the particle rotation rate and orbit shape. *Physical Review A* **81**, 016323.
- MANN, J., OTT, S., PECSELI, H.L. & TRULSEN, J. 2006 Laboratory studies of predator-prey encounters in turbulent environments: effects of changes in orientation and field of view. *Journal of Plankton Research* **28**, 509-522.
- MARCHIOLI, C. & SOLDATI, A. 2002 Mechanisms for particle transfer and segregation in a turbulent boundary layer. *J. Fluid Mech.* **468**, 283-315.
- MARCHIOLI, C., FANTONI M. & SOLDATI, A. 2010 Orientation, distribution, and deposition of elongated, inertial fibers in turbulent channel flow. *Phys. Fluids* **22**, 033301.
- MOIN, P. & MAHESH, K. 1998 Direct numerical simulation: a tool in turbulence research. *Ann. Rev. Fluid Mech.* **30**, 539-578.
- MORTENSEN, P.H., ANDERSSON, H.I., GILLISSEN, J.J.J. & BOERSMA, B.J. 2008 On the orientation of ellipsoidal particles in a turbulent channel flow. *Intl J. Multiphase Flow* **34**, 678-683.
- MORTENSEN, P.H., ANDERSSON, H.I., GILLISSEN, J.J.J. & BOERSMA, B.J. 2008 Dynamics of prolate ellipsoidal particles in a turbulent channel flow. *Phys. Fluids* **20**, 093303.
- NARAYANAN, C., LAKEHAL, D., BOTTO, L. & SOLDATI, A. 2003 Mechanisms of particle deposition in a fully developed turbulent open channel flow. *Phys. Fluids* **15**, 763-775.
- PAN, Y. & BANERJEE, S. 1996 Numerical simulation of particle interactions with wall turbulence. *Phys. Fluids* **8**, 2733-2755.
- PAN, Y., TANAKA, T. & TSUJI, Y. 2001 Direct numerical simulation of particle-laden rotating turbulent channel flow. *Phys. Fluids* **13**, 2320-2337.
- PEDINOTTI, S., MARIOTTI, G. & BANERJEE, S. 1992 Direct numerical simulation of particle behaviour in the wall region of turbulent flows in horizontal channels. *Intl J. Multiphase Flow* **18**, 927-941.
- PICCIOTTO, M., MARCHIOLI, C. & SOLDATI, A. 2005 Characterization of near-wall accumulation regions for inertial particles in turbulent boundary layers. *Phys. Fluids* **17**, 098101.
- POPE, S. B. 1972 Turbulent flows. *Cambridge University Press*.

- RASHIDI, M., HETSRONI, G. & BANERJEE, S. 1990 Particle-turbulence interaction in a boundary layer. *Int. J. Multiphase Flow* **16**, 935-949.
- SOLDATI, A. 2005 Particles turbulence interactions in boundary layers. *Z. Angew. Math. Mech.* **85**, 683-699.
- SOLTANI, M. & AHMADI, G. 1995 Direct numerical simulation of particle entrainment in turbulent channel flow. *Phys. Fluids* **7**, 647-657.
- SQUIRES, K. D., & EATON, J. K. 1990 Particle response and turbulence modification in isotropic turbulence. *Phy. Fluids A: Fluid Dynamics* **2**, 1191-1203.
- TENNEKES, H. & LUMLEY, J. L. 1972 A first course in turbulence. *MIT Press*.
- TRUESDELL, G. C. & ELGHOBASHI, S. 1994 Homogeneous turbulence and dispersed solid particles. II. Particle Dispersion. *Phys. Fluids* **6**, 1405-1407.
- VAN HAARLEM, B. 2000 The dynamics of particles and droplets in atmospheric turbulence. *PhD thesis* Delft University of Technology.
- VREMAN, A. W. 2007 Turbulence characteristics of particle-laden pipe flow. *J. Fluid Mech.* **584**, 235-279.
- WANG, Q., SQUIRES, K. D., CHEN, M. & MCLAUGHLIN, J. B. 1997 On the role of the lift force in turbulence simulations of particle deposition. *Int. J. Multiphase Flow* **23**, 749-763.
- YAMAMOTO, Y., POTTHOFF, M., TANAKA, T., KAJISHIMA, T. & TSUJI, Y. 2001 Large-eddy simulation of turbulence gas-particle flow in a vertical channel: effect of considering inter-particle collisions. *J. Fluid Mech.* **442**, 303-334.
- ZHANG, H., AHMADI, G., FAN, F. G. & MCLAUGHLIN, J.B. 2001 Ellipsoidal particle transport and deposition in turbulent channel flows. *Int. J. Multiphase Flow* **27**, 971-1009.

Part 2

Articles

Part 2.1

One-way coupled simulations of spherical particle suspensions

Article 1

Computation of particle-laden turbulent flows

H.I. ANDERSSON & LIHAO ZHAO

The 23rd Nordic Seminar on Computational Mechanics, Stockholm, Sweden, 2010.

COMPUTATION OF PARTICLE-LADEN TURBULENT FLOWS

HELGE I. ANDERSSON* AND LIHAO ZHAO*

* Division of Fluids Engineering
Department of Energy and Process Engineering
The Norwegian University of Science and Technology (NTNU)
N-7491 Trondheim, Norway
e-mail: helge.i.andersson@ntnu.no; lihao.zhao@ntnu.no

Key words: Particle Dynamics, Turbulence Modulation, Multiphase Flow, Chemical Engineering.

Summary. This paper aims to outline the mixed Eulerian-Lagrangian approach to simulations of dilute suspensions of spherical particles in turbulent fluid flows. An extension to non-spherical particles will also be discussed. Both one-way coupled and two-way coupling schemes will be addressed. Examples from ongoing research work at NTNU will be given.

1 INTRODUCTION

Dilute suspensions of solid particles in a turbulent gas or liquid flow offer problems of greater complexity than mono-phase turbulence, but are nevertheless of immense practical concern both in natural flows and in industry. The vast majority of investigations have naturally focused on the behaviour of *spherical* particles in a fluid flow and occasionally also on how the flow field is affected by the presence of the particles. The recent review article by Balachandar and Eaton¹ provides a useful introduction to the state-of-the-art in this vast area of research.

The particle-laden flows considered are either homogenous in space or of the shear-flow type like in boundary layers, channels and pipes. In the majority of applications, the fluid flow is turbulent and therefore inherently unsteady and three-dimensional. If the suspension is sufficiently dilute, the carrier fluid is unaffected by the presence of the particles and the focus is on the translational motion of the particles. It is known beyond any doubt¹ that spherical particles tend to concentrate in the near-wall region of a wall-bounded shear flow and furthermore that the particles are not evenly distributed but rather accumulate in preferred areas. For somewhat larger particle concentrations, the fluid flow is influenced by the solid particles embedded in the flow field. The current understanding of such particle-fluid interactions was summarized by Soldati².

Suspensions of *non-spherical* particles are also encountered in practice, for instance in the fields of aerosol science, phytoplankton dynamics, dispersion of carbon nano-tubes (CNTs), and transport of cellulose fibers in the pulp and paper industry. As far as the dynamics of non-spherical particles is of concern, not only their translational motion is of importance, but their rotational motion and their orientation become essential.

2 COMPUTATIONAL MODELLING APPROACH

A variety of different approaches have been taken to numerically simulate suspensions of solid particles in a fluid flow. Each approach has its own advantages and limitations. Here, we follow the mixed Eulerian-Lagrangian approach. Both the particle dynamics and the fluid motion are governed by the fundamental laws of mechanics and the modeling is therefore in accordance with so-called ‘*first principles*’.

2.1 Eulerian representation of the flow field

Since we are concerned with turbulent flow fields, the fluid motion is governed by the full Navier-Stokes equation. As long as the Reynolds number is not too high, the discretized Navier-Stokes equation is integrated on a three-dimensional mesh and in time. It is essential that the mesh sizes do not exceed the size of the smallest turbulent eddies, i.e. the Kolmogorov scales, since no turbulence models are to be used. Such direct numerical simulations (DNSs) are considered as true realizations of turbulent flow fields and serve as reliable computer experiments.

2.2 Lagrangian particle dynamics

The motion of the particles is governed by the Lagrangian equation of motion:

$$m dv/dt = \mu K(\mathbf{u} - \mathbf{v}). \quad (1)$$

Here, \mathbf{v} and \mathbf{u} denote the velocity vector of the particle and the fluid, respectively. The physical quantities involved are the particle mass m , the fluid viscosity μ and the resistance parameter K . Assuming that the particle Reynolds number based on the particle diameter $2a$ and the slip velocity $|\mathbf{u} - \mathbf{v}|$ is smaller than unity only Stokes drag is taken into account. For spherical particles these three quantities combine into the particle response time:

$$\tau = m/\mu K = 2\rho D a^2/9\mu \quad (2)$$

where D is the ratio between particle and fluid densities.

3 COUPLING BETWEEN PARTICLES AND FLUID

The presence of solid particles in a turbulent flow is known to affect the flow field. A point force from each and every particle in accordance with Newton’s third law is added to the Navier-Stokes equation which governs the fluid flow. In such *two-way coupled* simulations the amount of feedback from the particles on the carrier fluid depends on the particle size, shape and concentration. Recent two-way coupled simulations of spherical particles in turbulent channel flow by Zhao et al.³ showed pronounced turbulence modulations accompanied by a significant drag reduction. Figure 1 shows the uneven distribution of spherical particles in a turbulent channel flow obtained in a two-way coupled simulation.

4 NON-SPHERICAL PARTICLES

If non-spherical rather than spherical particles are considered, the Lagrangian equation of translational motion is still valid but the resistance parameter K in eq. (1) is then a tensor rather than a scalar. The particle response time τ in eq. (2) is no longer dependent only on the

particle radius a but also on the particle aspect ratio λ .

Even more important is the fact that the rotational motion becomes of major concern and determines, for instance, the instantaneous orientation of a given particle relative to the primary flow direction. The rotational motion of a solid particle is given, for instance, by

$$I_{xx} d\omega_x/dt - \omega_y\omega_z (I_{yy} - I_{zz}) = N_x. \quad (3)$$

Here, ω_x is the x -component of the angular velocity of a particle with principle moments of inertia I_{xx} , I_{yy} , and I_{zz} . N_x is the x -component of the torque on the particle and involves the spin of the particle relative to the fluid vorticity. The equations of translational and rotational particle motion (1) and (3) are integrated forward in time in a reference frame attached to the particle whereas the Navier-Stokes equation for the fluid flow is solved in a fixed frame of reference; see Zhang et al.⁴ Three independent Euler angles specify the transformation between these two coordinate systems. In practice, however, we adopted the four Euler parameters (*quaternions*) instead of the Euler angles. We first used this approach to study the spin of spherical particles and observed that the particle spin deviated from the fluid vorticity (Mortensen et al.⁵)

As a prototype model of a non-spherical particle we consider a *spheroid* which is characterized not only by the equatorial radius a but also by its aspect ratio λ . Results from one-way coupled turbulent channel flow simulations of prolate spheroids with some different aspect ratios and particle response times were presented by Mortensen et al.^{6,7} Figure 2 gives a first impression of the different orientations of prolate spheroids in a turbulent flow field.

5 CLOSING REMARKS

Our current investigations are proceeding along two different paths. We are continuing our investigations of two-way coupled simulations of spherical particles with the view to explore how the turbulence modulation is affected by the particle response time and the particle loading. In this context the energy exchange between the fluid and the particles is investigated by means of conditional averages. In parallel two-way coupled simulations of non-spherical particles are underway. For that purpose a novel method to account for torque-coupling between the fluid and the particles is explored.

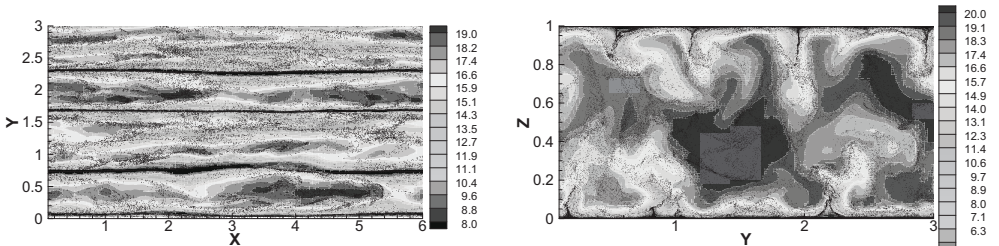


Figure 1: Contours of the streamwise velocity component in a wall-parallel X-Y plane (left) and a cross-sectional Y-Z plane (right). The black dots represent the instantaneous particle positions.

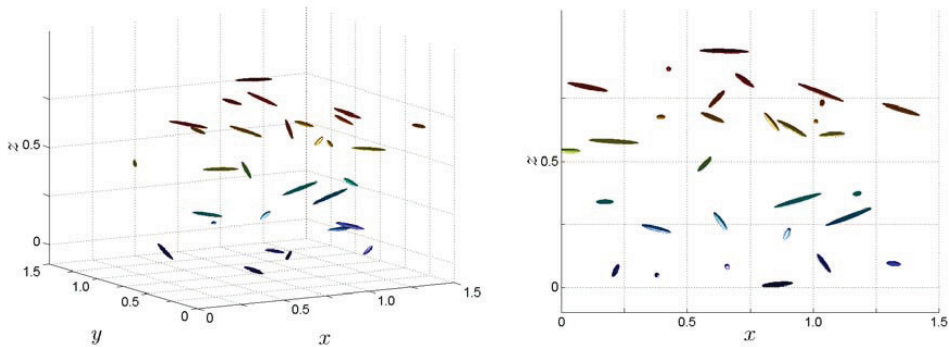


Figure 2: Instantaneous orientation of non-spherical particles in a turbulent channel flow. The orientation of the prolate spheroids varies in time and with position. A perspective view is shown to the left and a planar view to the right. Statistics of the particle orientations are deduced from the instantaneous orientations.

ACKNOWLEDGEMENTS

This work is currently funded by The Research Council of Norway (NFR) and A/S Norske Shell. Computing time on the ‘Stallo’ compute cluster HP BL 460c in Tromsø is granted by NFR (Programme for Supercomputing). The collaboration with Prof. B.J. Boersma and Dr. J.J.J. Gillissen (TU Delft) is greatly appreciated.

REFERENCES

- [1] S. Balachandar and J.K. Eaton, “Turbulent dispersed multiphase flow”, *Annu. Rev. Fluid Mech.*, **42**, 111-133 (2010).
- [2] A. Soldati, “Particles turbulence interactions in boundary layers”, *Z. Angew. Math. Mech.*, **85**, 683-699 (2005).
- [3] L.H. Zhao, H.I. Andersson and J.J.J. Gillissen, “Turbulence modulation and drag reduction by spherical particles”, *Phys. Fluids*, **22**, 081702 (2010).
- [4] H. Zhang, G. Ahmadi, F.G. Fan and J.B. McLaughlin, “Ellipsoidal particle transport and deposition in turbulent channel flows”, *Int. J. Multiphase Flow*, **27**, 971-1009 (2001).
- [5] P.H. Mortensen, H.I. Andersson, J.J.J. Gillissen and B.J. Boersma, “Particle spin in a turbulent shear flow”, *Phys. Fluids*, **19**, 078109 (2007).
- [6] P.H. Mortensen, H.I. Andersson, J.J.J. Gillissen and B.J. Boersma, “Dynamics of prolate ellipsoidal particles in a turbulent channel flow”, *Phys. Fluids*, **20**, 093302 (2008).
- [7] P.H. Mortensen, H.I. Andersson, J.J.J. Gillissen and B.J. Boersma, “On the orientation of ellipsoidal particles in a turbulent shear flow”, *Int. J. Multiphase Flow*, **34**, 678-683 (2008).

Article 2

Statistics of particle suspensions in turbulent channel flow

LIHAO ZHAO & H.I. ANDERSSON

Communications in Computational Physics, **11**, 1311-1322, 2012.

Statistics of Particle Suspensions in Turbulent Channel Flow

Lihao Zhao* and Helge I. Andersson

Fluids Engineering Division, Department of Energy and Process Engineering, Norwegian University of Science and Technology, 7491 Trondheim, Norway.

Abstract. Particle dynamics in a turbulent channel flow is considered. The effects of particle concentration and Reynolds number on the particle velocity statistics are investigated. Four different particle response times, $\tau^+ = 1, 5, 30$ and 100 , are examined for three different Reynolds numbers, $Re_* = 200, 360$ and 790 (based on channel height and friction velocity). The particle concentration evolves with time and statistics obtained during three different sampling periods might be distinctly different. The mean and fluctuating particle velocities are substantially affected both by the particle response time and by the Reynolds number of the flow.

AMS subject classifications: 76T15 76F10 76F65

Key words: spherical particles, DNS, turbulence, sampling, Reynolds number effects

1 Introduction

Solid spherical particles suspended in fluid turbulence are commonly encountered both in nature and industry, e.g. in sand storms, pollution in the atmosphere, in pneumatic transport and so on. The study of particles suspended in a carrier fluid has been an active area of research during several decades along with the development of computer resources and experiment technologies [1] [2]. It is commonly known that inertial particles will not follow the flow totally passive. Due to the inertial effect, there is a certain amount of slip velocity between particles and the local fluid flow. In other words, the inertial solid particles have a tendency to concentrate around locally calm regions [1]. In the channel flow case, for example, the particles tend to accumulate in the near-wall region and the greater the inertia of particles, the longer time is needed to achieve a steady state of the particle concentration. Several investigations have focused on the particle deposition and particle preferential concentration in wall turbulence or homogenous turbulence, see for instance Pedinotti *et al.* [2], Soltani and Ahmadi [3], Marchioli and Soldati [4], Narayanan *et al.* [5] and Picciotto *et al.* [6]. To obtain better understanding of particle transport and

*Corresponding author. *Email address:* lihao.zhao@ntnu.no

particle velocity statistics, several studies were reported by Marchioli and Soldati [4], Kulick *et al.* [7]. and Geashchenko *et al.* [8].

Depending on the particle volume fraction, there are several ways to make the coupling between the particle phase and the fluid phase, i.e. as one-way, two-way or four-way coupling, as defined by Elghobashi [9]. With *one-way* coupling, e.g. [4] [6], the particles are driven by the local flow, but there is no feedback effect from particles on the fluid. This approach is suitable for sufficiently dilute suspension flows when the particle volume fraction is small. *Two-way* coupling means interactions between the particle phase and the fluid phase based on Newton's third law, while *four-way* coupling not only considers the interaction between particles and fluid, but also includes the effect of inter-collisions among the particles themselves. Several investigations with two-way coupling, like Squires and Eaton [10] and Elghobashi and Truesdell [11] in homogeneous turbulence, Pan and Banerjee [12] and Zhao *et al.* [13] in wall-bounded turbulence, focus on the modulations of turbulence by the presence of particles. The present work is confined to one-way coupling as we assume a dilute suspension of the particles in the carrier fluid and focuses on the Reynolds number effect on the particle transport and particle depositions.

During the last two decades direct numerical simulations (DNSs) have become a powerful tool in the research of turbulent flow of particle suspensions, for example DNS simulations of particle-laden homogeneous and isotropic turbulence [10] [11] and also of particulate turbulent channel flow [2] [3] [4] [12] [13]. However, all these simulations were carried out at fairly low Reynolds numbers, most likely due to limitations of the available computer capacity.

In the present investigation a dilute suspension of solid particles in a turbulent channel flow is simulated with an Eulerian-Lagrangian approach where the fluid flow is obtained by means of DNS. In Section 2, the treatment of the flow and the particles is described. Results for four different particle categories are presented and compared in Section 3.1 for one particular Reynolds number whereas results for three different Reynolds numbers are presented in Section 3.3. The highest Reynolds number considered is substantially higher than in earlier DNS studies of particle-laden channel flows [2] [3] [4] [5] [6] [12] [13]. The major findings are discussed and summarized in Section 4, notably in view of the influence of the particle concentration on the velocity statistics.

2 Mathematical modeling and computational details

In the present work we consider the motion of tiny spherical particles in a turbulent plane channel flow. The equations governing the flow field and particle motion are simultaneously integrated forward in time. The flow solver and the particle treatment is the same as that used by Mortensen *et al.* [14] [15].

2.1 Governing equations of the fluid flow

DNS is used to solve the continuity and momentum conservation equations:

$$\nabla \cdot \vec{u} = 0 \quad (2.1)$$

$$\frac{\partial \vec{u}}{\partial t} + (\vec{u} \cdot \nabla) \vec{u} = -\nabla p + \frac{\nabla^2 \vec{u}}{Re_*} \quad (2.2)$$

for an isothermal and incompressible Newtonian fluid. Here, \vec{u} and p are the instantaneous velocity vector and pressure and ∇ is the gradient operator. The flow field is determined by the friction Reynolds number $Re_* = hu_*/\nu$ based on the wall distance h , the friction velocity u_* and the kinematic viscosity ν of the fluid. The flow is driven by a constant pressure gradient in the streamwise direction in order to overcome the wall friction. Here, simulations will be performed at three different Reynolds numbers 200, 360 and 790 from which some primary statistics will be compared.

The size of the computational domain is the same as in Refs. [14] and [15], namely a length $6h$ in the streamwise x -direction and a width $3h$ in the spanwise y -direction. Periodic boundary conditions are imposed in the homogeneous x - and y -directions and no-slip and impermeability were enforced at the solid walls at $z = 0$ and $z = h$. A mesh with $192 \times 192 \times 192$ grid points is used for the two lower Reynolds numbers and a finer mesh with $384 \times 384 \times 384$ grid points is used for $Re_* = 790$. The mesh sizes in wall units ν/u_* thus become $\Delta x^+ = 2\Delta y^+ = 6.25$ (11.25) and the grid spacing Δz^+ in the wall-normal direction varies from 0.49 to 1.59 (0.88 – 2.86) for $Re_* = 200$. The values in the parenthesis refer to the intermediate Reynolds number 360. The resolution for the highest Reynolds number is comparable with that for $Re_* = 360$.

The same numerical scheme as that used by Mortensen *et al.* [14] [15] and Gillissen *et al.* [16] is employed in the present study to integrate the Eulerian flow Eq. (2.1)(2.2). This is based on a pseudo-spectral method in which the spatial derivatives in the two homogeneous directions are obtained in spectral space by means of Fourier-series representations. A second-order accurate finite-difference scheme on a staggered grid system is used for the derivatives in the wall-normal directions. The time advancement is carried out with a second-order explicit Adams-Bashforth scheme. Mass conservation is assured by means of a standard projection method and the resulting Poisson equation is transformed to Fourier space in the homogeneous directions.

2.2 Governing equations for the particle motion

The translational motions of the particles are computed from Newton's second law, i.e. in a Lagrangian approach. Only the Stokes drag is considered in present work, while other forces, such as lift and virtual mass forces, are neglected. The particle Reynolds number Re_p should be smaller than unity in order to satisfy the assumption of Stokes flow in the immediate vicinity of a particle. The size of the particles is smaller than smallest eddies in

the flow such that the force on the particle can be treated as a point force. The governing equation of particle motion then becomes:

$$\frac{d\vec{v}}{dt} = \frac{1}{\tau}(\vec{u}(x_p, t) - \vec{v}) \quad (2.3)$$

In Eq. (2.3), v is the translational velocity of the particle and u is the velocity of fluid at the location x_p of the particle. τ is the *particle response time* defined as:

$$\tau = \frac{2Sa^2}{9\nu}, \quad \tau^+ = \tau \frac{u_*^2}{\nu} \quad (2.4)$$

Here, S is the density ratio between particle and fluid, and a is the radius of the particle. τ^+ denotes the particle response time normalized by the viscous time scale ν/u_*^2 . In order to determine the slip velocity which determines the Stokes drag in Eq. (2.3), the fluid velocity $u(x_p, t)$ at the particle position x_p is interpolated from the staggered grid on which the fluid motion is obtained onto the particle position. The interpolation scheme used is quadratic and involves the 27 closest grid points.

The particles are initially distributed randomly throughout the already fully developed turbulent flow field. The particle velocity is initially set equal to the local fluid velocity. The governing equation of particle motion (2.3) is integrated in time with a second-order accurate Adams-Bashforth scheme. The time-step used in this integration is the same as the time-step used for the integration of Navier-Stokes equation (2.2), which is sufficiently smaller than the particle response time.

3 Results

The present approach is based on the assumption that the particle suspension is sufficiently dilute and that the size of the particles is smaller than the Kolmogorov length scale. Based on these assumptions, the simulations are one-way coupled, which means that the particles are affected by the fluid but there is no feedback from the particles onto the flow. The flow field is obtained by means of DNS for the three different frictional Reynolds numbers 200, 360, and 790. The four different particle response times $\tau^+ = 1, 5, 30,$ and 100 (see Table 1) are considered at all the three Reynolds numbers. The same number of particles N_p is used in all the 12 simulations. At the low and intermediate Re_* an almost steady particle concentration distribution is reached during the course of the simulations.

3.1 Choice of sampling period – $Re_* = 200$

The initiation of statistics sampling and the duration T of the sampling period are believed to have a crucial impact on the particle statistics. Due to particle inertia, the majority of the particles tend to distribute inside of the viscous sublayer and the number

Case	τ^+	a^+	S	N_p
A	1	0.36	34.7	10^5
B	5	0.36	173.6	10^5
C	30	0.36	1041.7	10^5
D	100	0.36	3472.2	10^5

Table 1: Particle properties. The same four particle cases are considered for all three Reynolds numbers. The superscript + refers to normalization with viscous units.

of particles in the center part of the channel is accordingly reduced. This phenomenon can affect the quality of the sampled data and different sampling periods may give rise to different statistical results. The time development of number of particles in the region $z^+ < 12$ is shown in Fig. 1 for $Re_* = 200$. This means that we are counting only the particles in the innermost near-wall region, i.e. inside of where the turbulent kinetic energy reaches its peak level. Three different sampling periods are considered, each of length $T^+ = 2820$. During a sampling period 141 samples are taken, equally separated in time. The sampling periods labeled 1, 2, and 3 in Figure 1 are in an early stage of the simulation, at an intermediate state, and at an almost statistically steady state, respectively.

Primary particle velocity statistics for $\tau^+ = 5$ and $\tau^+ = 30$ are shown in Fig. 2 and Fig. 3, respectively. The results obtained during Sampling 2 and Sampling 3 (see Fig. 1) are almost indistinguishable. This observation implies that reliable sampling can be performed although the particle concentration still changes with time. However, if the sampling is done at a too early stage of the simulation, i.e. Sampling 1, the resulting statistics deviate from those obtained later on. This tendency is observed in the near-wall region for the $\tau^+ = 5$ particles in Fig. 2, but the effect is more pronounced for the slower particles in Fig. 3. A longer time is required for the $\tau^+ = 30$ particles to adapt to the local flow conditions in the viscous sub-layer. These findings are consistent with the recommendation made by Zhang *et al.* [17] that sampling should be performed under quasi-equilibrium conditions when the particle mass flux towards the wall has become almost constant. The above results demonstrate that not only the length of the sampling period matters. The start of the sampling is also of major concern to ensure reliable particle statistics.

3.2 Verification of the high-Reynolds-number case – $Re_* = 790$

The vast majority of DNSs of dilute particle suspensions are performed at fairly low Reynolds numbers; see e.g. Marchioli *et al.* [18] where the benchmarking were performed at Reynolds number $Re_* = 300$. In order to investigate the Reynolds number effect on the

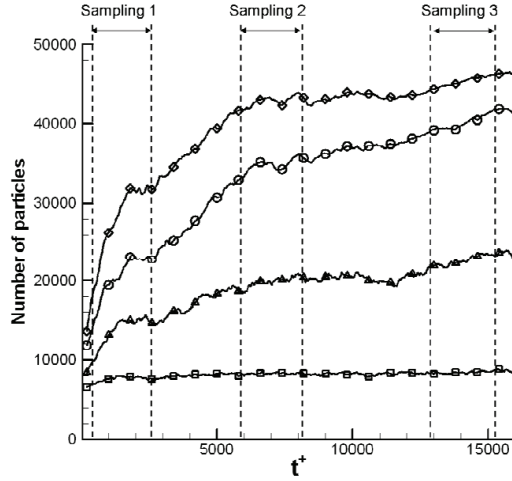


Figure 1: Development of particle concentration in the near-wall region $z^+ < 12$ for $Re_* = 200$. The double arrows show three different sampling periods each of duration 2820 viscous time units. $\tau^+ = 1$, squares; $\tau^+ = 5$, triangles; $\tau^+ = 30$, diamonds; $\tau^+ = 100$, circles.

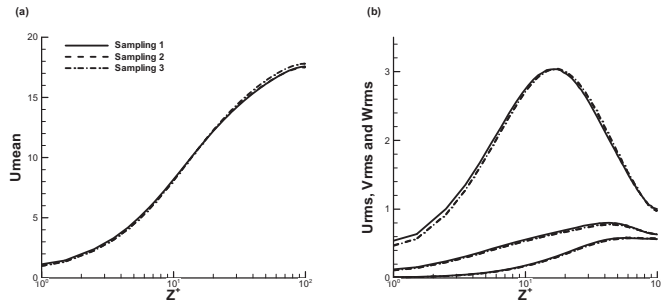


Figure 2: Streamwise mean particle velocity (a) and RMS velocity fluctuations (b) for $\tau^+ = 5$

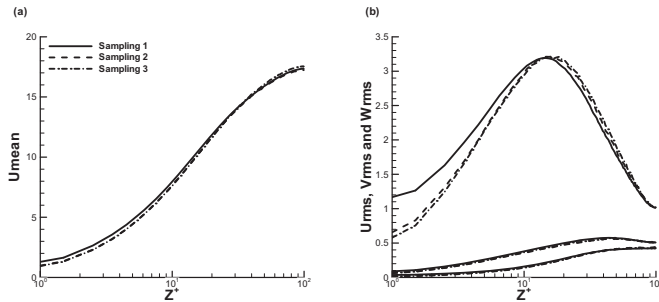


Figure 3: Streamwise mean particle velocity (a) and RMS velocity fluctuations (b) for $\tau^+ = 30$

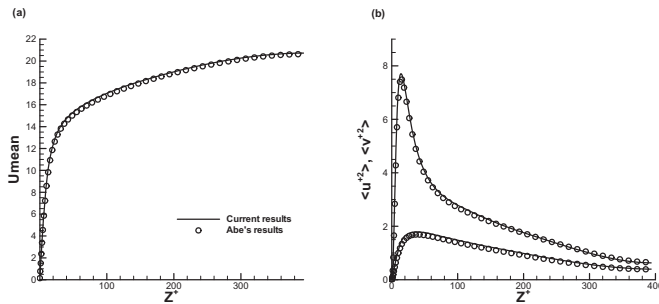


Figure 4: Mean streamwise fluid velocity (a) and velocity fluctuations $\langle u^{+2} \rangle$, $\langle v^{+2} \rangle$ (b). Results from the present simulation at $Re_* = 790$ (lines) are compared with DNS data from Abe *et al.* [19] [20] at the same Reynolds number.

particle dynamics, we also performed simulations at higher Re . In order to verify that the turbulent channel flow field is realistic, the mean fluid velocity and the streamwise and spanwise velocity variances $\langle u^{+2} \rangle$ and $\langle v^{+2} \rangle$ are compared with DNS data from Abe *et al.* [19] at the same Reynolds number. Their data is available at the database [20]. The comparisons in Figure 4 show an almost perfect agreement between the present results and those of Abe *et al.* [19], [20].

3.3 Reynolds number effects

Results for the three different Reynolds numbers considered will now be examined. First of all, let us recall that the variance of the fluid velocity components increases with increasing Reynolds number, in keeping with the earlier findings of Abe *et al.* [19] and others, see e.g. Figure 5 in which results for the fastest particles ($\tau^+ = 1$) are presented. It is noteworthy that the fluid and particle velocities coincide in almost all respects, except when the streamwise velocity fluctuations are considered in Figure 5(b). These fast

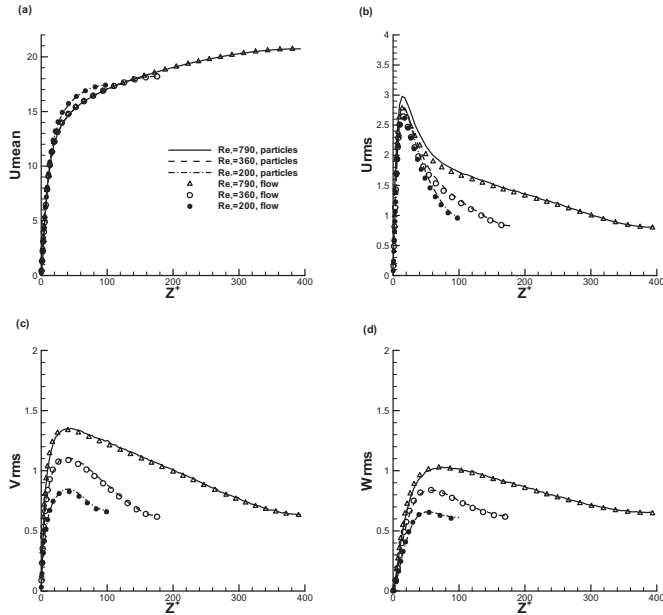


Figure 5: Comparison between fluid and particle mean velocity (a) and velocity fluctuations in the streamwise (b), spanwise (c), and wall-normal (d) directions for $\tau^+=1$. The symbols denote fluid velocities and the lines represent particle velocities. The profiles are terminated at the mid-plane of the channel.

particles behave almost as passive tracer particles. The modest deviation between particle and fluid streamwise velocities is due to preferential concentration of the particles in the near-wall region, see e.g. Eaton & Fessler [1] and Marchioli & Soldati [4]. Near-wall regions with locally low streamwise fluid velocity are left almost empty of particles.

Particle velocity statistics for the slower (or heavier) particles with response times $\tau^+=5, 30$ and 100 are shown in Figures 6 - 8, respectively. Notice that the fluid velocity statistics are the same throughout since the particles do not affect the flow field in the one-way coupled simulations. The mean particle velocity coincides with the mean fluid velocity, except for $\tau^+=30$ particles at $Re_*=200$ in Fig. 7(a) and for the slowest (heaviest) particles in Fig. 8(a). The deviation between mean particle and fluid velocities is most pronounced at the lowest Reynolds number and becomes almost negligible in the high-Re case in Figure 8(a).

The particle velocity fluctuations in the streamwise direction are distinctly different from the fluid velocity fluctuations already for $\tau^+=5$ particles, as shown in Figure 5(b), whereas the spanwise and wall-normal fluctuations in Fig. 5(c, d) are almost the same for the particle and the fluid. However, substantial differences are observed in all three directions for the slower particles. In spite of the large differences between fluid and

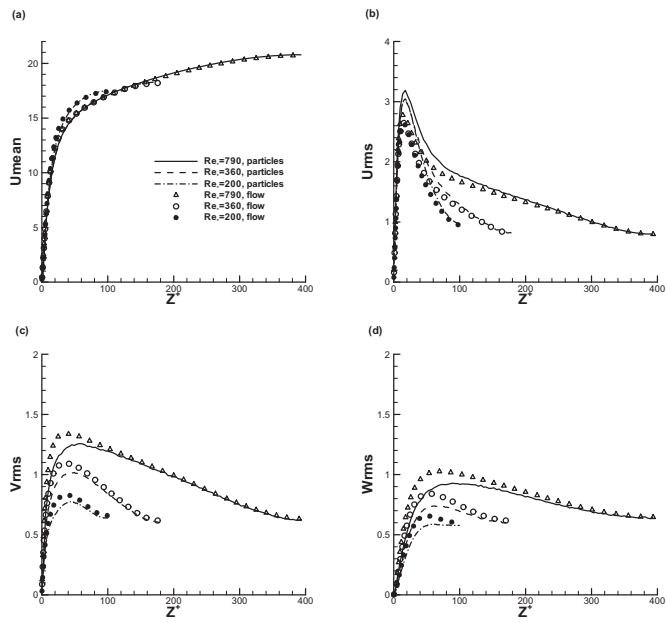


Figure 6: Comparison between fluid and particle mean velocity (a) and velocity fluctuations in the streamwise (b), spanwise (c), and wall-normal (d) directions for $\tau^+ = 5$. The symbols denote fluid velocities and the lines represent particle velocities. The profiles are terminated at the mid-plane of the channel.

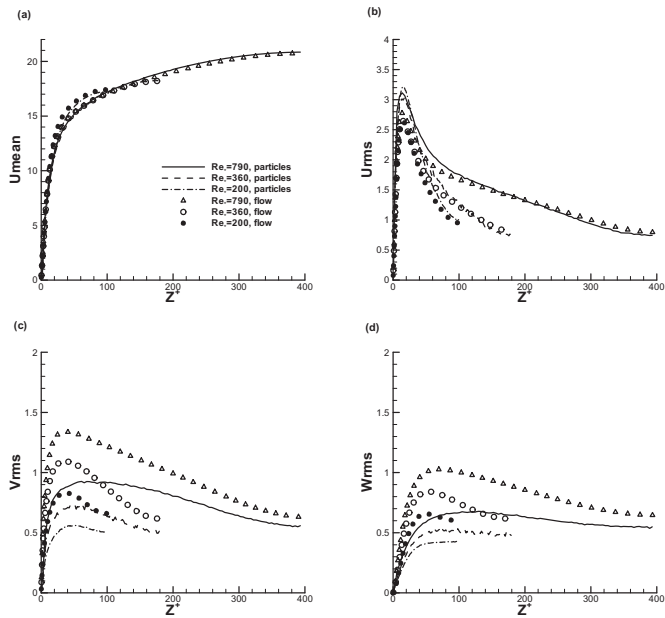


Figure 7: Comparison between fluid and particle mean velocity (a) and velocity fluctuations in the streamwise (b), spanwise (c), and wall-normal (d) directions for $\tau^+ = 30$. The symbols denote fluid velocities and the lines represent particle velocities. The profiles are terminated at the mid-plane of the channel.

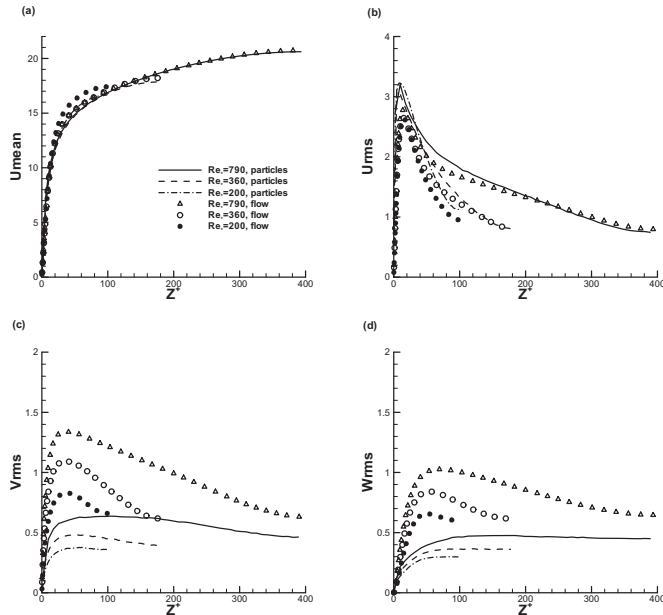


Figure 8: Comparison between fluid and particle mean velocity (a) and velocity fluctuations in the streamwise (b), spanwise (c), and wall-normal (d) directions for $\tau^+ = 100$. The symbols denote fluid velocities and the lines represent particle velocities. The profiles are terminated at the mid-plane of the channel.

particle velocity fluctuations, the latter show the same increasing trend with Re as the fluid velocity fluctuations.

4 Discussion and concluding remarks

The objective of the present investigation has been to compare particle statistics in turbulent channel flow at three different Reynolds numbers and for particles with four different relaxation times ranging from fast ($\tau^+ = 1$) to slow ($\tau^+ = 100$). Since almost all earlier DNS studies on particle dynamics in turbulent shear flows have been carried out at fairly low Reynolds numbers (e.g. at $Re_* = 300$ in [4], [18] and at $Re_* = 360$ in [14], [15]), an examination of Reynolds number effects was considered timely. First, however, we considered some different choices of the sampling period during which statistics were gathered. It was demonstrated that it is not required to postpone the sampling until the particle concentration has reached a steady state. On the contrary, a too early sampling may lead to misleading statistics.

A major observation regarding the particle velocity fluctuations is the pronounced in-

crease at higher Reynolds numbers. This is fully consistent with the well-known Reynolds number effect on the fluid velocity fluctuations, see e.g. Abe *et al.* [19]. This effect is most prominent for the spanwise (v) and wall-normal (w) fluctuations. The streamwise particle velocity fluctuations u , on the other hand, exhibit no distinct Reynolds number effect for the slowest particles in Fig. 8(b). It is also noteworthy that in spite of the increasing trend of v and w with Re , the *shape* of the intensity profiles in Fig. 8 is rather different from those of the fluid intensity profiles. The near-wall peaks of the turbulence intensity distributions are almost absent in the particle intensity profiles. This is probably due to the preferential particle clustering in near-wall areas where the fluid motion is predominantly in the streamwise direction.

It is generally observed that the differences between the particle and fluid velocities increase with increasing response times, i.e. for slower and/or heavier particles. Let us therefore recall that the present simulations were one-way coupled. The deviation between particle and fluid velocities will undoubtedly be altered in a two-way coupled simulation. Intuitively two-way coupling will tend to reduce the deviation between fluid and particle velocities, but the amount of adaption will obviously depend on the particle response time. The present data are nevertheless believed to exhibit the same qualitative features as more realistic two-way coupled simulations.

From the present data, we observed that the particles fluctuated less vigorously than the fluid in the spanwise and wall-normal direction, whereas the streamwise agitation of the particles exceeded the streamwise turbulence intensity (see e.g. Figs 7 and 8). We will therefore conjecture that the presence of the particles in a two-way coupled simulation will tend to enhance the streamwise fluid velocity fluctuations and correspondingly reduce the spanwise and wall-normal fluctuations. This happens to be the signature of drag reduction achieved by polymers, as reviewed recently by Graham [21]. We are therefore inclined to speculate, on the basis of the present results, that drag reduction can be achieved also by means of solid spherical particles. This conjecture was in fact approved while the present manuscript was being reviewed. Two-way coupled simulations with $\tau^+ = 30$ particles at a friction Reynolds number $Re_* = 360$ reported by Zhao *et al.* [13] exhibited the anticipated modulation of the turbulent flow field which resulted in a significant drag reduction.

Acknowledgments

This article is a slightly expanded version of a paper with the same title presented by the first author at "The 8th Asian Computational Fluid Dynamics Conference" in Hong Kong 10th – 14th January 2010. The research work reported herein has been supported by A/S Norske Shell through a research fellowship (contract no. 4610020178/C08156) and by The Research Council of Norway (Programme for Supercomputing) through a grant of computing time.

References

- [1] J. K. Eaton and J. R. Fessler, Preferential concentration of particles by turbulence. *Int. J. Multiphase Flow*, 20 (1994), 169-209.
- [2] S. Pedinotti, G. Mariotti and S. Banerjee, Direct numerical simulation of particle behaviour in the wall region of turbulent flows in horizontal channels. *Int. J. Multiphase Flow*, 18 (1992), 927-941.
- [3] M. Soltani and G. Ahmadi, Direct numerical simulation of particle entrainment in turbulent channel flow. *Phys. Fluids*, 7 (1995), 647-657.
- [4] C. Marchioli and A. Soldati, Mechanisms for particle transfer and segregation in a turbulent boundary layer. *J. Fluid Mech.*, 468 (2002), 283-315.
- [5] C. Narayanan, D. Lakehal, L. Botto and A. Soldati, Mechanisms of particle deposition in a fully developed turbulent open channel flow. *Phys. Fluids*, 15 (2003), 763-775.
- [6] M. Picciotto, C. Marchioli and A. Soldati, Characterization of near-wall accumulation regions for inertial particles in turbulent boundary layers. *Phys. Fluids* 17 (2005), 098101.
- [7] J. D. Kulick, J. R. Fessler and J. K. Eaton, Particle response and turbulence modification in fully developed channel flow. *J. Fluid Mech.*, 227 (1994), 109-134.
- [8] S. Geashchenko, N. Sharp, S. Neuscamman and Z. Warhaft, Lagrangian measurements of inertial particle accelerations in a turbulent boundary layer. *J. Fluid Mech.*, 617 (2008), 255-281.
- [9] E. Elghobashi, On predicting particle-laden turbulent flows. *Appl. Sci. Res.*, 52 (1994), 309C329.
- [10] K. D. Squires and J. K. Eaton, Particle response and turbulence modification in isotropic turbulence. *Phys. Fluids A* 2 (1990), 1191-1203.
- [11] S. Elghobashi and G. C. Truesdell, On the two-way interaction between homogeneous turbulence and dispersed solid particles. I: Turbulence modification. *Phys. Fluids A* 5 (1993), 1790-1801.
- [12] Y. Pan and S. Banerjee, Numerical simulation of particle interactions with wall turbulence. *Phys. Fluids* 8 (1996), 2733-2755.
- [13] L. H. Zhao, H. I. Andersson and J. J. J. Gillissen, Turbulence modulation and drag reduction by spherical particles. *Phys. Fluids* 22 (2010), 081702.
- [14] P. H. Mortensen, H. I. Andersson, J. J. J. Gillissen and B. J. Boersma, Statistics of dilute particle suspensions in wall-bounded turbulence. *Proc. 4th National Conference on Computational Mechanics*, Tapir Academic Press (2007), 259 C 271.
- [15] P. H. Mortensen, H. I. Andersson, J. J. J. Gillissen and B. J. Boersma, Particle spin in a turbulent shear flow. *Phys. Fluids*, 19 (2007), 078109.
- [16] J. J. J. Gillissen, B. J. Boersma, P. H. Mortensen and H. I. Andersson, On the performance of the moment approximation for the numerical computation of fibre stress in turbulent channel flow. *Phys. Fluids*, 19 (2007), 035102.
- [17] H. Zhang, G. Ahmadi, F.-G. Fan and J. B. McLaughlin, Ellipsoidal particles transport and deposition in turbulent channel flows. *Int. J. Multiphase Flow*, 27 (2001), 971-1009.
- [18] C. Marchioli, A. Soldati, J. G. M. Kuerten, B. Arcen, A. Tanire, G. Goldensohn, K.D. Squires, M. F. Cargnelutti and L.M. Portela, Statistics of particle dispersion in direct numerical simulations of wall-bounded turbulence: Results of an international collaborative benchmark test. *Int. J. Multiphase Flow*, 34 (2008), 879-893.
- [19] H. Abe, H. Kawamura, H. Choi, Very large-scale structures and their effects on the wall shear-stress fluctuations in turbulent channel flow up to $Re_\tau = 640$. *J. Fluids Eng.*, 126 (2004),

835 - 843.

[20] Database <http://murasun.me.noda.tus.ac.jp> .

[21] M. D. Graham, Drag reduction in turbulent flow of polymer solutions. *Rheology Reviews* (2004), 143 C 170.

Article 3

Particle slip velocity in wall-bounded turbulence and implications for dispersion models

LIHAO ZHAO, C. MARCHIOLI & H.I. ANDERSSON

Physics of Fluids, accepted for publication, 2012.

Stokes number effects on particle slip velocity in wall-bounded turbulence and implications for dispersion models

L.H. Zhao¹, C. Marchioli², H.I. Andersson¹

¹ *Department of Energy and Process Engineering,
Norwegian University of Science and Technology, 7491 Trondheim, Norway*

² *Department of Energy Technology,
University of Udine, 33100 Udine, Italy*

(Dated: January 20, 2012)

Abstract

The particle slip velocity is adopted as an indicator of the behavior of heavy particles in turbulent channel flow. The statistical moments of the slip velocity are evaluated considering particles with Stokes number, defined as the ratio between the particle response time and the viscous time scale of the flow, in the range $1 < St < 100$. The slip velocity fluctuations exhibit a monotonic increase with increasing particle inertia, whereas the fluid-particle velocity covariance is gradually reduced for $St \geq 5$. Even if this covariance equals the particle turbulence intensity, a substantial amount of particle slip may occur. Relevant to two-fluid modeling of particle-laden flows is the finding that the standard deviation of the slip velocity fluctuations is significantly larger than the corresponding mean slip velocity.

The motion of a tiny solid particle in a turbulent flow is characterized by its Lagrangian velocity vector, \mathbf{u}_p . When the particle velocity differs from that of the surrounding fluid, e.g. due to particle inertia [1] or gravity [2], significant decorrelation of the fluid velocity fluctuations along the particle trajectory occurs and a *particle slip velocity* can be observed. The particle slip velocity vector, defined as $\Delta\mathbf{u} = \mathbf{u}_f - \mathbf{u}_p$ with \mathbf{u}_f the fluid velocity at the particle location (referred to as *fluid velocity seen* hereinafter), is a primary variable in two-fluid modelling of particle-laden flows [3, 4], for which new data might provide useful guidance. Its importance has long been recognized [5] with reference to crossing trajectory effects on the time decorrelation tensor of \mathbf{u}_f , a crucial parameter for the development of Lagrangian stochastic models of particle dispersion, for instance in gas-solid turbulent flows [2], but also for the closure of Eulerian models [6–8]. More recently, accurate characterization of the slip velocity has become a key issue in modelling particle dynamics at the sub-grid scale level in large-eddy simulations [9]. The particle slip velocity is furthermore an outstanding measure of the interactions between the discrete particle phase and the continuous fluid phase being the only flow variable which determines (together with some fluid and particle physical properties) the drag experienced by the particles. The reaction force from the particles on the fluid in two-way coupled simulations is equally dependent on $\Delta\mathbf{u}$, which accordingly is essential for the modulation of the turbulent flow field [10].

In this Letter we examine from a statistical viewpoint the slip velocity of particles with different inertia to explore their dynamics in turbulent channel flows and to provide information for possible inclusion in models. To these aims, statistics are computed considering conditional averaging rather than averaging on discrete Eulerian grid points. We used pseudo-spectral direct numerical simulation [9, 11] of turbulent Poiseuille flow (incompressible and Newtonian) in a channel at $Re_\tau = u_\tau h/\nu = 150$, where $u_\tau = \sqrt{\tau_w/\rho}$ is the friction velocity with τ_w the wall shear stress and ρ the fluid density, ν is the kinematic fluid viscosity and h is the channel half-height. The reference geometry consists of two infinite flat parallel walls with periodic boundary conditions in the streamwise (x) and spanwise (y) directions and no-slip conditions in the wall-normal direction (z). The computational domain has dimensions $(L_x, L_y, L_z) = (4\pi h, 2\pi h, 2h)$,

discretized with 128^3 grid nodes [12]. We tracked swarms – $O(10^5)$ – of particles, treated as pointwise, rigid, elastically-rebounding spheres with Stokes number $St = \tau_p/\tau_f = 1, 5, 30$ and 100 . Here, $\tau_p = \rho_p d_p^2/18\mu$ is the particle characteristic time scale, with ρ_p and d_p the particle density and diameter respectively, and $\tau_f = \nu/u_\tau^2$ is the viscous time scale of the flow. To characterize the collective behavior of particles, we chose a simplified numerical setting (one-way coupling approach) that applies to dilute flow regimes. Our findings are thus valid in the limit of negligible turbulence modulation and particle-particle interactions. One-way coupling also allows to investigate slip velocity statistics by letting different-inertia particles evolve in the same instantaneous flow field.

In many real applications the slip velocity is strongly influenced by gravity which acts to decorrelate the particle velocity from the fluid velocity seen [2, 5]. In this work, gravity is ignored to isolate effects due solely to turbulence, and the Lagrangian equation of particle motion includes only inertia and Schiller-Naumann corrected Stokes drag [13] aimed to allow for finite particle Reynolds numbers. In vector form: $d\mathbf{u}_p/dt = (\Delta u/\tau_p)[1+0.15(|\Delta\mathbf{u}| d_p/\nu)^{0.687}]$. The results shown in this paper are given in wall units (obtained using ν and u_τ , and identified with superscript “+”), and were validated by running simulations with two independent codes [9, 11]. Statistics were collected over a time window $\Delta t^+ = 3900$ starting at time $t^+ = 3000$ after particle injection: within this window slip velocity statistics are at steady state, while particle concentration and transport fluxes are not [12]. In Fig. 1(a), we contrast the wall-normal particle velocity ($\langle w_p \rangle^+$, symbols) against the wall-normal fluid velocity seen ($\langle w_f \rangle^+$, lines) at varying particle inertia. Brackets $\langle \dots \rangle$ denote variables averaged in time and space (over the homogeneous directions x and y). Focusing first on particle velocity, it can be seen that the profiles exhibit the same qualitative behavior but differ quantitatively. All profiles start from zero in the channel center, attain negative values as the wall is approached (indicating that $\langle w_p \rangle^+$ is directed to the wall), develop a maximum in the region $20 < z^+ < 50$, and drop again to zero at the wall. This behavior was observed before for $St < 25$ [14] and is a manifestation of a net particle flux towards the wall. From a quantitative viewpoint, inertia induces strong changes

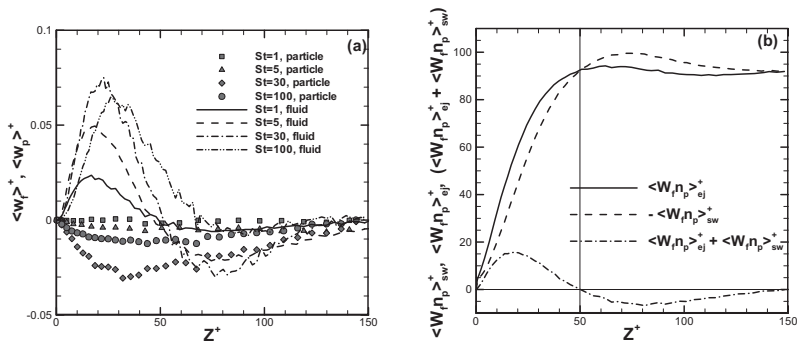


FIG. 1: (a) Mean values of the wall-normal component of the fluid velocity seen, $\langle w_f \rangle^+$, and of the particle velocity, $\langle w_p \rangle^+$. (b) Density-weighted fluid velocities seen by particles entrained in ejections or sweeps for $St=5$.

in the magnitude of $\langle w_p \rangle^+$: in the region where $\langle w_p \rangle^+$ develops a maximum, a decrease of more than one order of magnitude is observed for the $St = 1$ and $St = 5$ particles compared to the $St = 30$ particles. A decrease of $\langle w_p \rangle^+$ is found also for the $St = 100$ particles, confirming that that wall accumulation increases with inertia up to an *optimum* value of the Stokes number ($St = 30$ in this study), while decreasing on either side of the optimum.

This non-monotonic Stokes number dependence is observed also for the fluid velocity seen. Another interesting feature, relevant for the present analysis, is that $\langle w_f \rangle^+$ undergoes a sign change while approaching the wall and becomes positive in the region where $\langle w_p \rangle^+$ reaches large negative values. A straightforward interpretation of this result would lead to conclude that particles move toward the wall within regions of the flow where the fluid moves away from wall. This conclusion is however incorrect, as the phenomenology of near-wall turbulence is ignored. Regions characterized by off-the-wall fluid velocity represent coherent ejections of low momentum fluid away from the wall, which co-exist with coherent sweeps of high-momentum fluid to the wall. Sweeps and ejections are known to govern particle transfer flux to/off the wall [1], and it is precisely their capability to entrain particles and modulate the flow field seen that generates the counter-intuitive behavior of $\langle w_f \rangle^+$. This is demonstrated, only for the $St = 5$ particles to simplify discussion, in Fig.

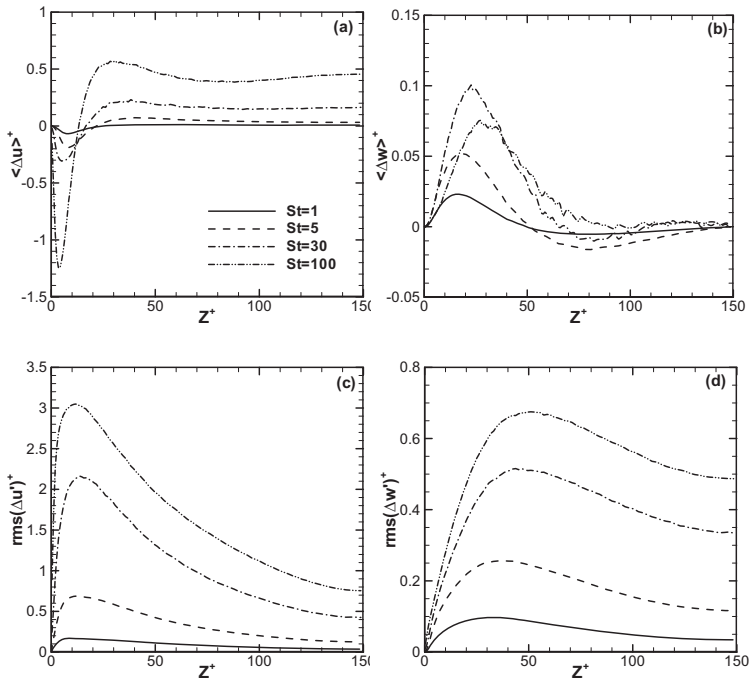


FIG. 2: Stokes number effects on mean and rms slip velocity statistics: (a-b) mean streamwise and wall-normal slip velocity, $\langle \Delta u \rangle^+$ and $\langle \Delta w \rangle^+$; (c-d) rms of streamwise and wall-normal slip velocity fluctuations, $\langle \text{rms}(\Delta u') \rangle^+$ and $\langle \text{rms}(\Delta w') \rangle^+$.

1(b) where we plot the density-weighted fluid velocity seen by particles entrained either in ejections, $\langle w_f \cdot n_p \rangle_{ej}^+$ with $w_f > 0$, or in sweeps, $\langle w_f \cdot n_p \rangle_{sw}^+$ with $w_f < 0$. The quantity n_p denotes particle number density. We also plot the sum $\langle w_f \cdot n_p \rangle_{ej}^+ + \langle w_f \cdot n_p \rangle_{sw}^+$, which is almost proportional to the dashed $\langle w_f \rangle^+$ profile shown in Fig. 1(a). Near the wall ($z^+ < 50$ in our simulations), $\langle w_f \cdot n_p \rangle_{ej}^+ > \langle w_f \cdot n_p \rangle_{sw}^+$ and therefore $\langle w_f \rangle^+ > 0$ even if $\langle w_p \rangle^+ < 0$. The opposite reasoning applies away from the wall. From a physical viewpoint, this behavior can be explained interpreting particle preferential sampling of $\langle w_f \rangle^+ > 0$ regions as a sort of continuity effect of the fluid velocity field for which sweeps are more intense and spatially concentrated than ejections [14]. In addition, sweeps dominate Reynolds stress production very near the wall whereas ejections dominate farther from it [1]: hence, the ejection-dominated region covers a much wider proportion of the $z^+ < 50$ fluid slab.

The deviations between $\langle w_p \rangle^+$ and $\langle w_f \rangle^+$ observed in Fig. 1 indicate that the slip velocity is largely dependent on the wall distance, z^+ . Let us now decompose the slip velocity vector into a mean and a fluctuating part:

$$\langle \Delta \mathbf{u} \rangle = \langle \mathbf{u}_f \rangle - \langle \mathbf{u}_p \rangle, \quad \Delta \mathbf{u}' = \mathbf{u}'_f - \mathbf{u}'_p. \quad (1)$$

The streamwise and wall-normal mean slip velocity components, $\langle \Delta u \rangle^+$ and $\langle \Delta w \rangle^+$, are shown in Figs. 2(a-b) together with the corresponding standard deviations (root-mean-square values), $rms(\Delta u')^+$ and $rms(\Delta w')^+$, shown in Figs. 2(c-d). First, we notice that the streamwise mean slip velocity $\langle \Delta u \rangle^+$ shows the same characteristic variation regardless of the Stokes number: negative values near the wall ($z^+ < 20$), indicating that the particles lead the fluid, positive values throughout the central region, where the particles lag behind the fluid. This behavior is known from mean velocity profiles [14]. The sign change of $\langle \Delta u \rangle^+$ implies that the direction of the mean drag force changes with the distance from the wall. Interestingly, this change occurs at $z^+ \simeq 18$ irrespective of the Stokes number. Second, we observe that the magnitude of the mean slip velocities increases monotonically with St : in the core region of the channel, this increase indicates that the ability of particles to adapt to the fluid motion is gradually reduced with increasing inertia; closer to the wall, it corresponds to an increased capability of maintaining streamwise momentum while drifting to the wall due to turbophoresis. This explains why $\langle u_p \rangle$ exceeds $\langle u_f \rangle$ near the wall. Arcen *et al.* [15] found a similar variation of the streamwise drag force per unit mass, but also observed a drag decrease with increasing particle inertia in the range $1.2 < St < 27.1$. This reduction stems from the increasing St since the drag force to a first approximation is proportional to $\Delta u / St$.

The wall-normal component of the mean slip velocity, shown in Fig. 2(b), is largest for the $St=30$ particles as follows from discussion of Fig. 1, and attains positive values for $z^+ < 50$ regardless of the Stokes number. This implies that the mean drag force counteracts particle drift to the wall within the buffer layer. In the core region, particles with low inertia are driven to the wall by a negative mean drag force, whereas large-inertia particles ($St \geq 30$) still experience a weak positive drag force. Figs. 2(c-d) show that the

streamwise and wall-normal slip velocity fluctuations increase monotonically with St . Profiles of $rms(\Delta v')^+$ (not shown) exhibit the same trend, suggesting that the slip velocity fluctuations are weakly influenced by the inertial bias that shows in the behavior of $\langle \Delta w \rangle^+$. It is noteworthy that the largest values of $rms(\Delta u')^+$ occur close to the wall, with peaks located in the buffer layer for both the heavier $St = 100$ particles ($z^+ \simeq 11$) and the lighter $St = 1$ particles ($z^+ \simeq 9$). The opposite behavior is observed for $rms(\Delta w')^+$, whose maximum values shift away from the wall at increasing particle inertia: the peak is located well outside the buffer layer (at $z^+ \approx 45$) for $St=100$. The most relevant result provided by Fig. 2, however, is the magnitude of the rms values over the channel cross-section. Regardless of the coordinate direction, the standard deviation typically exceeds the corresponding mean value by roughly 3 to 5 times, revealing that the instantaneous slip velocity and, in turn, the drag force may frequently change sign.

A more complete understanding of the statistical characterization of $rms(\Delta \mathbf{u}')$ can be achieved if the fluctuating slip velocity components are normalized either by the fluid velocity fluctuations along the particle trajectories, as in Figs. 3(a-b), or by the particle velocity fluctuations, as in Figs. 3(c-d). All profiles in Fig. 3 increase monotonically with the Stokes number. Profiles in Fig. 3(a-b) are nearly flat outside of the buffer layer, i.e. beyond $z^+ \approx 30$. In this region, the rms ratio is rather low for the $St = 1$ particles since these light particles closely follow the local fluid motion and therefore exhibit small standard deviations compared to the fluid; the heavier $St = 100$ particles tend to move independently of the fluid and one may conjecture that $rms(\Delta \mathbf{u}') \approx rms(\mathbf{u}'_p)$ in the limit $St \rightarrow \infty$. Inside the viscous sub-layer, however, the rms ratios attain values significantly above unity. The fluid velocity fluctuations are substantially damped in the immediate vicinity of the solid wall, whereas the inertial particles are able to maintain the momentum acquired farther from it during their interaction with the turbulent coherent structures. This behavior has been observed also in a spatially-developing turbulent boundary layer [16] where the globally-averaged rms ratios may exceed unity and, consistently with our findings, increase with St . Rms ratios close to unity are observed at the wall in Figs. 3(c-d) except for the lighter particles.

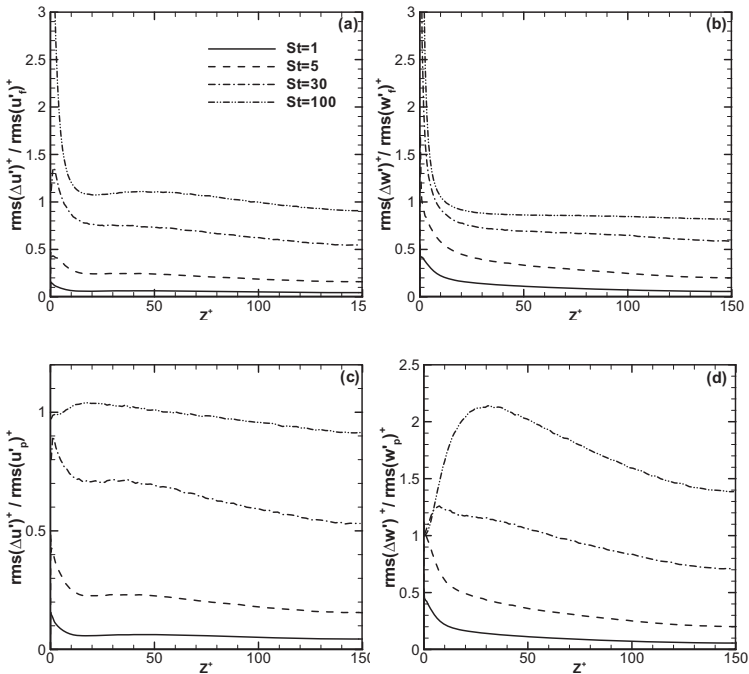


FIG. 3: Stokes number effects on the rms of slip velocity fluctuations normalized either by the rms of the fluid velocity fluctuations along the particle trajectory (a-b) or by the rms of the particle velocity fluctuations (c-d)

Thus, for particles with $St \geq 30$ the slip velocity fluctuations $rms(\Delta \mathbf{u}')$ in the vicinity of the wall stem from the particle velocity fluctuations $rms(\mathbf{u}'_p)$ since the fluid velocity fluctuations $rms(\mathbf{u}'_f)$ are suppressed by the no-slip and impermeability conditions imposed at the wall. The variation of the rms ratios in the core region of the channel resembles the trends observed in Figs. 3(a-b).

We conclude our discussion by considering the fluid-particle velocity *covariance*, an important quantity in Lagrangian[3] and Eulerian models[6, 8], e.g. to compute integral time scales. For the present analysis, the streamwise and wall-normal components, $\langle u'_f u'_p \rangle$ and $\langle w'_f w'_p \rangle$ respectively, are the most interesting. In agreement with previous observations [15, 17], Fig. 4 shows that $\langle u'_f u'_p \rangle$ exceeds $\langle w'_f w'_p \rangle$ and that both components are substantially reduced as St increases. The only exception from this general trend is the modest, yet significant increase of $\langle u'_f u'_p \rangle$ for the $St = 5$ particles as compared with the

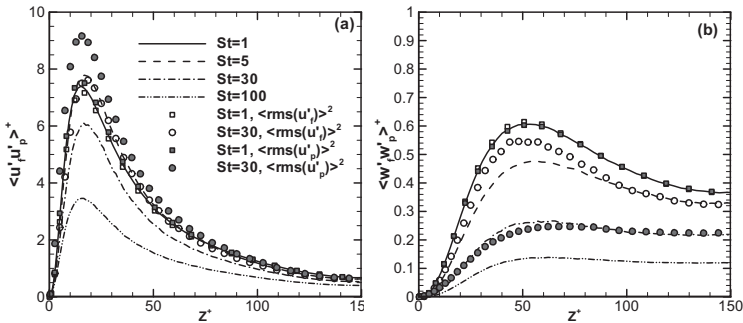


FIG. 4: Stokes number effects on the fluid-particle velocity covariance. Panels: (a) streamwise covariance, $\langle u'_f u'_p \rangle$; (b) wall-normal covariance, $\langle w'_f w'_p \rangle$. Fluid and particle fluctuations ($St = 1$ and 30 only) are also shown for comparison purposes (open symbols: $\langle rms(u'_f) \rangle^2$; filled symbols: $\langle rms(u'_p) \rangle^2$).

$St = 1$ particles. This increase was not observed by Arcen et al. [15, 18], who however adopted slightly different values of Re_τ and St and no drag force correction, nor by Vance et al. [17], who focused on relatively heavy particles ($30 \leq St \leq 470$).

The streamwise covariance is related to the streamwise slip velocity fluctuations through the equality:

$$\langle \Delta u'^2 \rangle = \langle u'^2_f \rangle - 2\langle u'_f u'_p \rangle + \langle u'^2_p \rangle. \quad (2)$$

Analogous equalities apply in the other coordinate directions. Since both fluid and particle intensities in the streamwise direction are modestly affected by the particle Stokes number, the reduction of $\langle u'_f u'_p \rangle$ observed in Fig. 4(a) is directly linked to the increase of $\langle \Delta u'^2 \rangle$ in Fig. 2(c). For the lower Stokes numbers, $\langle u'_f u'_p \rangle \approx \langle u'^2_p \rangle$ and can therefore infer from Eq. (2) that: $\langle \Delta u'^2 \rangle = \langle u'^2_f \rangle - \langle u'^2_p \rangle$. However, it can by no means be concluded that the slip velocity fluctuations vanish and that the particles exactly follow the local fluid motion, i.e. that $\langle u'^2_p \rangle \approx \langle u'^2_f \rangle$. For $St = 1$, Fig. 4(a) shows that the results are fairly close to this limit and Fig. 4(b) shows that $\langle w'_f w'_p \rangle \approx \langle w'^2_p \rangle \approx \langle w'^2_f \rangle$, which is consistent with the almost negligible slip fluctuations $\langle \Delta w'^2 \rangle$ in Fig. 2(d). For the heavier $St = 30$ particles $\langle w'_f w'_p \rangle \approx \langle w'^2_p \rangle \ll \langle w'^2_f \rangle$, hence the condition $\langle w'_f w'_p \rangle \approx \langle w'^2_p \rangle$ which applies to low- or intermediate- St particles

is not sufficient to warrant that particles passively follow the fluid, as argued by [17]. This conclusion is in accordance with the Cauchy-Schwartz inequality: $\langle w'_f w'_p \rangle^2 \leq \langle w'^2_f \rangle \langle w'^2_p \rangle$ from which one only can deduce that $\langle w'_f w'_p \rangle^2 \leq \langle w'^2_f \rangle^2$ in such cases, e.g. that of Fig. 4(b). In the limit of $St \rightarrow \infty$, particle motion is not at all influenced by the flow field and u'_p is completely suppressed. Eq. (2) accordingly simplifies to $\langle \Delta u'^2 \rangle = \langle u'^2_f \rangle$. Inspections of the data presented in Figs. 3 and 4 demonstrate that even the results for the heaviest $St = 100$ particles are far apart from this limit, although these particles experience a substantial velocity slip.

In this Letter we have demonstrated that the particle slip velocity is a useful measure of particle-turbulence interactions in wall-bounded flows and that its statistical characterization may provide new information about the physics and useful indications for modeling turbulent particle dispersion. To summarize, our results show that the slip velocity fluctuations $\Delta \mathbf{u}'$ are significantly larger than the corresponding mean slip velocity $\langle \Delta \mathbf{u} \rangle$, with the consequence that a given directional component of the instantaneous slip velocity vector $\Delta \mathbf{u}$ may frequently attain the sign opposite to that of $\langle \Delta \mathbf{u} \rangle$. The statistical behavior of the slip velocity is thus expected to depend strongly on the distribution of the turbulent velocity fluctuations, which is highly anisotropic in wall-bounded flows. We have also pointed out that the condition of particle-fluid covariance equals to the particle turbulence intensity in a given direction is not sufficient to ensure that particles passively follow the fluid motion.

Computing time was granted by CINECA Supercomputing Center (Bologna, Italy), which also provided data storage (<http://cfd.cineca.it>), and by the Research Council of Norway (Programme for Supercomputing). COST Actions MP0806 and FP1005 are gratefully acknowledged. C.M. also thanks Prof. A. Soldati for providing part of the raw data that were used in this study.

-
- [1] C. Marchioli, and A. Soldati, “Mechanisms for particle transfer and segregation in turbulent boundary layer,” *J. Fluid Mech.*, **468**, 283 (2002).
- [2] B. Oesterlé “On heavy particle dispersion in turbulent shear flows: 3-D analy-

- sis of the effects of crossing trajectories” *Boundary-Layer Meteorol.*, **130**, 71 (2009).
- [3] B. Arcen, and A. Tanière, “Simulation of a particle-laden turbulent channel flow using an improved stochastic Lagrangian model,” *Phys. Fluids*, **21**, 043303 (2009).
- [4] X. Pialat, O. Simonin, and P. Villedieu, “A hybrid Eulerian-Lagrangian method to simulate the dispersed phase in turbulent gas-particle flows”, *Int. J. Multiphase Flow*, **33**, 766 (2007).
- [5] G.T. Csanady, “Turbulent diffusion of heavy particles in the atmosphere”, *J. Atmos. Sci.*, **20**, 201 (1963).
- [6] O. Simonin, E. Deutsch, and J.P. Minier, “Eulerian prediction of fluid-particle correlated motion in turbulent two-phase flows”, *Appl. Sci. Res.*, **51**, 275 (1993).
- [7] S. Cerbelli, A. Giusti, and A. Soldati, “ADE approach to predicting dispersion of heavy particles in wall-bounded turbulence”, *Int. J. Multiphase Flow*, **27**, 1861 (2001).
- [8] M.W. Reeks, “On model equations for particle dispersion in inhomogeneous turbulence”, *Int. J. Multiphase Flow*, **31**, 93 (2005).
- [9] A. Soldati, and C. Marchioli, “Physics and modelling of turbulent particle deposition and entrainment: Review of a systematic study,” *Int. J. Multiphase Flow.*, **35**, 827 (2009).
- [10] L.H. Zhao, H.I. Andersson, and J.J.J. Gillissen, “Turbulence modulation and drag reduction by spherical particles,” *Phys. Fluids*, **22**, 081702 (2010).
- [11] J.J.J. Gillissen, B.J. Boersma, P.H. Mortensen, and H.I. Andersson, “On the performance of the moment approximation for the numerical computation of fibre stress in turbulent channel flow,” *Phys. Fluids* **19**, 035102 (2007).
- [12] C. Marchioli, A. Soldati, J.G.M. Kuerten, B. Arcen, A. Tanière, G. Goldensohn, K.D. Squires, M. F. Cargnelutti, and L.M. Portela, “Statistics of particle dispersion in Direct Numerical Simulations of wall-bounded turbulence: results of an international collaborative benchmark test,” *Int. J. Multiphase Flow*, **34**, 879 (2008).
- [13] L. Schiller, and A.Z. Naumann, “Über die grundlegenden Berechnungen bei der

- Schwerkraftaufbereitung,” *Z. Ver. Dtsch. Ing.* , **77**, 318 (1933).
- [14] M. Picciotto, C. Marchioli, M. Reeks, and A. Soldati, “Statistics of velocity and preferential accumulation of micro-particles in boundary layer turbulence,” *Nucl. Eng. Des.*, **235**, 1239 (2005).
- [15] B. Arcen, A. Tanière, and B. Oesterlé, “On the influence of near-wall forces in particle-laden channel flows,” *Int. J. Multiphase Flow*, **32**, 1326 (2006).
- [16] A. Dorgan, and E. Loth, “Simulation of particles released near the wall in a turbulent boundary layer,” *Int. J. Multiphase Flow*, **30**, 649 (2004).
- [17] M.W. Vance, K.D. Squires, and O. Simonin, “Properties of the particle velocity field in gas-solid turbulent channel flow,” *Phys. Fluids*, **18**, 063302 (2006).
- [18] B. Arcen, A. Tanière, and L. I. Zaichik, “Assessment of a statistical model for the transport of discrete particles in a turbulent channel flow,” *Int. J. Multiphase Flow*, **34**, 419 (2008).

Part 2.2

Two-way coupled simulations of spherical particle suspensions

Article 4

Turbulence modulation and drag reduction by spherical particles

LIHAO ZHAO, H.I. ANDERSSON & J.J.J. GILLISSEN

Physics of Fluids, **22**, 081702, 2010.

Turbulence modulation and drag reduction by spherical particles

L. H. Zhao,¹ H. I. Andersson,¹ and J. J. J. Gillissen²

¹*Department of Energy and Process Engineering, Norwegian University of Science and Technology, 7491 Trondheim, Norway*

²*Department of Multi-Scale Physics, TU Delft, 2628 BW Delft, The Netherlands*

(Received 13 May 2010; accepted 21 July 2010; published online 16 August 2010)

This letter reports on the pronounced turbulence modulations and the accompanying drag reduction observed in a two-way coupled simulation of particle-laden channel flow. The present results support the view that drag reduction can be achieved not only by means of polymeric or fiber additives but also with spherical particles. © 2010 American Institute of Physics.

[doi:10.1063/1.3478308]

The inevitable pressure loss associated with transport of fluids in pipelines determines the pumping requirements. The pressure loss arises in order to overcome the skin-friction drag. Several investigations of turbulent drag reduction have thus been motivated by the economical benefits of pressure-loss reduction. Drag reduction can be achieved in many different ways, for instance, by means of additives suspended into an otherwise Newtonian fluid (see, e.g., the reviews by Lumley¹ and Gyr and Bewersdorff²). A notable example is the substantial drag reduction observed when flexible polymers are dissolved in the carrier fluid as reported in Refs. 3 and 4 (see also the recent reviews^{5,6}). However, the findings with respect to drag reduction are not as clear-cut for additives other than polymers and chemicals. Pressure drop measurements reported from a variety of solid-fluid systems were scrutinized by Radin *et al.*⁷ While drag reduction was obtained with fibrous additives (e.g., nylon or cotton), no drag reduction was reported for nonfibrous additives irrespective of the shape of the solid (spherical, platelet, or needle-shaped). More recently, drag reduction has been reported from computer experiments by Paschkewitz *et al.*⁸ and Gillissen *et al.*⁹ also for rigid fibers.

Suspensions of *spherical* particles in turbulent pipe and channel flows have been extensively studied during the years with the view to better understand the particle transport, dispersion, and segregation in wall-turbulence and also the influence of the presence of the solid spheres on the turbulence of the carrier fluid. The current understanding of the complex behavior of inertial spherical particles in turbulent wall flows was summarized in a keynote lecture by Soldati.¹⁰ The survey of experimental studies and two-way coupled computer simulations by Balachandar and Eaton¹¹ furthermore addressed the turbulence modulation observed in the presence of inertial particles. In dilute suspensions where particle collisions are of negligible importance, the fluid turbulence may be affected by an enhanced dissipation due to the particles, kinetic energy transfer between the fluid and the particles, and wakes formed in the lee of the solid particles. The relative importance of these mechanisms depends on the particle Reynolds number, the particle-to-fluid density ratio, and the particle-to-turbulence length-scale ratio. By adopting the turbulence intensity as a measure of the turbulence activity,

Gore and Crowe¹² showed that a particle diameter of 1/10 the size of the most energetic eddies represents a demarcation between increase and decrease of the carrier-phase turbulence such that smaller particles tended to attenuate the turbulence.

In this letter, turbulence attenuation in a dilute suspension of spherical particles is further explored. A reduced turbulence activity in the presence of tiny spheres has been observed in several laboratory experiments^{13,14} and computer simulations.^{15–17} In most cases, the attenuation of the turbulence is associated with a substantial reduction of the velocity fluctuations perpendicular to the mean flow, whereas the streamwise turbulence intensity might be enhanced. These alterations of the fluctuating velocity field reflect a higher degree of asymmetry. The same trends have been reported in conjunction with drag reduction, for instance, in dilute polymer solutions.^{3,4} Evidence of drag reduction achieved by means of spherical particles is, however, almost nonexistent. Rashidi *et al.*¹⁸ showed that the presence of small particles reduced the number of wall ejections, turbulence intensity, and also the skin friction. A modest pressure-loss reduction was also reported for the smallest particle case considered in the pipe-flow experiments by Kartushinsky *et al.*¹⁹ More recent pressure-drop measurements by Bari and Yunus²⁰ showed substantial drag reduction for suspensions of either alumina or sand particles in kerosene over a fairly wide range of turbulent Reynolds numbers. Drag reduction was also found in the computer experiments by Li *et al.*,¹⁶ but their mesh was too coarse to assure accurate results. The more reliable simulations by Dritselis and Vlachos²¹ suggested a modest drag reduction, although not commented by the authors. For a given bulk velocity, the wall-friction was reduced by 4% in the particle-laden flow. On the basis of the above observations, it may be conjectured that significant drag reduction can be achieved also by means of small spherical particles, provided that the particle size, density, and loading are properly selected.

We consider the fully developed turbulent flow in a plane channel. The motion of the incompressible Newtonian fluid is governed by the continuity and momentum conservation equations

$$\nabla \cdot \vec{u} = 0, \quad \rho \left[\frac{\partial \vec{u}}{\partial t} + (\vec{u} \cdot \nabla) \vec{u} \right] = -\nabla p + \mu \nabla^2 \vec{u} + \vec{F}_p. \quad (1)$$

Here, \vec{u} and p are the instantaneous fluid velocity vector and pressure, respectively, whereas \vec{F}_p denotes the force per unit volume from the particles. ρ and μ are the density and the dynamic viscosity of the Newtonian carrier fluid.

The translational motion of individual spherical particles is governed by Newton's second law. Only the Stokes drag is considered in present work, while other forces, such as lift and virtual-mass forces, are neglected. The particle Reynolds number $\text{Re}_p = 2a|\vec{u} - \vec{v}|/\mu$, based on the particle diameter $2a$ and the slip velocity between the fluid and particle, should be smaller than unity to satisfy the assumption of Stokes flow in the particle vicinity. The size of the particles is smaller than smallest eddies in the flow such that the force $\vec{f}_i(\vec{x}_p)$ on particle number i can be treated as a point force

$$\vec{f}_i(\vec{x}_p) = 6\pi\mu a[\vec{u}(\vec{x}_p, t) - \vec{v}]. \quad (2)$$

Here, \vec{v} is the translational velocity of the particle and \vec{u} is the fluid velocity evaluated at the particle location \vec{x}_p . The motion of a particle and its trajectory are obtained from

$$\frac{d\vec{v}}{dt} = \frac{1}{\tau}[\vec{u}(\vec{x}_p, t) - \vec{v}], \quad \frac{d\vec{x}_p}{dt} = \vec{v}. \quad (3)$$

The particle response time τ can be expressed as

$$\tau = \frac{2\rho D a^2}{9\mu}, \quad (4)$$

under the Stokes flow approximation where $D = \rho_p/\rho$ is the ratio between the particle and fluid densities. The particles collide elastically with the walls. If a particle hits a wall, it bounces back into the flow with the only change that the wall-normal velocity component switches sign.

The Lagrangian particle equations (3) are integrated forward in time along with the Eulerian equation (1) for the fluid motion in a two-way coupled simulation. Each and every particle acts back onto the fluid with a point force $-\vec{f}_i(\vec{x}_p)$, in accordance with Newton's third law. The feedback from the n_p particles within a given grid cell volume V_{cell} adds up

$$\vec{F}_p = -\frac{1}{V_{\text{cell}}} \sum_{i=1}^{n_p} \vec{f}_i(\vec{x}_p). \quad (5)$$

This is the force per unit volume in the particle-laden Navier–Stokes equation (1). This point-force approach to two-way coupled simulations is essentially the same as that introduced by Squires and Eaton²² for isotropic turbulence and subsequently adopted for wall-bounded turbulence.^{16,21,23}

The governing equations for the fluid and particle motions can be normalized by the skin-friction velocity u_* and the channel height h . This gives the following set of partial and ordinary differential equations:

$$\nabla \cdot \vec{u} = 0, \quad \frac{\partial \vec{u}}{\partial t} + (\vec{u} \cdot \nabla) \vec{u} = +2\bar{\epsilon}_x - \nabla p + \text{Re}^{-1} \nabla^2 \vec{u} + \vec{F}_p, \quad (6)$$

$$\frac{d\vec{v}}{dt} = \frac{1}{\bar{\tau}}[\vec{u}(\vec{x}_p, t) - \vec{v}], \quad \frac{d\vec{x}_p}{dt} = \vec{v}. \quad (7)$$

All dependent and independent variables are now dimensionless quantities, although we stick to the same notation as for the dimensional variables. The first term to the right of Eq. (6) is the imposed mean pressure gradient, which drives the flow in the positive x -direction. The normalized particle relaxation time $\bar{\tau}$ in Eq. (7) is

$$\bar{\tau} = \frac{\tau}{h/u_*} = \frac{2}{9} D (\bar{a})^2 \text{Re}, \quad (8)$$

where $\bar{a} = a/h$ and $\text{Re} = \rho u_* h / \mu$ is the wall-friction Reynolds number. The particles in a given grid cell act on the fluid flow by means of the force

$$\vec{F}_p = -6\pi \text{Re}^{-1} \bar{a} \frac{1}{V_{\text{cell}}} \sum_{i=1}^{n_p} [\vec{u}(\vec{x}_p, t) - \vec{v}]. \quad (9)$$

Here, V_{cell} is the dimensionless volume of the grid cell.

In *one-way coupled* simulations, the influence of the particles on the flow field through \vec{F}_p is either ignored or negligibly small and the flow field is determined only by the friction Reynolds number, Re . The particle dynamics are fully determined when also $\bar{\tau}$ is given. Thus, for a given Re , a short particle relaxation time, i.e., a fast particle response, corresponds to either light or small particles (low values of either D or \bar{a}) according to Eq. (8). In *two-way coupled* simulations, on the other hand, the feedback from the particles on the fluid motion is given by Eq. (9), which shows that the magnitude of the feedback is determined by the particle size \bar{a} but is independent of the relative particle density D . Thus, \bar{a} and D play different roles in two-way coupled simulations and cannot be combined into a single parameter $D(\bar{a})^2$ as in one-way coupled simulations.

The turbulent channel flow was driven by the prescribed pressure gradient corresponding to a friction Reynolds number $\text{Re} = 360$. The sizes of the computational domain were $6h$ and $3h$ in the streamwise x -direction and the spanwise y -direction, respectively. Periodic boundary conditions were imposed in these homogeneous directions and no-slip and impermeability were enforced at the solid walls at $z=0$ and $z=h$. The computational mesh consisted of 128^3 grid points. The direct numerical simulations (DNSs) were performed with the same Navier–Stokes solver as used by Gillissen *et al.*²⁴ and Mortensen *et al.*²⁵ After the turbulent flow field first had evolved into a statistically steady state, 4×10^6 spherical particles were randomly released into the flow field. The particle radius \bar{a} was 0.001 and the density ratio $D = 1042$. This corresponds to $a^+ = 0.36$ and $\tau^+ = 30$ in terms of the viscous scales ν/u_* and ν/u_*^2 for length and time, respectively. The particle characteristics were thus the same as those in the one-way coupled simulations (case C) by Mortensen *et al.*²⁵

The particle-laden channel flow was assumed to be sufficiently dilute so that particle-particle collisions were of negligible importance, i.e., the flow was in the two-way coupling regime according to the updated classification map due

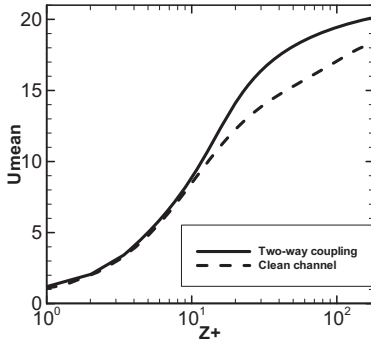


FIG. 1. Mean fluid velocity profile $U^*(z^+)$ for the particle-laden channel flow (solid line) and for the unladen flow (broken line).

to Elghobashi.²⁶ For a given grid cell, the force \vec{F}_p from the particles on the fluid is a sum of point forces according to Eq. (9). In practice, a point force, which originated from the hydrodynamic force (2) on an individual particle at \vec{x}_p , was considered as a body force $-\vec{f}_i(\vec{x}_p)/V_{\text{cell}}$ that acted in the cell center. In accordance with the quasistaggered grid system, however, the wall-normal force component was assigned to the nearest wall-parallel cell face rather than to the cell center. No smoothing of the forces from the particles onto the fluid was required.

The same time step $\Delta t = 0.0001h/u_*$ as in the DNS was used for the integration of the particle equations of motion (7). This time step corresponds to $\Delta t^+ = 0.036$ measured in viscous time units. The particles were released into an already statistically steady unladen channel flow. The simulation of the particle-laden flow was first run for $20h/u_*$ ($7200\nu/u_*^2$). During this time span, the particles accumulated in the near-wall region. The bulk flow was monitored and seemed to reach an almost steady state during this period of time. The simulation was thereafter continued for another $5h/u_*$, during which fluid and particle statistics were gathered.

The results of the two-way coupled simulation will be compared with results from a clean or unladen channel simulation, i.e., with $\vec{F}_p = 0$ in the particle-laden Navier–Stokes equation (1). The same computational domain and the same grid were used in both simulations and the wall-friction Reynolds number was the same, i.e., $\text{Re} = 360$. The mean fluid velocity in Fig. 1 is substantially increased compared with that in the clean channel. Since Re and thus u_* are the same in both cases, the enhanced mean velocity is equivalent with drag reduction. Here, the bulk flow rate is 14% higher than for the particle-free flow driven by the same pressure gradient. In view of this finding, it is not surprising to observe the dramatic alterations of the turbulence field in Fig. 2. The streamwise turbulence intensity shown in Fig. 2(a) is enhanced and the peak position is shifted somewhat further away from the wall than in the unladen channel. On the contrary, the velocity fluctuations perpendicular to the mean-flow direction are reduced considerably, as seen in Figs. 2(b) and 2(c). The increased anisotropy of the fluid turbulence due to the solid particles can either be due to different time

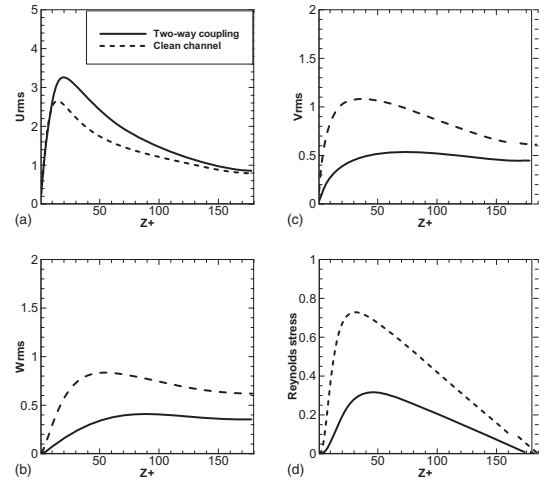


FIG. 2. Turbulence intensities and Reynolds shear stress for the particle-laden channel flow (solid lines) and for the unladen flow (broken lines). (a) Streamwise intensity u_{rms} ; (b) cross-stream intensity v_{rms} ; (c) wall-normal intensity w_{rms} ; and (d) Reynolds shear stress $-\overline{u'w'}$.

scales (or frequencies) of the different components of the instantaneous velocity vector or a hampered intercomponential energy transfer due to pressure-strain interactions. The pronounced reduction of the Reynolds shear stress $-\overline{u'w'}$ in Fig. 2(d) is partly due to the reduced wall-normal fluctuations and also a consequence of a decorrelation between the streamwise and wall-normal velocity components.

The trends exhibited by the fluid statistics in Figs. 1 and 2 are the same as when drag reduction is achieved by means of polymeric additives, e.g., Ptasincki *et al.*,³ Dubief *et al.*,⁴ and Graham.⁵ Spherical particles have occasionally given rise to the same qualitative effect on the turbulence field, but

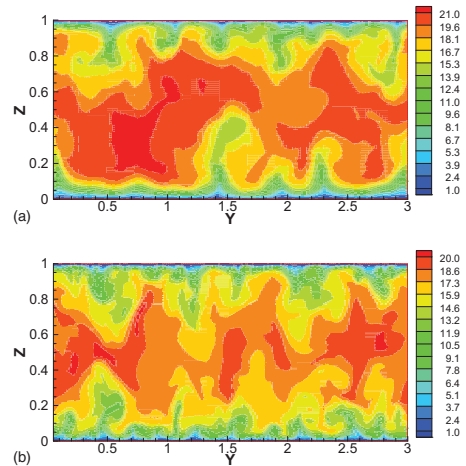


FIG. 3. (Color online) Instantaneous contours of the streamwise velocity component in a cross-sectional (y, z)-plane. Not to scale. (a) Particle-laden flow and (b) unladen flow.

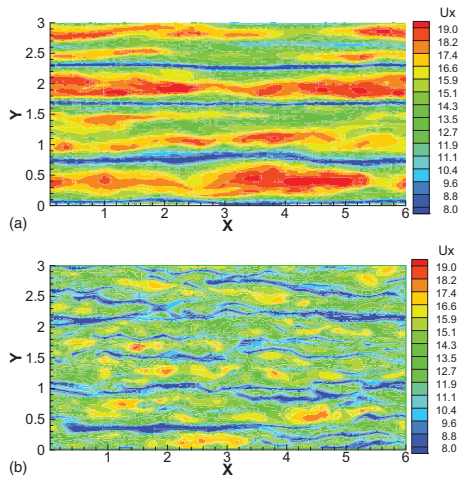


FIG. 4. (Color online) Instantaneous contours of the streamwise velocity component in a (x, y) -plane at $z^*=20$. Not to scale. (a) Particle-laden flow and (b) unladen flow.

without any reported drag reduction except in the under-resolved DNS-study of Li *et al.*¹⁶

Contours of the instantaneous streamwise fluid velocity are presented in Figs. 3 and 4. The smaller scales, which appear as distortions of the large-eddy contours, have been damped in the particle-laden flow, both in the cross-sectional plane in Fig. 3 and in the wall-parallel plane in Fig. 4. The streamwise coherence of the near-wall flow structures is considerably increased in the presence of particles. The alternating high- and low-velocity bands in Fig. 4(a) appear wider and more regular than in the unladen flow. This is a typical feature of drag-reduced flows independent of the actual cause of drag reduction, for instance, polymer-induced drag reduction (see, e.g., Ref. 6). The close resemblance of the present flow modulations and the turbulence modulations associated with fiber- and polymer-induced drag reduction makes us believe that also the spherical particles interrupt the turbulence generating cycle by a reduction of the strength and number of quasistreamwise vortices, which, in turn, leads to stabilization and widening of the near-wall streaks.

Pronounced turbulence modulations have been observed in the present two-way coupled simulation of turbulent channel flow laden with spherical particles. The enhancement of the turbulence anisotropy and the attenuation of the Reynolds shear stress are typical findings when drag reduction is achieved by means of polymeric or fiber additives. It is therefore not unexpected that significant drag reduction is found also when the turbulence is modulated by tiny spherical particles. The present results support the recently measured pressure-loss reductions achieved by means of sand or alumina particles in a liquid circulation loop.²⁰

This work has been supported by A/S Norske Shell through a research fellowship (Contract No. 4610020178/C08156) and by The Research Council of Norway (Programme for Supercomputing) through a grant of computing time.

- ¹J. L. Lumley, "Drag reduction by additives," *Annu. Rev. Fluid Mech.* **1**, 367 (1969).
- ²A. Gyr and H. W. Bewersdorff, *Drag Reduction of Turbulent Flows by Additives* (Kluwer, Dordrecht, 1995).
- ³P. K. Ptasiński, B. J. Boersma, F. T. M. Nieuwstadt, M. A. Hulsen, B. H. A. A. van den Brule, and J. C. R. Hunt, "Turbulent channel flow near maximum drag reduction: Simulations, experiments and mechanisms," *J. Fluid Mech.* **490**, 251 (2003).
- ⁴Y. Dubief, C. M. White, V. E. Terrapon, E. S. G. Shaqfeh, P. Moin, and S. K. Lele, "On the coherent drag-reducing and turbulent-enhancing behaviour in wall flows," *J. Fluid Mech.* **514**, 271 (2004).
- ⁵M. D. Graham, "Drag reduction in turbulent flow of polymer solutions," *Rheology Reviews* (British Society of Rheology, Norwich, UK, 2004), pp. 143–170.
- ⁶C. M. White and G. Mungal, "Mechanics and prediction of turbulent drag reduction with polymer additives," *Annu. Rev. Fluid Mech.* **40**, 235 (2008).
- ⁷I. Radin, J. L. Zakin, and G. K. Patterson, "Drag reduction in solid-fluid systems," *AIChE J.* **21**, 358 (1975).
- ⁸J. S. Paschkewitz, Y. Dubief, C. D. Dimitropoulos, E. S. G. Shaqfeh, and P. Moin, "Numerical simulation of turbulent drag reduction using rigid fibres," *J. Fluid Mech.* **518**, 281 (2004).
- ⁹J. J. J. Gillissen, B. J. Boersma, P. H. Mortensen, and H. I. Andersson, "Fibre-induced drag reduction," *J. Fluid Mech.* **602**, 209 (2008).
- ¹⁰A. Soldati, "Particles turbulence interactions in boundary layers," *Z. Angew. Math. Mech.* **85**, 683 (2005).
- ¹¹S. Balachandar and J. K. Eaton, "Turbulent dispersed multiphase flow," *Annu. Rev. Fluid Mech.* **42**, 111 (2010).
- ¹²R. A. Gore and C. T. Crowe, "Modulation of turbulence by a dispersed phase," *Trans. ASME J. Fluids Eng.* **113**, 304 (1991).
- ¹³J. D. Kulick, J. R. Fessler, and J. K. Eaton, "Particle response and turbulence modification in fully developed channel flow," *J. Fluid Mech.* **277**, 109 (1994).
- ¹⁴S. Geiss, A. Dreizler, Z. Stojanovic, M. Chrigui, A. Sadiki, and J. Janicka, "Investigation of turbulence modification in a non-reactive two-phase flow," *Exp. Fluids* **36**, 344 (2004).
- ¹⁵Y. Pan and S. Banerjee, "Numerical simulation of particle interactions with wall turbulence," *Phys. Fluids* **8**, 2733 (1996).
- ¹⁶Y. Li, J. B. McLaughlin, K. Kontomaris, and L. Portela, "Numerical simulation of particle-laden turbulent channel flow," *Phys. Fluids* **13**, 2957 (2001).
- ¹⁷J. K. Eaton, "Two-way coupled turbulence simulations of gas-particle flows using point-particle tracking," *Int. J. Multiphase Flow* **35**, 792 (2009).
- ¹⁸M. Rashidi, G. Hetsroni, and S. Banerjee, "Particle-turbulence interaction in a boundary layer," *Int. J. Multiphase Flow* **16**, 935 (1990).
- ¹⁹A. Kartushinsky, A. Mulgi, S. Tisler, and E. E. Michaelides, "An experimental study of the effect of particles on the shear stress in particulate turbulent pipe flow," *Proc. Estonian Acad. Sci. Eng.* **11**, 161 (2005).
- ²⁰H. A. A. Bari and R. B. M. Yunus, "Drag reduction improvement in two phase flow system using traces of SLES surfactant," *Asian J. Ind. Eng.* **1**, 1 (2009).
- ²¹C. D. Dritselis and N. S. Vlachos, "Numerical study of educed coherent structures in the near-wall region of a particle-laden channel flow," *Phys. Fluids* **20**, 055103 (2008).
- ²²K. D. Squires and J. K. Eaton, "Particle response and turbulence modification in isotropic turbulence," *Phys. Fluids A* **2**, 1191 (1990).
- ²³M. Picciotto, A. Giusti, C. Marchioli, and A. Soldati, "Turbulence modulation by micro-particles in boundary layers," *IUTAM Symposium on Computational Approaches to Multiphase Flow*, edited by S. Balachandar and A. Prosperetti (Springer, Dordrecht, 2006), pp. 53–62.
- ²⁴J. J. J. Gillissen, B. J. Boersma, P. H. Mortensen, and H. I. Andersson, "On the performance of the moment approximation for the numerical computation of fibre stress in turbulent channel flow," *Phys. Fluids* **19**, 035102 (2007).
- ²⁵P. H. Mortensen, H. I. Andersson, J. J. J. Gillissen, and B. J. Boersma, "Particle spin in a turbulent shear flow," *Phys. Fluids* **19**, 078109 (2007).
- ²⁶S. Elghobashi, "An updated classification map of particle-laden turbulent flows," *IUTAM Symposium on Computational Approaches to Multiphase Flow*, edited by S. Balachandar and A. Prosperetti (Springer, Dordrecht, 2006), pp. 3–10.

Article 5

On particle spin in a two-way coupled turbulent channel flow simulation

LIHAO ZHAO & H.I. ANDERSSON

Physics of Fluids, **23**, 093302, 2011.

On particle spin in two-way coupled turbulent channel flow simulations

Lihao Zhao and Helge I. Andersson

Department of Energy and Process Engineering, The Norwegian University of Science and Technology, NO-7491 Trondheim, Norway

(Received 24 March 2011; accepted 28 July 2011; published online 6 September 2011)

The rotational motion of spherical particles suspended in a turbulent flow field may not necessarily adapt to the fluid rotation, i.e., the particle spin may be different from the fluid vorticity. The translational and rotational motions of tiny particles are described in a Lagrangian framework using the point-particle approximation. The turbulence of the fluid phase is obtained by means of direct numerical simulations in which the feed-back from the particles onto the flow field is accounted for by a two-way coupling scheme. Particles with three different response times are considered, each for which millions of particles are released randomly in a turbulent channel flow at a frictional Reynolds number 360. The lightest particles with rotational response time 0.3 times the viscous time scale exhibited preferential concentration in areas with low streamwise vorticity but rotated passively along with the local fluid. The heaviest particles with a 30 times longer response time spun strikingly different from the particle spin observed in a one-way coupled simulation. This phenomenon can be ascribed primarily to the substantial modulation of the carrier-phase turbulence caused by the feed-back from the particles in the two-way coupled approach. Due to their higher rotational inertia, these particles did not even adjust to the rotational motion of the local fluid. © 2011 American Institute of Physics. [doi:10.1063/1.3626583]

INTRODUCTION

Spin of solid spherical particles suspended in a turbulent carrier fluid has received considerably less attention than their translational motions. In the vast majority of applications, the actual orientation of a spherical particle is irrelevant and the majority of the earlier investigations have focused on particle dispersion and deposition; e.g., Squires and Eaton,¹ Brooke *et al.*,² Zhang and Ahmadi,³ Marchioli and Soldati,⁴ and Marchioli *et al.*⁵ The presence of solid particles in a fluid may in a certain parameter range even alter the turbulent flow field, as observed in both experimental studies, e.g., Rashidi *et al.*,⁶ Kulick *et al.*,⁷ Kaftori *et al.*,⁸ Hussainov *et al.*,⁹ Geiss *et al.*,¹⁰ Hosokawa and Tomiyama,¹¹ and Bari and Yunus,¹² and in numerical simulations, e.g., Squires and Eaton,¹³ Elghobashi and Truesdell,¹⁴ Pan and Banerjee,¹⁵ Hwang and Eaton,¹⁶ Vreman,¹⁷ Dritselis and Vlachos,^{18,19} Bijlard *et al.*,²⁰ and Eaton.²¹

To fully comprehend the particle dynamics, however, knowledge about the particle spin is required. The optical probe invented by Frish and Webb²² as a means of direct measurement of fluid vorticity assumes that spherical particles suspended in the flow rotate with an angular velocity equal to half the local fluid vorticity, i.e., that the particles perfectly follow the fluid rotation. Ye and Roco,²³ however, measured the rotational velocity of neutrally buoyant particles and observed that the mean particle spin exceeded the mean angular fluid velocity in the core region of a planar Couette flow. Bluemink *et al.*²⁴ considered a sphere with a fixed centre but free to rotate in a solid-body-rotation flow. Their experimental observations showed that the particle spins faster than the fluid when the sphere is sufficiently far from the axis of solid-body rotation. Pan *et al.*^{25,26} investigated particle-laden turbulent channel flow subjected to

system rotation. In their four-way coupled simulations, particle spin was considered both in the particle-wall collision and inter-particle collision models, although the focus of their study was on the translational particle motion and the turbulence modulation. Mortensen *et al.*²⁷ performed one-way coupled simulations of tiny spherical particles suspended in wall-bounded turbulence and observed that the mean particle spin exceeded the mean fluid angular velocity close to the channel walls.

The importance of an angular slip velocity between particle and local fluid has also been addressed in some other flow configurations and parameter regimes by Yang *et al.*,²⁸ Zeng *et al.*,²⁹ and Lee and Balachandar.³⁰ Particle rotation may give rise to a lift force perpendicular to the direction of the flow, which in turn changes the trajectory of the spinning particle. This lift force might sometimes be of importance in industrial gas-solid flows as demonstrated, for instance, by Kajishima.³¹ Knowledge about the particle spin becomes an essential ingredient of the particle dynamics as soon as the particle shape deviates from spherical, as for oblate or prolate ellipsoidal particles (e.g., Mortensen *et al.*³²).

This study is a sequel to the work by Mortensen *et al.*²⁷ in which particle spin was examined in a *one-way* coupled Eulerian-Lagrangian simulation. The purpose of the present study is to examine how particle spin is affected by the sometimes pronounced turbulence modulation observed in *two-way* coupled simulations, as compared with data from the one-way coupled simulation.²⁷

THE POINT-FORCE APPROXIMATION TO TWO-WAY COUPLING

Dilute suspensions of spherical particles in a viscous fluid is routinely treated in a mixed Eulerian-Lagrangian

approach. The particle motion is modelled in a Lagrangian framework and the fluid flow is formulated in an Eulerian way. *One-way coupled* simulations mean that the particle motion is affected by the fluid flow but the fluid is not influenced by the particles. *Two-way coupled* simulations imply that the fluid flow is also affected by forces from the particles.

The fully developed turbulent flow in a plane channel is considered as being a prototype wall-bounded shear flow. The motion of the incompressible Newtonian fluid is governed by the continuity and momentum conservation equations,

$$\nabla \cdot \vec{u} = 0, \quad \rho \left[\frac{\partial \vec{u}}{\partial t} + (\vec{u} \cdot \nabla) \vec{u} \right] = -\nabla p + \mu \nabla^2 \vec{u} + \vec{f}^p. \quad (1)$$

Here, \vec{u} and p are the instantaneous fluid velocity vector and pressure, respectively, \vec{f}^p denotes the force per unit volume from the particles, whereas the gravity force is ignored. ρ and μ are the density and the dynamic viscosity of the carrier fluid.

Let us consider the motion of spherical particles with radius a , mass m , and moment of inertia $I = 2ma^2/5$. The equations governing the translational and rotational motion of one single particle are Newton's 2nd law of motion,

$$m \frac{d\vec{v}}{dt} = \vec{F} \quad (2)$$

and Euler's equation,

$$I \frac{d\vec{\omega}}{dt} = \vec{N}. \quad (3)$$

Here, \vec{v} is the translational and $\vec{\omega}$ is the angular velocity of the particle. These ordinary differential equations for \vec{v} and $\vec{\omega}$ can be integrated forward in time along with the partial differential equations (1) for the flow field \vec{u} and p , as soon as the force \vec{F} and the torque \vec{N} are specified.

If the particles are sufficiently small so that the neighboring flow can be considered as Stokesian, the force \vec{F} and the torque \vec{N} acting on the particle from the surrounding fluid can be expressed as

$$\vec{F} = 6\pi\mu a [\vec{u}(\vec{x}_p, t) - \vec{v}(t)] \quad (4)$$

and

$$\vec{N} = 8\pi\mu a^3 [\vec{\Omega}(\vec{x}_p, t) - \vec{\omega}(t)], \quad (5)$$

respectively. Here, $\vec{u}(\vec{x}_p, t)$ is the fluid velocity at the particle position \vec{x}_p at time t and $\vec{\Omega}(\vec{x}_p, t) = 1/2\nabla \times \vec{u}(\vec{x}_p, t)$ is thus the angular velocity of the flow field at the particle position. The force acting on the particle is, therefore, *linearly* dependent on the *translational slip velocity*, i.e., the difference in translational velocity between the fluid and the particle. Similarly, the torque is linearly dependent on the difference in angular velocity between the fluid and the particle, i.e., the *angular slip velocity*. The particle Reynolds number $\text{Re}_p = 2a|\vec{u}(\vec{x}_p, t) - \vec{v}(t)|/\nu$ is assumed to be rather small,

and the *non-linear* correction $(1 + 0.15 \text{Re}_p^{0.687})$ to the Stokes force (4) and a corresponding correction to the linear torque (5) were, therefore, not taken into account in this study. The validity of this assumption, which was also made by Mortensen *et al.*,²⁷ will be justified further below.

The equations governing the translational and rotational particle motion, with the force \vec{F} given in Eq. (4) and the torque \vec{N} as in Eq. (5), can be written as

$$\frac{d\vec{v}}{dt} = \frac{1}{\tau_t} (\vec{u}(\vec{x}_p, t) - \vec{v}(t)), \quad \text{where} \quad \tau_t = \frac{2Da^2}{9\nu} \quad (6)$$

and

$$\frac{d\vec{\omega}}{dt} = \frac{1}{\tau_r} (\vec{\Omega}(\vec{x}_p, t) - \vec{\omega}(t)), \quad \text{where} \quad \tau_r = \frac{Da^2}{15\nu}. \quad (7)$$

D is the ratio between the particle density and the fluid density ρ , and the rotational response time τ_r is exactly 3/10 of the translational response time τ_t . The ratio 3/10, which readily follows from the preceding equations, is valid only for spherical particles and implies that particle spin adjusts about 3 times faster to the fluid spin than the particle velocity adjusts to the fluid velocity.

The force from an individual particle on the fluid is equal to $-\vec{F}_i$, according to Newton's 3rd law "*action equals reaction*." The feedback from n_p particles within a given volume Δ adds up to

$$\vec{f}^p = -\frac{1}{\Delta} \sum_{i=1}^{n_p} \vec{F}_i. \quad (8)$$

This force per unit volume can be included in the momentum equation in Eq. (1) to account for the effect of the solid particles on the fluid motion. This is known as the *point-force approximation* to two-way coupling; see, e.g., the recent reviews by Eaton²¹ and Balachandar and Eaton.³³ This approach was probably first introduced by Squires and Eaton¹³ in order to study the modulation of isotropic turbulence and, subsequently, adopted for wall-bounded turbulence by Li *et al.*³⁴ and several others.

Forces other than Stokes drag will not be taken into account in the present study since other forces, like buoyancy and Basset forces, are negligibly small when the spherical particles are heavier than the fluid, i.e., $D \gg 1$ (Ref. 35). Wang *et al.*³⁶ showed that the particle deposition rate was only marginally reduced when lift forces were neglected, whereas Pan *et al.*²⁶ retained a lift force in their direct numerical simulation (DNS) study and found only a modest influence as compared with the drag force. Arcen *et al.*³⁷ demonstrated that the wall-corrections of the drag force and the optimum lift force, as defined by Wang *et al.*,³⁶ have a negligible effect for particle response times of the same order as those in the present study.

In accordance with the aim of the present investigation, namely, to study how the particle spin is affected by the modulation of the flow field in two-way coupled simulations, exactly the same modeling of the particle dynamics is adopted as in the one-way coupled simulations by Mortensen

et al.,²⁷ i.e., the linear laws (4) and (5) are used for the viscous drag force and torque, respectively. For this reason, we also impose the same wall-conditions as in Ref. 27, i.e., a particle which happens to hit a wall bounces elastically back while retaining its previous velocity and spin, besides that the wall-normal velocity component changes sign.

FLOW CONFIGURATION AND COMPUTATIONAL APPROACH

Particle-laden fully developed turbulent channel flow at a Reynolds number $Re = 360$ based on the channel height h and the wall-friction velocity u_* is considered. The Eulerian flow field \vec{u} of the carrier phase is obtained by means of DNS, and the DNS-solver is the same as that used by Gillissen *et al.*³⁸ and Mortensen *et al.*²⁷ A pseudo-spectral method using Fourier series in the two homogeneous directions and a second-order finite-difference scheme in the wall-normal direction are employed for the spatial derivatives on a staggered grid system. The time advancement is carried out with a second-order explicit Adams-Bashforth scheme. Periodic boundary conditions are used in the homogenous directions and no-slip boundary conditions are imposed at the channel walls.

The computational domain is $6h$, $3h$, and h in the streamwise (x), spanwise (y), and wall-normal (z) directions, respectively. This is exactly the same domain size as in Ref. 27 and essentially the same as in the collaborative testing campaign reported by Marchioli *et al.*⁵ The computational mesh consisted of 128^3 grid points, i.e., the same as used by the majority of the groups who contributed to Ref. 5. Mortensen *et al.*,²⁷ however, used a finer 192^3 grid, but the different resolutions have a marginal influence on the results.

After the flow field is advanced forward one time step ($\Delta t^+ = 0.036$ when normalized with the viscous time scale ν/u_*^2) in accordance with Eq. (1), the fluid velocity and angular velocity are required at the particle positions \vec{x}_p in order to also advance the particle velocity and the particle spin forward in time in accordance with Eqs. (6) and (7). Therefore, a second-order quadratic interpolation scheme is employed to interpolate the discrete fluid variables onto the particle location \vec{x}_p .

Three different particle classes, denoted as A, B, and C, are considered in order to explore the effect of various particle relaxation times; see Table I. The particle radius scaled with the viscous length ν/u_* is $a^+ = 0.36$ in all cases, whereas the ratio τ_t^+ between the translational particle relaxation time and the viscous time scale varies from 1 in Case A to 30 in Case C. The particle properties in the three different

TABLE I. Overview of the three different particle classes considered. The number of particles is N_p and the particle volume fraction is V_p . The superscripts + denote scaling with the viscous scales for length ν/u_* and time ν/u_*^2 . Some results for Case C were reported by Zhao *et al.* (Ref. 41).

Case	N_p	V_p	τ_t^+	D	a^+
A	$5 \cdot 10^6$	$1.16 \cdot 10^{-3}$	1	35	0.36
B	$5 \cdot 10^6$	$1.16 \cdot 10^{-3}$	5	174	0.36
C	$4 \cdot 10^6$	$0.93 \cdot 10^{-3}$	30	1041	0.36

cases considered here are thus identical with those in the one-way coupled simulations reported by Mortensen *et al.*,²⁷ with which comparisons will be made in the "Results and Discussion" section.

Several million (N_p) mono-sized spherical particles are released randomly into an already developed turbulent flow field with velocity and spin initially equal to the local fluid velocity and spin. It is not a straightforward task, however, to foresee when the particle distribution reaches a statistically steady state (as pointed out by one of the reviewers). According to Marchioli *et al.*,⁵ the time needed for $\tau_t^+ = 25$ particles to achieve a steady-state particle number density is distinctly shorter than for $\tau_t^+ = 1$ and $\tau_t^+ = 5$ particles. Marchioli *et al.*³⁹ included time evolution results also for lighter $\tau_t^+ = 0.2$ and heavier $\tau_t^+ = 125$ particles and showed that the rate of development towards a steady particle state is indeed non-linear in τ_t^+ . This non-linear dependency on the particle response time is confirmed by our recent study (Zhao and Andersson⁴⁰), which suggested that the lighter particles adjust faster to the flow field into which they are embedded as long as τ_t^+ does not exceed above 30. However, these findings based on one-way coupled simulations are not necessarily valid for two-way coupled simulations. In the present case, we, therefore, monitor the number of particles in the near-wall sublayer together with the bulk flow velocity in order to observe when a steady state of the particulate flow is reached. The simulation for the heaviest particles (Case C) is thus first run for 5400 viscous time units before fluid and particle statistics are obtained during the subsequent 3600 time units. For the lighter particles (Case A and Case B), statistics are also gathered over 3600 time units, but the sampling is initiated after 3600 time units.

The translational slip velocity $\vec{u}(\vec{x}_p, t) - \vec{v}(t)$ will probably attain the highest values for the heaviest particles considered in this study. The particle Reynolds number Re_p based on the magnitude of the mean slip velocity is seen to reach its maximum value of about 0.8 in the buffer layer and to reduce to about 0.2 in the channel center for the $\tau_t^+ = 30$ particles. The non-linear correction $0.15 Re_p^{0.687}$ to the Stokes force in Eq. (4) thus amounts to less than 15%. An alternative particle Reynolds number based on the root-mean-square value of the translational slip velocity exhibits almost the same variation as Re_p but the nominal value is somewhat lower than Re_p . The adoption of the linear Stokes force (4), as used also by Mortensen *et al.*,²⁷ can, therefore, be justified.

RESULTS AND DISCUSSION

Statistical results from the present two-way coupled simulations are compared with results from one-way coupled simulations by Mortensen *et al.*²⁷ Let us first take a brief look at the fluid flow. Irrespective of the particle response time and mass loading, the velocity field resulting from a one-way coupled simulation, i.e., with $\vec{f}^P = 0$ in Eq. (1), is indistinguishable from that of an unladen or clean channel flow.

The turbulence intensities and Reynolds shear stress are shown in Figure 1. The lightest particles (Case A) have only an almost negligible effect on the fluid turbulence due to

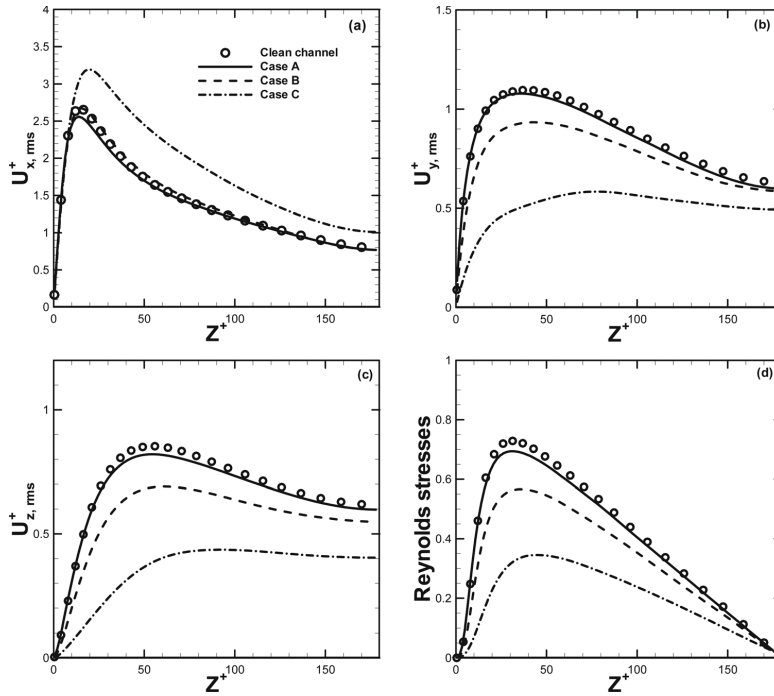


FIG. 1. Turbulence intensities and Reynolds shear stress $-\overline{u'_x u'_z}$ for the two-way coupled simulations (lines) compared with data from a one-way coupled simulation (circles). ($\tau_i^+ = 1$ —; $\tau_i^+ = 5$ - - -; $\tau_i^+ = 30$ - · - ·).

their modest inertia. The intermediate Case B particles tend to attenuate the turbulence intensities in the spanwise and wall-normal directions, whereas the streamwise velocity fluctuations are left almost unaffected. The Reynolds shear stress $-\overline{u'_x u'_z}$ is, nevertheless, distinctly reduced. For the heaviest particles (Case C), the streamwise velocity fluctuations are enhanced, whereas, the velocity fluctuations in the two other directions are damped considerably, as reported already by Zhao *et al.*⁴¹ Although the streamwise fluid velocity fluctuations u'_x are enhanced by the presence of the inertial particles, the substantial damping of wall-normal velocity fluctuations u'_z suffices to reduce also the Reynolds shear stress. The almost 50% reduction of $-\overline{u'_x u'_z}$ as compared with the one-way coupled simulation is probably also an outcome of a de-correlation between the streamwise and wall-normal velocity components caused by the presence of the $\tau_i^+ = 30$ particles.

The angular velocity or spin of the carrier fluid, defined here as half of the fluid vorticity, is shown in Figure 2. Here, and in the following, the spin of the fluid and of the particles will be scaled with the reciprocal of the viscous time scale ν/u_s^2 . The variation of the mean spanwise spin $\overline{\Omega}_y^+$ with the distance z^+ from the wall in Fig. 2(a) stems directly from the slope of the fluid mean velocity profile $U(z)$. The mean spin in Cases A and B shows almost the same variation as in the unladen (i.e., one-way coupled) channel flow, whereas the mean spin in Case C exceeds $\overline{\Omega}_y^+$ in the unladen flow in the near-wall region $z^+ < 40$. This variation of $\overline{\Omega}_y^+$ with τ_i^+ is caused by the monotonic attenuation of the shear stress $-\overline{u'_x u'_z}$ with increasing particle response time, as observed in

Figure 1(d), which tends to increase dU/dz in the near-wall region and flatten the mean velocity profile $U(z)$ in the core region of the channel.

When the spin intensities $\Omega_{i,rms}^+$ (i.e., the rms values of the angular velocity fluctuations) are considered, the two-way coupling makes the results distinctly different from those of the unladen flow, except for Case A in which the lightest particles turn out to be unable to affect the fluid vorticity. With two-way coupling, all three components of the fluctuating spin vector are substantially reduced in the presence of Case C particles as compared with the one-way coupled results reported by Mortensen *et al.*²⁷ The most significant damping is in the streamwise direction (Figure 2(b)). This is consistent with the pronounced modulation of the turbulent velocity field caused by Case C particles shown in Figure 1. This modulation shows up not only in the fluctuating velocity field but also in the fluctuating vorticity field. The damping of the fluid spin intensities is primarily associated with the attenuation of the velocity fluctuations u'_y and u'_z in the spanwise and wall-normal directions, respectively.

The attenuation is most pronounced for $\Omega_{x,rms}^+$, which is independent of the augmentation of the streamwise velocity fluctuations u'_x . The profile peaks at about $z^+ \approx 20$ in the unladen flow, and this peak is associated with the coherent near-wall structures which carry streamwise vorticity, as argued for instance by Kim *et al.*⁴² This peak is still clearly visible for the intermediate $\tau_i^+ = 5$ particles in Figure 2(b) but has almost vanished for the heavier $\tau_i^+ = 30$ particles. Zhao *et al.*⁴¹ recently reported that the near-wall streaks were widened in this particle-laden case. The near-wall

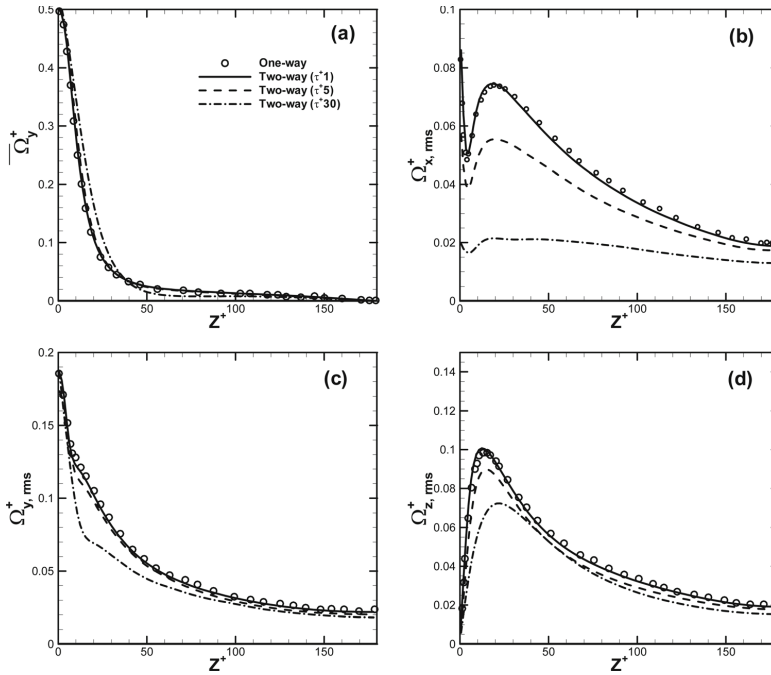


FIG. 2. Fluid spin. Results from the present two-way coupled simulations (lines) and the one-way coupled simulation (circles) by Mortensen *et al.* (Ref. 27). $\tau_i^+ = 1$ —; $\tau_i^+ = 5$ - - -; $\tau_i^+ = 30$ - · - ·. (a) mean spanwise spin, (b) rms streamwise spin, (c) rms spanwise spin, (d) rms wall-normal spin.

vortical structures are, therefore, probably weakened and the near-wall peak of the streamwise spin intensity vanishes. It is furthermore noteworthy from Figure 2(b) that $\Omega_{x,rms}^+$ remains roughly constant across the entire channel in Case C, except in the viscous sublayer. Moreover, the vorticity fluctuations, which are almost isotropic in the core region of an unladen channel flow (see Ref. 42), become anisotropic in the particle-laden channel due to the substantial damping of $\Omega_{x,rms}^+$.

The fluid flow field is substantially modulated by the presence of the solid particles through the particle force term \hat{f}^P in the particle-laden Navier-Stokes Equation (1). One can, therefore, expect that the particle motion will also be affected. The mean spanwise particle spin ω_y and the particle spin intensities $\omega_{i,rms}$ are compared with corresponding results from Mortensen *et al.*²⁷ in Figure 3. The profiles in Figure 3(a) show that the heavier particles (Cases B and C) rotate faster than the lightest Case A particles in the region $10 < z^+ < 80$ in the two-way coupled simulations. In the one-way simulations, on the contrary, the mean particle spin for the intermediate $\tau_i^+ = 5$ particles was distinctly higher than for the lighter $\tau_i^+ = 1$ particles as well as for the heavier $\tau_i^+ = 30$ particles in this region. Mortensen *et al.*²⁷ ascribed their findings to the ability of inertial particles to accumulate in preferred areas of high rate of strain; see, e.g., Rashidi *et al.*,⁶ Eaton and Fessler,⁴³ and Marchioli and Soldati.⁴ The relatively high mean fluid spin for the heavy particles in the region $10 < z^+ < 40$ in Fig. 2(a) may explain the high mean particle spin in Figure 3(a) for the $\tau_i^+ = 30$ particles, i.e., as an indirect effect of the turbulence modulation. The equally high mean particle spin of the $\tau_i^+ = 5$ particles are, however,

caused by the preferential particle concentration, just as in the one-way coupled simulation.

The streamwise spin intensity $\omega_{x,rms}^+$ shown in Fig. 3(b) is gradually attenuated with increasing particle response times, similar to the fluid spin intensities in Figure 2(b). In the one-way coupled simulations, however, the streamwise spin intensity is lowest for the intermediate $\tau_i^+ = 5$ particles, except in the viscous sublayer. The profiles of the spanwise spin intensity $\omega_{y,rms}^+$ in Figure 3(c) are almost unaffected by the two-way coupling as far as Case A and Case B particles are concerned. However, distinctly different profiles are obtained for the heaviest $\tau_i^+ = 30$ particles, and the shape of the particle spin intensity distribution resembles that of the fluid spin intensity profile in Figure 2(c). In the vicinity of the wall, $\omega_{y,rms}^+$ found in the two-way coupled simulation exceeds the near-wall level in the one-way coupled simulation²⁷ for Case C. Mortensen *et al.*²⁷ observed that $\omega_{y,rms}^+ < \Omega_{y,rms}^+$ close to wall. It is known that the spin difference between a particle and the fluid, i.e., the angular slip velocity, could be reduced due to particle-fluid interactions. This may explain why $\omega_{y,rms}^+$ becomes higher in the near-wall region than in the one-way coupled simulation.

The wall-normal particle spin intensity $\omega_{z,rms}^+$ reduces with increasing τ_i^+ inside of $z^+ \approx 20$, whereas the $\tau_i^+ = 30$ particles are spinning faster than the others in the interval from $z^+ \approx 20$ to 120. Two-way coupled simulations make the wall-normal spin intensity lower than in one-way coupled simulations for the $\tau_i^+ = 1$ and $\tau_i^+ = 5$ particles, whereas two-way coupling results in enhanced wall-normal spin for $\tau_i^+ = 30$. For the latter particles, the peak position of $\omega_{z,rms}^+$ is about twice as far from the wall as in the one-way coupled

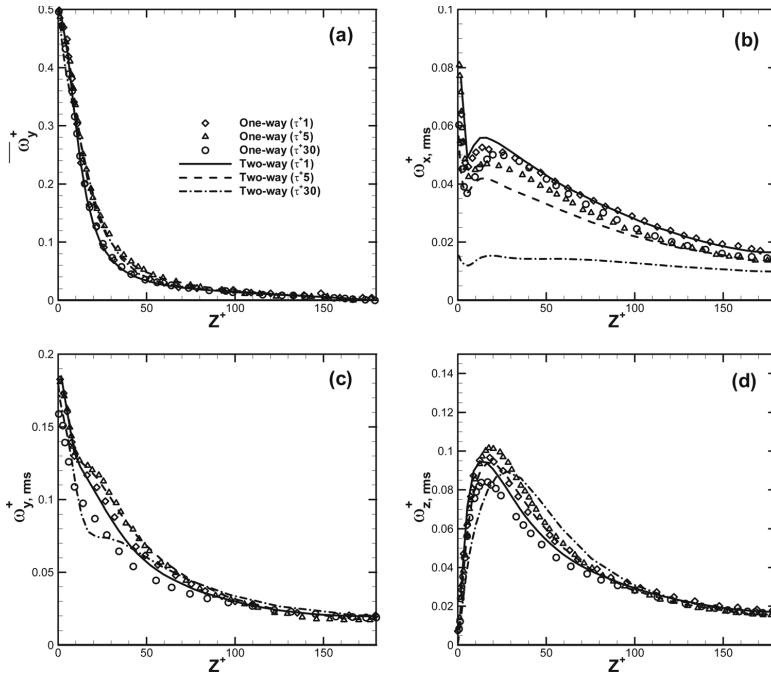


FIG. 3. Particle spin. Results from the present two-way coupled simulations (lines) and the one-way coupled simulations by Mortensen *et al.* (Ref. 27). $\tau_t^+ = 1$ —, diamond; $\tau_t^+ = 5$ - - -, triangle; $\tau_t^+ = 30$ -.-.-, circle (a) mean spanwise spin, (b) rms streamwise spin, (c) rms spanwise spin, (d) rms wall-normal spin.

simulation. Since the wall-normal fluid spin intensity depends on the streamwise and spanwise velocity fluctuations, the shift of the peak position of wall-normal particle spin away from the wall can be caused by the shift of the peak position of streamwise turbulence intensity in Fig. 1(a).

The streamwise intensities of both particle and fluid spins are substantially reduced in the two-way coupled simulations, as shown in Figures 2(b) and 3(b). The fluid spin intensity, nevertheless, remains higher than the corresponding particle spin intensity, and both exhibit a remarkably modest variation across the shear layer for the heaviest particles. The reduction of the streamwise spin intensity is apparently a direct consequence of the damping of the velocity fluctuations in the cross-stream and spanwise directions, which results from the feed-back from the particles onto the flow field (e.g., Zhao *et al.*⁴¹).

In order to explain the subtle variations of the particle spin observed in Figure 3, it is essential to examine how the particle spin compares with the *conditionally averaged* fluid spin in Figures 4–6. Here, the evaluation of the conditionally averaged fluid spin is conditioned on the presence of a solid particle. As long as the particles are evenly distributed throughout the flow field, as in the limit of a vanishing particle response time, the conditionally averaged fluid spin becomes identical with the unconditioned averages shown in Figure 2. For particle response times comparable to the relevant turbulent time scale, however, particles are known to concentrate preferentially in low-speed fluid velocity regions (Rashidi *et al.*,⁶ Eaton and Fessler,⁴³ Marchioli and Soldati⁴).

For the light and intermediate particles with $\tau_t^+ = 1$ and $\tau_t^+ = 5$, respectively, the particle spin intensities in the streamwise direction in Figure 4(a), in the spanwise direction

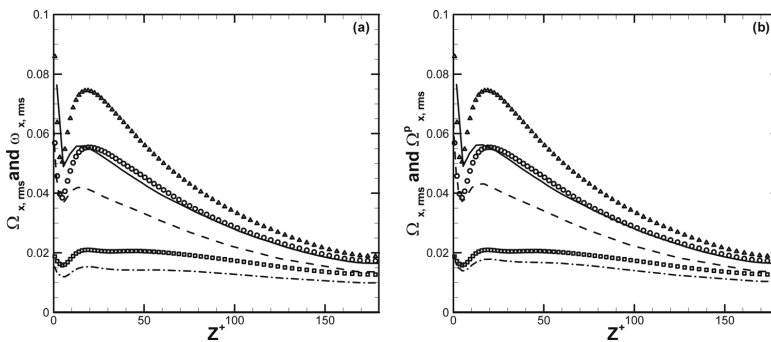


FIG. 4. Comparison between fluid spin intensities $\Omega_{x,rms}$ (symbols), conditionally averaged fluid spin intensities $\Omega_{x,rms}^P$ (lines), and particle spin intensities $\omega_{x,rms}$ (lines). $\tau_t^+ = 1$: triangle and solid line; $\tau_t^+ = 5$: open circle and dashed line; $\tau_t^+ = 30$: square and dashed dotted lines. (a) fluid and particles and (b) fluid and conditionally averaged fluid at particle positions.

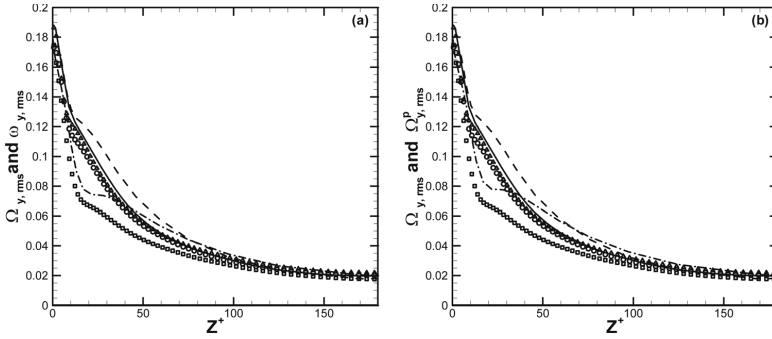


FIG. 5. Comparison between fluid spin intensities $\Omega_{y,rms}$ (symbols), conditionally averaged fluid spin intensities $\Omega_{y,rms}^P$ (lines), and particle spin intensities $\omega_{y,rms}$ (lines). $\tau_t^+ = 1$: triangle and solid line; $\tau_t^+ = 5$: open circle and dashed line; $\tau_t^+ = 30$: square and dash dot line. (a) fluid and particles and (b) fluid and conditionally averaged fluid at particle positions.

in Figure 5(a), and in the wall-normal direction in Figure 6(a) are almost indistinguishable from the corresponding conditionally averaged fluid spin intensities $\Omega_{z,rms}^P$ presented in Figures 4(b), 5(b), and 6(b), respectively. Here, the superscript P is used to denote the average of a fluid variable conditioned on the presence of a solid particle. This observation suggests that these relatively light particles follow the rotational motion of the fluid elements almost passively. The torque \vec{N} acting on a particle from the surrounding fluid, as given by Eq. (5), will, therefore, attain only negligibly small values. The spin intensities for the $\tau_t^+ = 30$ particles, however, are consistently lower than the corresponding conditionally averaged fluid spin intensities across most of the channel cross-section. This finding applies for all three directional components of the fluctuating particle spin vector and is most easily seen when the dash-dotted lines in panels (a) and (b) in Figures 4 and 6 are compared. This suggests that Case C particles either avoid regions of locally high streamwise fluid vorticity or that the rotational inertia of these particles is sufficiently high to allow the particles to spin slower than the surrounding fluid.

The comparison in Figure 4(b) of the unconditionally and conditionally averaged streamwise fluid spin intensities reveals beyond any doubt substantial differences between the two for all particles classes considered. More specifically, the conditionally averaged spin $\Omega_{x,rms}^P$ is distinctly lower than the unconditionally averaged $\Omega_{x,rms}$. These differences can only be explained in terms of a preferential concentration of the particles in regions of low streamwise vorticity. Moreover,

since $\omega_{x,rms}$ is lower than $\Omega_{x,rms}^P$ for heaviest particles, the rotational inertia of the $\tau_t^+ = 30$ particles is sufficient to allow these particles to spin slower than the surrounding fluid.

The wall-normal spin behaves somewhat differently. The peak of the particle spin intensity $\omega_{z,rms}$ in Fig. 6(a) is somewhat lower than the peak of the conditionally averaged fluid spin $\Omega_{z,rms}^P$ in Figure 6(b), and these particles are, therefore, spinning slower than the local fluid. However, both the particle spin intensity and the conditionally averaged fluid spin are substantially higher than the unconditionally averaged fluid spin. The inertial particles are thus concentrating in areas with locally high wall-normal vorticity but their rotational inertia does not allow them to fully adjust their rotation to the local fluid vorticity.

The dependence of the particle spin on the particle relaxation time τ_t^+ (and thereby also on τ_r^+) is rather complex. The particle inertia is proportional to τ_t^+ and τ_r^+ and, therefore, directly affects the translational and rotational motion of the particles in accordance with Eqs. (6) and (7). However, inertial particles may also distribute themselves unevenly in a turbulent flow field, and this preferential concentration yields an indirect effect on particle motion. In two-way coupled simulations, the particle inertia may moreover affect the turbulence, and this turbulence modulation will in turn also influence the particle motion.

The latter effect is apparently the most dominant in the three cases considered in this study. The lightest particles ($\tau_t^+ = 1$) adapt to the rotational motion of the local fluid, but nevertheless, spin differently than the unconditionally

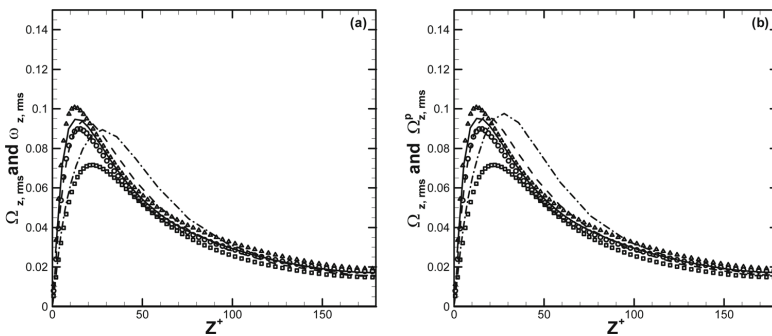


FIG. 6. Comparison between fluid spin intensities $\Omega_{z,rms}$ (symbols), conditionally averaged fluid spin intensities $\Omega_{z,rms}^P$ (lines), and particle spin intensities $\omega_{z,rms}$ (lines). $\tau_t^+ = 1$: triangle and solid line; $\tau_t^+ = 5$: open circle and dashed line; $\tau_t^+ = 30$: square and dash dot line. (a) fluid and particles and (b) fluid and conditionally averaged fluid at particle positions.

averaged fluid rotation. This means that these particles concentrate preferentially in the flow field but otherwise follow the fluid passively due to their modest rotational inertia. The heaviest particles, on the other hand, have sufficient inertia to partly penetrate the coherent near-wall vortical structures and the tendency towards preferential concentration is reduced, in line with the view of Eaton and Fessler.⁴³ Their rotational inertia moreover delays their spin-up by the surrounding fluid, and an angular slip velocity is observed. The largest effects on the particle spin is anyhow associated with the substantial modulation of the turbulent flow field achieved in these two-way coupled simulations as illustrated by the substantial reduction of the Reynolds shear stress shown in Figure 1(d). The gradually increasing turbulence modulation with increasing particle inertia makes the heaviest particles move and rotate in a completely different environment than the lightest particles considered.

CONCLUDING REMARKS

The rotational motion or spin of spherical particles embedded in a turbulent channel flow has been considered. The particles were treated in a Lagrangian framework and affected both by inertia and linear forces and torques. The flow field was obtained by direct numerical simulations in which two-way force-coupling between the particles and the fluid was achieved by means of a point-force approximation. The Reynolds number was fixed to 360, and three different particle response times were considered.

The present results show that the rotational motion of spherical particles suspended in a turbulent carrier fluid attains appreciable levels. The lightest particles rotate almost passively along with the local fluid rotation. Significant spin-slip occurs for inertial point-particles with relaxation times such that the translational and rotational Stokes numbers become $\tau_+^+ = 30$ and $\tau_+^+ = 9$, respectively. The assumption that the fluid and particle angular velocities equal, on which the vorticity probe of Frish and Webb²² was based, is therefore, far from being fulfilled for these particular particles. The inertial particles are driven to move and rotate by the large-scale turbulent eddies but could not fully respond to the smallest eddies and, therefore, partially attain their angular velocity.

The spin resulting from the present two-way coupled simulations is in most aspects strikingly different from the spin reported earlier in one-way coupled simulations by Mortensen *et al.*²⁷ The distinctly different particle spins are an *indirect* effect of the two-way coupling between the continuous fluid phase and the discrete particles. The force \vec{f}^P in the particle-laden Navier-Stokes Equation (1) is known to modulate the turbulent flow field in this parameter range, as recently reported by Zhao *et al.*⁴¹ This modulation of the turbulence by the presence of inertial solid particles affects not only the fluid velocity but also the fluid vorticity as shown herein. The particle spin, which is governed by Euler's Equation (3), is therefore indirectly affected. The angular slip velocity, which appears in the torque in Eq. (5), turned out to be negligibly small for the lightest particles considered but attained appreciable values for Case C particles.

The inclusion of two-way coupling in Eulerian-Lagrangian simulations of dilute particle suspensions does not only cause modulations of the turbulent flow field but also affects the mean spin and the spin intensities of the suspended inertial particles. Turbulence modulation achieved by particle additives depends crucially on the particle relaxation time and the particle volume fraction. The findings reported herein are, therefore, not necessarily applicable in other parameter ranges.

ACKNOWLEDGMENTS

The authors appreciate the constructive and exceptionally detailed feedback from the anonymous reviewers, which greatly assisted us in the preparation of the final paper. This work has been supported by A/S Norske Shell (Contract No. 4610020178/C08156) through a research fellowship to the first author and by The Research Council of Norway (Programme for Supercomputing) through a grant of computing time.

- ¹K. D. Squires and J. K. Eaton, "Preferential concentration of particles by turbulence," *Phys. Fluids A* **3**, 1169 (1991).
- ²J. W. Brooke, K. Kontomaris, T. J. Hanratty, and J. B. McLaughlin, "Turbulent deposition and trapping of aerosols at a wall," *Phys. Fluids A* **4**, 825 (1992).
- ³H. Zhang and G. Ahmadi, "Aerosol particle transport and deposition in vertical and horizontal turbulent duct flows," *J. Fluid Mech.* **406**, 55 (2000).
- ⁴C. Marchioli and A. Soldati, "Mechanisms for particle transfer and segregation in a turbulent boundary layer," *J. Fluid Mech.* **468**, 283 (2002).
- ⁵C. Marchioli, A. Soldati, J. G. M. Kuerten, B. Arcen, A. Tanière, G. Goldensoph, K. D. Squires, M. F. Cargnelutti, and L. M. Portela, "Statistics of particle dispersion in direct numerical simulations of wall-bounded turbulence: Results of an international collaborative benchmark test," *Int. J. Multiphase Flow* **34**, 879 (2008).
- ⁶M. Rashidi, G. Hetsroni, and S. Banerjee, "Particle-turbulence interaction in a boundary layer," *Int. J. Multiphase Flow* **16**, 935 (1990).
- ⁷J. D. Kulick, J. R. Fessler, and J. K. Eaton, "Particle response and turbulence modification in fully-developed channel flow," *J. Fluid Mech.* **277**, 109 (1994).
- ⁸D. Kaftori, G. Hetsroni, and S. Banerjee, "The effect of particles on wall turbulence," *Int. J. Multiphase Flow* **24**, 3 (1998).
- ⁹M. Hussainov, A. Kartushinsky, Ü. Rudi, I. Shecheglov, G. Kohnen, and M. Sommerfeld, "Experimental investigation of turbulence modulation by solid particles in a grid-generated vertical flow," *Int. J. Heat Fluid Flow* **21**, 365 (2000).
- ¹⁰S. Geiss, A. Dreizler, Z. Stojanovic, M. Chrigui, A. Sadiki, and J. Janicka, "Investigation of turbulence modification in a non-reactive two-phase flow," *Exp. Fluids* **36**, 344 (2004).
- ¹¹S. Hosokawa and A. Tomiyama, "Turbulence modification in gas-liquid and solid-liquid dispersed two-phase pipe flows," *Int. J. Heat Fluid Flow* **25**, 489 (2004).
- ¹²H. A. A. Bari and R. B. M. Yunus, "Drag reduction improvement in two phase flow system using traces of SLES surfactant," *Asian J. Ind. Eng.* **1**, 1 (2009).
- ¹³K. D. Squires and J. K. Eaton, "Particle response and turbulence modification in isotropic turbulence," *Phys. Fluids A* **2**, 1191 (1990).
- ¹⁴S. E. Elghobashi and G. C. Truesdell, "On the two-way interaction between homogeneous turbulence and dispersed particles. I: Turbulence modification," *Phys. Fluids A* **5**, 1790 (1993).
- ¹⁵Y. Pan and S. Banerjee, "Numerical simulation of particle interactions with turbulence," *Phys. Fluids* **8**, 2733 (1996).
- ¹⁶W. Hwang and J. K. Eaton, "Homogeneous and isotropic turbulence modulation by small heavy ($St \sim 50$) particles," *J. Fluid Mech.* **564**, 361 (2006).
- ¹⁷A. W. Vreman, "Turbulence characteristics of particle-laden pipe flow," *J. Fluid Mech.* **584**, 235 (2007).
- ¹⁸C. D. Dritselis and N. S. Vlachos, "Numerical study of educed coherent structures in the near-wall region of a particle-laden channel flow," *Phys. Fluids* **20**, 055103 (2008).

- ¹⁹C. D. Dritselis and N. S. Vlachos, "Numerical investigation of momentum exchange between particles and coherent structures in low Re turbulent channel flow," *Phys. Fluids* **23**, 025103 (2011).
- ²⁰M. J. Bijlard, R. V. A. Oliemans, L. M. Portela, and G. Ooms, "Direct numerical simulation analysis of local flow topology in a particle-laden turbulent channel flow," *J. Fluid Mech.* **653**, 35 (2010).
- ²¹J. K. Eaton, "Two-way coupled turbulence simulations of gas-particle flows using point-particle tracking," *Int. J. Multiphase Flow* **35**, 792 (2009).
- ²²M. B. Frish and W. W. Webb, "Direct measurement of vorticity by optical probe," *J. Fluid Mech.* **107**, 173 (1981).
- ²³J. Ye and M. C. Roco, "Particle rotation in a Couette flow," *Phys. Fluids A* **4**, 220 (1992).
- ²⁴J. J. Bluemink, D. Lohse, A. Prosperetti, and L. Van Wijngaarden, "A sphere in a uniformly rotating or shearing flow," *J. Fluid Mech.* **600**, 201 (2008).
- ²⁵Y. Pan, T. Tanaka, and Y. Tsuji, "Turbulence modulation by dispersed solid particles in rotating channel flows," *Int. J. Multiphase Flow* **28**, 4 (2002).
- ²⁶Y. Pan, T. Tanaka, and Y. Tsuji, "Direct numerical simulation of particle-laden rotating turbulent channel flow," *Phys. Fluids* **13**, 2320 (2001).
- ²⁷P. H. Mortensen, H. I. Andersson, J. J. J. Gillissen, and B. J. Boersma, "Particle spin in a turbulent shear flow," *Phys. Fluids* **19**, 078109 (2007).
- ²⁸B. H. Yang, J. Wang, D. D. Joseph, H. H. Hu, T.-W. Pan, and R. Glowinski, "Migration of a sphere in tube flow," *J. Fluid Mech.* **540**, 109 (2005).
- ²⁹L. Zeng, F. Najjar, S. Balachandar, and P. Fischer, "Forces on a finite-sized particle located close to a wall in a linear shear flow," *Phys. Fluids* **21**, 033302 (2009).
- ³⁰H. Lee and S. Balachandar, "Drag and lift forces on a spherical particle moving on a wall in a shear flow at finite Re," *J. Fluid Mech.* **657**, 89 (2010).
- ³¹T. Kajishima, "Influence of particle rotation on the interaction between particle clusters and particle-induced turbulence," *Int. J. Heat Fluid Flow* **25**, 721 (2004).
- ³²P. H. Mortensen, H. I. Andersson, J. J. J. Gillissen, and B. J. Boersma, "Dynamics of prolate ellipsoidal particles in a turbulent channel flow," *Phys. Fluids* **20**, 093303 (2008).
- ³³S. Balachandar and J. K. Eaton, "Turbulent dispersed multiphase flow," *Annu. Rev. Fluid Mech.* **42**, 111 (2010).
- ³⁴Y. Li, J. B. McLaughlin, K. Kontomaris, and L. Portela, "Numerical simulation of particle-laden turbulent channel flow," *Phys. Fluids* **13**, 2957 (2001).
- ³⁵S. Elghobashi and G. C. Truesdell, "Direct simulation of particle dispersion in a decaying isotropic turbulence," *J. Fluid Mech.* **242**, 655 (1992).
- ³⁶Q. Wang, K. D. Squires, M. Chen, and J. B. McLaughlin, "On the role of the lift force in turbulence simulations of particle deposition," *Int. J. Multiphase Flow* **23**, 749 (1997).
- ³⁷B. Arcen, A. Tanière, and B. Oesterlé, "On the influence of near-wall forces in particle-laden channel flows," *Int. J. Multiphase Flow* **32**, 1326 (2006).
- ³⁸J. J. J. Gillissen, B. J. Boersma, P. H. Mortensen, and H. I. Andersson, "On the performance of the moment approximation for the numerical computation of fibre stress in turbulent channel flow," *Phys. Fluids* **19**, 035102 (2007).
- ³⁹C. Marchioli, M. Picciotto, and A. Soldati, "Particle dispersion and wall-dependent turbulent flow scales: Implications for local equilibrium models," *J. Turbul.* **7**, 60 (2006).
- ⁴⁰L. H. Zhao and H. I. Andersson, "Statistics of particle suspensions in turbulent channel flow," *Comm. Comp. Phys.* (to be published).
- ⁴¹L. H. Zhao, H. I. Andersson, and J. J. J. Gillissen, "Turbulence modulation and drag reduction by spherical particles," *Phys. Fluids* **22**, 081702 (2010).
- ⁴²J. Kim, P. Moin, and R. Moser, "Turbulence statistics in fully developed channel flow at low Reynolds number," *J. Fluid Mech.* **117**, 133 (1987).
- ⁴³J. K. Eaton and J. R. Fessler, "Preferential concentration of particles by turbulence," *Int. J. Multiphase Flow* **20**, 169 (1994).

Article 6

Two-way coupled simulations of particle-laden wall turbulence

LIHAO ZHAO & H.I. ANDERSSON

*Particles in turbulence 2011 - International Conference on Fundamentals,
Experiments, Numeric and Applications, Potsdam, Germany, 2011.*

Two-way coupled simulations of particle-laden wall turbulence

Lihao Zhao, Helge I. Andersson

Department of Energy and Process Engineering, Norwegian University of Science and Technology, 7491 Trondheim, Norway

lihao.zhao@ntnu.no

Abstract. To study the modulation of shear-flow turbulence by a modest amount of spherical particles suspended in a channel flow, two-way coupled numerical simulations with an Eulerian-Lagrangian point-particle approach are performed. The turbulence is obtained by Direct Numerical Simulation (DNS) in an Eulerian framework while the translational motion of the particles is described by a Lagrangian approach. The particle equations of motion are integrated along with the particle-laden Navier-Stokes equations for the carrier fluid. Since the feedback effect of the particles on the local fluid field is of primary concern, a two-way force-coupling method using a volume-force concept has been implemented in accordance with Newton's third law. Two cases with different particle volume fractions are designed to analyze the influence of solid particles on the fluid turbulence. Comparisons between the particle-laden flows and an unladen channel flow are made. The results demonstrate that the presence of the particles leads to a remarkable increase of the mean bulk velocity provided that the particle loading is sufficiently high. This is equivalent with a drag reduction. Moreover, the streamwise turbulence intensity is augmented in the high loading case whereas the spanwise turbulent intensity and, in particular, the Reynolds shear stress are attenuated compared with the low loading case and the unladen flow. Additionally, the overall turbulence level is damped, the small-scale turbulence seems to have been suppressed and the resulting flow field comprises larger eddies than a clean flow without particles.

1. Introduction

Particle suspension flows have been studied for several decades in both experimental work and numerical simulations [1, 2]. This kind of flows is commonly seen in the environment (e.g. sand storms and volcanic ash) and also in industrial applications, such as fluidized beds. Depending on the purpose of the study and the actual particle mass loading in the flow, one-way, two-way and four-way coupling approaches are used in numerical simulations [3]. One-way coupling is normally employed to study dilute suspension flows while two-way and four-way coupling methods are appropriate to investigate interactions between the fluid and the particles and particle-particle interactions, respectively. By utilizing the two-way coupling approach, the turbulence is observed to be attenuated or augmented depending on the type of particle [4]. In channel flow an increased mean flow velocity has been discovered in the presence of spherical particles in laboratory experiments [5, 6] and some simulation studies have reported on this phenomenon, e.g. Li et al. [7] and Zhao et al. [8]. However, the physical mechanisms involved in the turbulence modulation due to the solid particles are still poorly understood.

The present study aims to investigate the modulations of wall-bounded turbulence caused by the presence of particles. A two-way coupling scheme is implemented in a Navier-Stokes solver by means of a volume-force derived from a point-force approximation. In this paper the alterations of the turbulent properties and instantaneous flow structures are examined with the view to assess the importance of the particle loading.

2. Numerical model and methodology

2.1. Eulerian representation of the fluid flow

We consider the fully-developed turbulent flow in a plane channel. The flow is driven by a constant pressure gradient in the streamwise direction. The motion of the incompressible carrier fluid is governed by the continuity and momentum conservation equations:

$$\nabla \cdot \vec{u} = 0; \quad \rho \left[\frac{\partial \vec{u}}{\partial t} + (\vec{u} \cdot \nabla) \vec{u} \right] = -\nabla p + \mu \nabla^2 \vec{u} + \vec{F}_p \quad (2.1)$$

Here, \vec{u} , ρ and p are the instantaneous fluid velocity vector, density and pressure, respectively, and μ is the dynamic viscosity of the Newtonian fluid. The last term \vec{F}_p represents the force per unit volume from the particles, which becomes essential in the two-way coupled formulation but is absent in one-way coupled simulations. The size of the computational domain is $6h$, h and $3h$ in the streamwise x -direction, the wall-normal y -direction, and the spanwise z -direction, respectively. Periodic boundary conditions are imposed in the homogeneous x - and z -directions and no-slip conditions are enforced at the solid walls at $y = 0$ and $y = h$. A rectangular mesh with 128^3 grid points is used. The Reynolds number Re based on the wall-friction velocity u_τ and the wall-separation distance h is 360.

The computer simulations were performed with the same Navier-Stokes solver as employed by Gillissen *et al.* [9] and Mortensen *et al.* [10], but with the particle force \vec{F}_p implemented in the momentum equations. A pseudo-spectral method using Fourier series in the two homogeneous directions and a second-order finite-difference scheme in the wall-normal direction is employed for the spatial derivatives on a staggered grid system. The time stepping is accomplished with a second-order explicit Adams-Bashforth scheme.

2.2. Lagrangian particle treatment

The particles are represented in a Lagrangian framework in which each and every individual particle is tracked at every time step. The translational motion of the individual spherical particles is affected only by Stokes' drag force, while other forces such as those due to lift and gravity are neglected. The particle Reynolds number $Re_p = 2a|\vec{u} - \vec{v}| \rho / \mu$, based on the particle radius a and the slip velocity between the particle and local fluid is assumed to be smaller than unity in order to justify the assumption of Stokesian flow in the immediate vicinity of the particle. The particle size is smaller than the size of the tiniest turbulent eddies, i.e. a is smaller than the Kolmogorov length scale. The force from the fluid on a particle can then be simply treated as a point force:

$$\vec{f}_i(\vec{x}_p) = 6\pi\mu a \left[\vec{u}(\vec{x}_p, t) - \vec{v} \right] \quad (2.2)$$

Here, \vec{u} is the fluid velocity evaluated at the particle location \vec{x}_p and \vec{v} is the velocity of the particle. The translational motion of a given particle can thus be obtained from Newton's law of motion:

$$\frac{d\vec{v}}{dt} = \frac{1}{\tau} \left[\vec{u}(\vec{x}_p, t) - \vec{v} \right]; \quad \frac{d\vec{x}_p}{dt} = \vec{v}. \quad (2.3)$$

Here, the particle response time τ can be expressed as

$$\tau = \frac{2\rho D a^2}{9\mu} \quad (2.4)$$

where $D = \rho_p/\rho$ is the density ratio between the particle and fluid densities.

The Lagrangian particle equations (2.3) are integrated forward in time along with the integration of the Eulerian equation (2.1) for the fluid motion. According to the Newton's third law, each and every particle acts back onto the local fluid with a point force $-\vec{f}_i(\vec{x}_p)$. The feedback from the n_p particles within a given grid cell volume V_{cell} adds up to:

$$\vec{F}_p = -\frac{1}{V_{cell}} \sum_{i=1}^{n_p} \vec{f}_i(\vec{x}_p) \quad (2.5)$$

This is the force per unit volume in the particle-laden Navier-Stokes equation (2.1). This point-force approach to two-way coupled simulations is essentially the same as that followed by Squires & Eaton [11] in the simulation of isotropic turbulence and also Li *et al.* [7], Dritselis & Vlachos [12] and Zhao *et al.* [8] for particle-laden turbulent channel flow simulations.

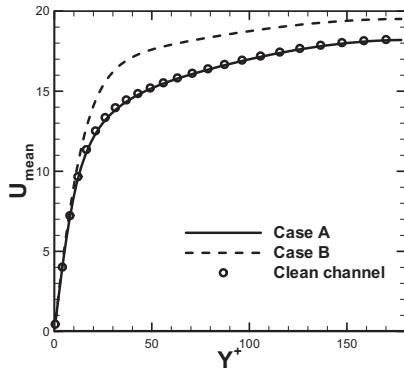
3. Results

Results from simulations with two different particle loadings will be compared in this section with the view to demonstrate the importance of the loading. The particle parameters in the two simulations are the same, see Table 1, except that the number of particles N_p in Case B is 40 times higher than in Case A. These numbers correspond to volume fractions $9.3 \cdot 10^{-4}$ and $2.3 \cdot 10^{-5}$, respectively. $Re = 360$ and the particle response time is 30 times the viscous time scale in both cases.

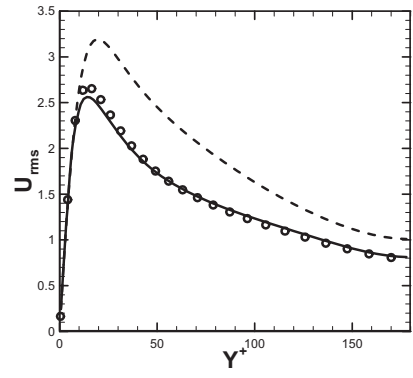
The mean flow velocity profile, the turbulence intensities and the Reynolds shear stress are shown in Fig. 1. It is immediately observed that the flow field and turbulence statistics are practically unaffected by the solid particles in Case A with modest particle loading. The data are almost indistinguishable from the results from the unladen channel flow simulation. Second, in Case B with a substantially higher loading of the same particles, the mean velocity has been increased, in accordance with the laboratory measurements by Sato & Hishida [13] and the computer experiments by Li *et al.* [7] and Zhao *et al.* [8]. The turbulence field has also been severely affected. The streamwise turbulence intensity is augmented whereas the velocity fluctuations in the spanwise and wall-normal directions have been damped, along with a substantial attenuation of the Reynolds shear stress in Fig. 1(e). The same increased turbulence anisotropy was reported by Zhao *et al.* [8].

Table 1 Particle properties for two different two-way coupled simulations

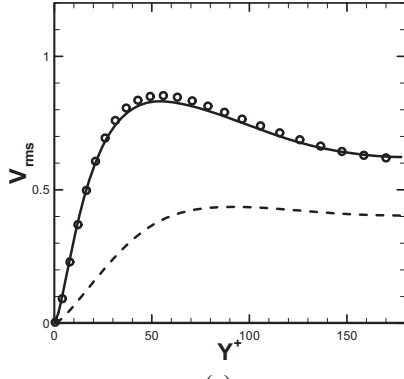
Case	N_p	τ^+	ρ_p / ρ	a^+
A	10^5	30	1041	0.36
B	$4 \cdot 10^6$	30	1041	0.36



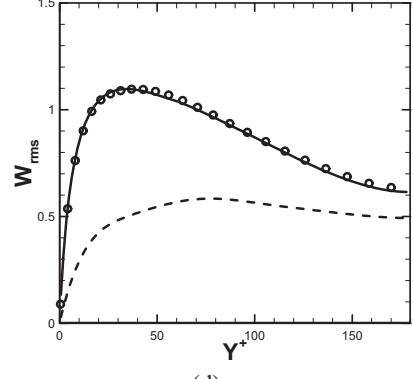
(a)



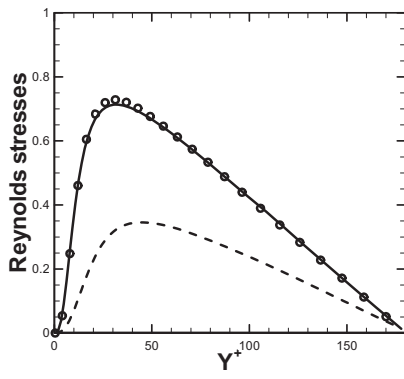
(b)



(c)



(d)



(e)

Figure 1. Comparison between the unladen channel flow (\circ) and particle-laden flows (— Case A and - - Case B). (a) Mean velocity distribution; (b) Velocity fluctuations in streamwise; (c) Velocity fluctuations in wall-normal; (d) Velocity fluctuations in spanwise; (e) Reynolds shear stress.

Let us now examine in some detail the fluid and particle motions at one arbitrarily chosen instant of time. The cross-sectional views in Figure 2 give a visual impression of the particle-laden channel flow. The uneven distribution of the particles, known as *preferential concentration*, is readily seen in Figure 2(a). Densely populated areas coincide with ejections of low-speed fluid away from the channel walls, for instance at $Z \approx 0.9, 2.0,$ and 2.6 along the lower wall and the exceptionally strong ejection at $Z \approx 0.5$ away from the upper wall. Such events are characterised by fluid velocities being below the average at a particular wall-distance. Recall that $Y = 0.1$, for instance, corresponds to $y^+ = 36$, i.e. the innermost part of the logarithmic law-of-the-wall.

The topology of the turbulent flow field suggests that the small-scale eddies have been suppressed and the resulting flow field thus comprises larger eddies than an unladen flow. The instantaneous particle distribution reflects the large-scale structure of the flow and local void areas seem to coincide with areas where the streamwise fluid velocity component u_x is below its average. Besides the near-wall regions and the ejection events, the highest particle densities are found in areas with locally high streamwise fluid velocities. The streamwise particle velocity v_x depicted in Figure 2(b) also attains high values in areas where the streamwise fluid velocity is above its average. It is noteworthy that negative values of neither u_x nor v_x have been observed.

Fig. 2(c) shows the same particle distribution as in Fig. 2(b), but now with a colour-coding which represents the wall-normal component of the particle velocity. Besides the near-wall regions where v_y generally attains low values, densely populated clusters of particles move either towards the upper ($v_y > 0$) or lower ($v_y < 0$) walls. Such collective particle motions are apparently caused by large-scale eddies which carry the particles for a certain while.

The streamwise component of the instantaneous Stokes force $\vec{f}_i(\vec{x}_p)$ on the particles is shown in Fig. 2(d). In practice, the Stokes force for all particles inside a given grid volume were summed up and the resulting force divided by the grid cell volume, as in eq. (2.5). The Stokes drag is generally fairly modest over most of the cross-section, except in the near-wall region, say within $y^+ \approx 30$, and further away from the walls around strong ejections. It is noteworthy that f_x is negative almost everywhere in the innermost wall-layers. Thus, since the dominating contribution to the work of the particles on the fluid is proportional to $-f_x \cdot u_x$, we can conclude that the particles exert work on the fluid flow in the near-wall layers.

Comparably high positive and negative values of the Stokes force are only occasionally observed further away from the walls. These localised areas of high Stokes forces almost always coincide with the ejection events. Zones with $f_x > 0$ associated the ejections imply that the fluid flow exerts work on the particles since $f_x \cdot v_x$ attains large positive values. This suggests that the high contour levels in Fig. 2(d) identify local regions where the energy exchange rate is relatively higher than elsewhere. Moreover, the exchange of kinetic energy between the fluid flow and the suspended particles are distinctly different in the near-wall region and the core region of the channel flow.

4. Summary

In the present paper we have examined the effect of particle loading on the ability of tiny solid particles to modulate the turbulent flow field in a wall-bounded shear flow. The study was motivated by earlier computational studies which showed rather different and apparently contradictory results. A particle-laden turbulent channel flow was simulated in an Eulerian-Lagrangian approach at a frictional Reynolds number 360. A finite number of inertial point particles were released randomly and their equations of motion were integrated along with the particle-laden Navier-Stokes equation. A two-way force-coupling scheme using the volume-force method was employed to account for the feedback of the particles onto the local fluid flow. Only the Stokes drag force was considered in the present study.

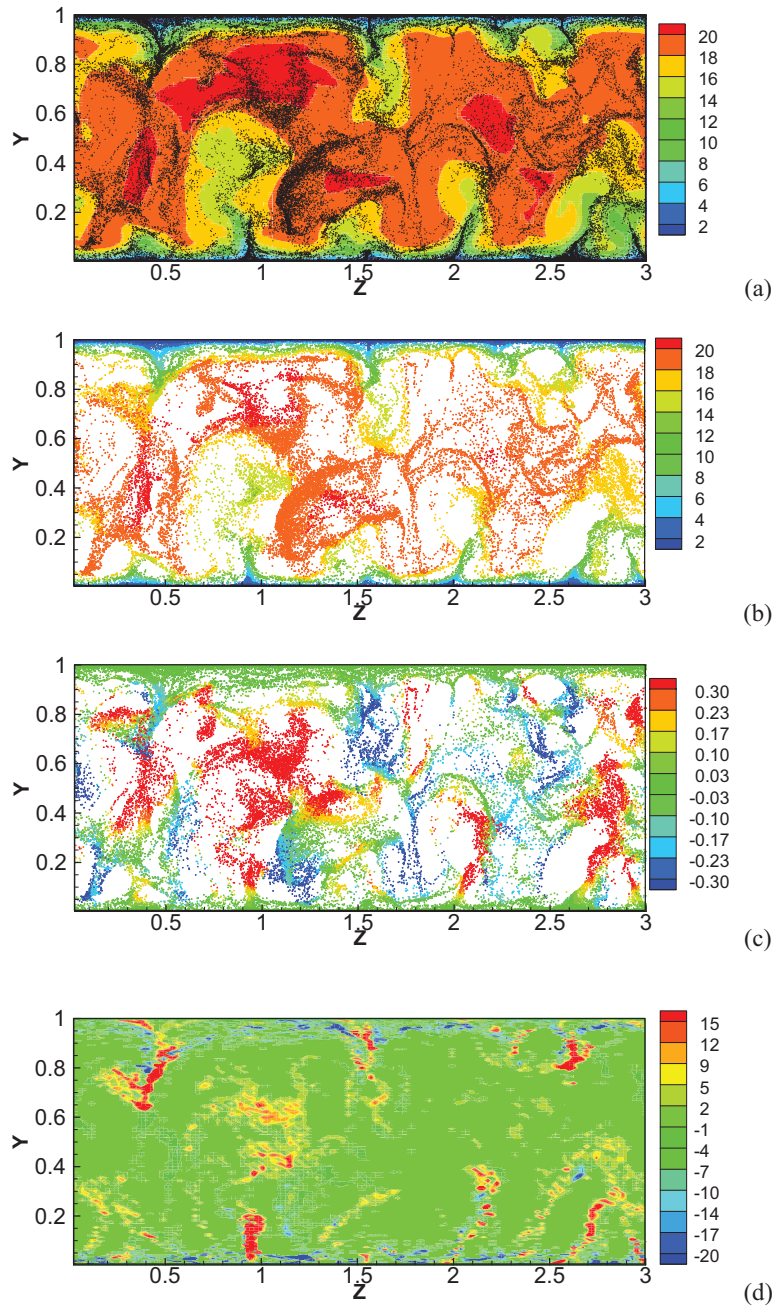


Figure 2. Instantaneous view over the entire channel cross-section (not to scale) for Case B. (a) Contours of the streamwise fluid velocity component u_x ; (b) streamwise particle velocities v_x ; (c) wall-normal particle velocities v_y ; (d) Stokes drag force in the streamwise direction f_x .

Only negligible differences from the unladen flow field were observed at the lowest particle loading. When the volume fraction was increased by a factor 40, the streamwise velocity fluctuations were augmented whereas the turbulent fluctuations in the spanwise and wall-normal directions were attenuated. Such modulations have also been observed in turbulent channel flow with fiber-like additives [9, 14]. Another distinct effect of the particles on the flow field is the increase of the mean velocity in the channel relative to that observed in the unladen flow. Since the unladen and the particle-laden flows were driven by exactly the same streamwise pressure-gradient, the excess mean velocity is equivalent with drag reduction. A higher anisotropy of the turbulence field has also been observed in conjunction with rather different drag-reduction schemes.

The inertial particles are partially driven by the large-eddy motion which is characterized by a larger time scale than the small-scale turbulence. The effective Stokes number is therefore lower than 30. The suspended particles exert mechanical work on the fluid flow in the innermost wall-regions. Around strong ejections the particle works on the fluid. These findings suggest that kinetic energy is transferred from the fluid to the particles in the logarithmic part of the wall-layer and from the particles to the fluid in the viscous and buffer layers.

Acknowledgments

The present work has been supported by A/S Norske Shell through a research fellowship (contract no. 4610020178/C08156) and by The Research Council of Norway (Programme for Supercomputing) through a grant of computing time.

References

- [1] M. Rashidi, G. Hetsroni and S. Banerjee, *Int. J. Multiphase Flow* **16**, 935-949 (1990).
- [2] Y. Pan and S. Banerjee, *Phys. Fluids* **8**, 2733-2755 (1996).
- [3] S. Elghobashi, in *IUTAM Symposium on Computational Approaches to Multiphase Flow*. **81**, S. Balachandar and A. Prosperetti, Eds.: Springer Netherlands, 3-10 (2006).
- [4] J.K. Eaton, *Int. J. Multiphase Flow* **35**, 792-800 (2009).
- [5] G. Gust, *J. Fluid Mech.* **75**, 29-47 (1976).
- [6] H.A.A. Bari and R.B.M. Yunus, *Asian J. Ind. Eng.* **1**, 1-11 (2009).
- [7] Y. Li, J.B. McLaughlin, K. Kontomaris and L. Portela, *Phys. Fluids* **13**, 2957-2967 (2001).
- [8] L.H. Zhao, H.I. Andersson and J.J.J. Gillissen, *Phys. Fluids* **22**, 081702 (2010).
- [9] J.J.J. Gillissen, B.J. Boersma, P.H. Mortensen and H.I. Andersson, *Phys. Fluids* **19**, 115107 (2007).
- [10] P.H. Mortensen, H.I. Andersson, J.J.J. Gillissen and B.J. Boersma, *Phys. Fluids* **19**, 078109 (2007).
- [11] K.D. Squires and J.K. Eaton, *Phys. Fluids A* **2**, 1191-1203 (1990).
- [12] C.D. Dritselis and N.S. Vlachos, *Phys. Fluids* **20**, 055103 (2008).
- [13] Y. Sato and K. Hishida, *Int. J. Heat Fluid Flow* **17**, 202-210 (1996).
- [14] C.M. White and M.G. Mungal, *Annu. Rev. Fluid Mech.* **40**, 235-256 (2008).

Article 7

On particle stress in gas-solid channel flows

LIHAO ZHAO & H.I. ANDERSSON

In preparation for submission.

Is not included due to copyright

Article 8

Interphasial energy transfer and particle dissipation in particle-laden wall turbulence.

LIHAO ZHAO, H.I. ANDERSSON & J.J.J. GILLISEN

Submitted to *Journal of Fluid Mechanics*, 2011.

Interphasial energy transfer and particle dissipation in particle-laden wall turbulence

Lihao Zhao¹, Helge I. Andersson¹ and Jurriaan J.J. Gillissen²

1. Department of Energy and Process Engineering, Norwegian University of Science and Technology, 7491 Trondheim, Norway

2. Department of Multi-Scale Physics, TU Delft, 2628 BW Delft, The Netherlands

Abstract

Transfer of mechanical energy between particle additives and a carrier fluid has been explored by two-way coupled direct numerical simulations. The inertial particles have been treated as individual point-particles in a Lagrangian framework and their feedback on the fluid phase is incorporated in the particle-laden Navier-Stokes equations. Three different particle suspensions were simulated in order to examine the effect of particle loading on channel-flow turbulence and it was observed that the modulation of the turbulence field increased non-linearly with the number of particles. Simulations with three different particle response times showed that the Reynolds shear stress and the turbulence intensities in the spanwise and wall-normal directions were attenuated whereas the velocity fluctuations were augmented in the streamwise direction. These observations were crucially dependent on the particle response time in the range from 5 to 50 viscous time units.

The physical mechanisms involved in the particle-fluid interactions were analyzed in detail for one of the particle classes. It was observed that the fluid transferred energy to the particles in the core region of the channel whereas the fluid received kinetic energy from the particles in the wall region. Locally an imbalance in the work performed by the particles on the fluid and the work exerted by the fluid on the particles was observed. This imbalance gave rise to a particle-induced energy dissipation which represents a loss of mechanical energy from the fluid-particle suspension. An independent examination of work associated with the different directional components of the Stokes force revealed that the dominating energy transfer was associated with the streamwise component. The streamwise turbulence intensity was enhanced in the buffer region due to work performed by the particles on the local fluid. Both the mean and fluctuating parts of the Stokes force promoted streamwise fluctuations in the near-wall region. The kinetic energy of the flow field in a cross-sectional plane was damped due to work done by the particles, and the energy was dissipated rather than recovered as particle kinetic energy. This explained the significant damping of the cross-plane velocity components. Novel component-wise scatter plots of instantaneous velocity versus instantaneous slip velocity provided further insight into the energy transfer mechanism beyond that of the statistical data. The observed modulations of the turbulence field could be thereby completely understood.

1. Introduction

Particle-laden flows are commonly seen in our local environment and are also of crucial importance in many engineering applications. Turbulent flows of particle suspensions have been extensively studied during the past decades with a variety of different motivations. Either attenuation or augmentation of the turbulent kinetic energy in the presence of solid particles has been observed in both experiments and numerical simulations. Rashidi *et al.* (1990) performed measurements with two different sizes of polystyrene particles in wall turbulence and observed that the larger particles increase the number of wall ejections and also enhance the Reynolds shear stress. On the other hand, the smallest particles have the opposite effects on the turbulence. Kulick *et al.* (1994) conducted experiments in a vertical downward channel flow with small heavy particles. Their data indicated that the degree of turbulence attenuation increased with the Stokes number and the mass loading of the particles. From their experimental study Hussainov *et al.* (2000) also reported an attenuation of the turbulence intensity as well as a reduction of the energy density at high frequencies in the presence of small glass beads. In two-way coupled numerical simulations Squires & Eaton (1990), Elghobashi & Truesdell (1993) and Truesdell & Elghobashi (1994) focused on the turbulence modulation in homogeneous *isotropic* turbulence. Squires & Eaton (1990) observed an increase of the dissipation rate in the presence of tiny particles and the attenuation of the turbulent kinetic energy increased with higher mass loadings. Numerical studies have also explored particle dynamics and transport in wall-bounded turbulence. Pan & Banerjee (1996) carried out two-way coupled simulations by means of direct numerical simulations (DNS) and their results revealed a suppression of the sweeps by the smaller particles and an enhancement of sweep activity by the larger particles. Yamamoto *et al.* (2001) performed a large-eddy simulation (LES) of turbulent gas-particle flow in a vertical channel with four-way coupling and obtained good agreement with the experimentally observed attenuation of the turbulence for small Stokes numbers. Li *et al.* (2001) performed two-way coupled DNSs and found an increased flow rate in the presence of small particles as well as an enhancement of the velocity fluctuations in the streamwise direction, whereas the turbulence intensities in the two other directions were damped. Both two-way and four-way coupled simulations of particle-laden pipe flow were conducted by Vreman (2007). Various different aspects of particle-laden wall-bounded turbulence have been considered. Dritselis & Vlachos (2008, 2009), for instance, focused on the coherent structure around the wall region and found that the diameter and the streamwise extent of the mean vortices were increased due to the momentum exchange between the particles and fluid. More recently Bijlard *et al.* (2010) studied the topology of the local flow around solid particles and observed that the turbulent flow became more two dimensional in the viscous sublayer in two-way coupled simulations due to the feedback from the particles on the local fluid.

According to earlier findings it seems that tiny inertial particles tend to attenuate the turbulent kinetic energy whereas larger particles enhance the turbulent energy. Even in dilute particle suspensions, several different factors may contribute to the attenuation or augmentation of the fluid turbulence. These physical mechanisms include the kinetic energy transfer between the particles and fluid, the extra dissipation induced by the particles, and the wake formation and eventual vortex shedding behind the particles. Gore & Crowe (1989) proposed a dimensionless parameter, i.e. the ratio of the particle diameter to a characteristic size of large eddies, to distinguish between augmentation and attenuation of the turbulence. In a more recent work by Tanaka & Eaton (2008) a novel dimensionless parameter is introduced, the so-called particle moment number, in order to categorize the turbulence modulations. Furthermore, as discussed also by Balachandar & Eaton (2010), turbulence attenuation may occur when the particle inertia increases or when there is an increase of dissipation from the flow passing the particles or if the effective viscosity of the suspension is enhanced. On the contrary, the formation of a wake and vortex shedding behind the particles can lead to an increased turbulence level and this happens typically when the particle Reynolds number is above a few hundred.

In spite of the many earlier studies on particle-laden turbulent flows, the underlying physical mechanisms of the turbulence attenuation in the presence of tiny particles are still not fully comprehended. The point-particle two-way coupled method implemented both in DNS or LES codes enables a close look into the interaction processes between the point particles and the surrounding fluid. Such two-way coupled simulations of turbulent channel and pipe flows have been carried out, for instance, by Pan *et al.* (1996), Li *et al.* (2001), Rani *et al.* (2004) and Zhao *et al.* (2010) but with rather different focuses.

In the present computational study of particle-laden channel flow, we therefore focus on the interactions between the turbulence and the inertial point-particles in a turbulent channel flow. Two-way coupled point-particle Eulerian-Lagrangian DNS simulations will be performed. The size of particles is smaller than the smallest eddies in the turbulence. Five different simulations are performed with the view to study the influence of the particle characteristics, i.e. particle volume fraction and particle response time, on the particle-turbulence interactions. Data from one of the simulations are further analyzed in order to explore the kinetic energy exchange between the particles and local fluid as well as the extra energy dissipation caused by the particles. The mechanical energy exchanged between the two phases are examined by means of instantaneous data in a cross-sectional plane, long-time averages of the transferred power, as well as scatter plots of the involved flow variables. This novel approach enables us to pinpoint the different roles of the streamwise and cross-sectional components of the fluctuating slip velocity vector.

2. Mathematical model and methodology

2.1 Eulerian fluid representation

Turbulent channel flow is studied by means of DNS of the particle-laden Navier-Stokes equations in an Eulerian frame of reference. The motion of the incompressible and isothermal fluid is governed by the mass and momentum conservation equations:

$$\nabla \cdot \vec{u} = 0; \quad \rho \left[\frac{\partial \vec{u}}{\partial t} + (\vec{u} \cdot \nabla) \vec{u} \right] = -\nabla p + \mu \nabla^2 \vec{u} + \vec{f}^P \quad (2.1)$$

where, \vec{u} and p are the instantaneous fluid velocity vector and pressure, respectively. The flow is driven by a constant mean pressure gradient ∇p in the streamwise x -direction. In two-way coupled simulations, the last term \vec{f}^P is added in the momentum equation and represents the feedback force per unit volume due to the presence of the particles. Moreover, ρ and μ are the density and dynamic viscosity of the Newtonian carrier fluid. The present simulations were performed with the same Navier-Stokes solver as used by Gillissen *et al.* (2008), Zhao *et al.* (2010) and Zhao and Andersson (2011). A pseudo-spectral method, Fourier series in the homogeneous directions and a second-order finite-difference scheme in the wall-normal direction, is employed for the spatial derivatives on a staggered Cartesian grid system. The time advancement is carried out with a second-order explicit Adams-Bashforth scheme.

2.2 Lagrangian particle dynamics

The particles in the flow are represented by means of the Lagrangian point-particle approach; see e.g. Balachandar & Eaton (2010). Each individual particle is tracked at every time step of the DNS, i.e. the particle velocity and the particle position are altered in accordance with Newtonian dynamics and kinematics. The translational motion of the individual spherical particles is only affected by the Stokes drag force in present work, while other forces, such as gravity, lift and virtual-mass forces, are neglected. The size of the particles is smaller than the smallest eddy scales in the flow field and, consequently, the force on particle can be simply treated as a point force. The Stokes drag force on a given particle with radius a is expressed as:

$$\vec{F} = 6\pi\mu a \left[\vec{u}(\vec{x}_p, t) - \vec{v} \right] \quad (2.2)$$

where \vec{u} is the local fluid velocity evaluated at the particle location \vec{x}_p at time t and \vec{v} is the velocity of the particle. The local fluid information, e.g. the local fluid velocity, is obtained by interpolation using discrete velocity data in the surrounding

27 grid points onto the particle position \vec{x}_p . The position of a particle and its velocity can be obtained by:

$$\frac{d\vec{x}}{dt} = \vec{v} ; \quad \frac{d\vec{v}}{dt} = \frac{1}{\tau} [\vec{u}(\vec{x}_p, t) - \vec{v}], \quad \tau = \frac{2\rho D a^2}{9\mu} \quad (2.3)$$

where τ is the particle response time and $D = \rho_p/\rho$ is the density ratio between the particles and the fluid.

The Lagrangian particle eq. (2.3) is integrated forward in time with the same time step as the Eulerian fluid eq. (2.1) in the course of the simulation. According to Newton's third law, each and every particle acts back onto the local fluid with a point force $-\vec{F}_l$.

The feedback force on the fluid from n_p particles within a given cell volume V_{cell} can be added up as:

$$\vec{f}^p = -\frac{1}{V_{cell}} \sum_{l=1}^{n_p} \vec{F}_l \quad (2.4)$$

This is the expression of force per unit volume which is shown in momentum eq. (2.1). This two-way coupled scheme in the point-particle approach is essentially the same as that followed by Squires & Eaton (1990) in the simulation of isotropic turbulence and later by Li *et al.* (2001), Picciotto *et al.* (2006), Dritselis & Vlachos (2008) and Zhao *et al.* (2010) for particle-laden turbulent channel flows.

3. Kinetic energy transfer, conversion and dissipation

The transfer of kinetic energy between the particle phase and the fluid phase in particle-laden flow is of primary concern in the present work. A mathematical analysis of the relationship between the work done by particles on the surrounding fluid and the work by the local fluid on the particles is provided in this section. The outcome of the analysis will be used in the interpretation of the results of the DNSs.

The mechanical work done by a force on an object is the dot product of the force vector and the displacement vector. In two-way coupled simulations, the only linkage between the fluid and the particles is the Stokes drag force as given in eq. (2.2) and the reaction force in eq. (2.4). Based on Newton's third law, the point force on particles \vec{F} and the force on the local fluid $-\vec{F}$ always have the same magnitude but opposite signs. The work W^p done by the local fluid to move a particle a distance $\vec{L}^p = \vec{v}dt$ during one time step dt can be expressed as:

$$W^p = \vec{F} \cdot \vec{L}^p = \vec{F} \cdot \vec{v}dt = 6\pi\mu a [\vec{u}(\vec{x}_p, t) - \vec{v}] \cdot \vec{v}dt . \quad (3.1)$$

The time rate of the work, i.e. the power, is denoted by a dot and is thus defined as $\dot{W}^P = W^P / dt$. In order to distinguish between the power associated with motions in different directions, the subscript β is introduced to identify a particular coordinate direction. The power associated with the motion in the β -direction can be written as:

$$\dot{W}_\beta^P = 6\pi\mu\alpha[u_\beta - v_\beta]v_\beta = \alpha[u_\beta - v_\beta]v_\beta . \quad (3.2)$$

The usual summation convention does not apply for repeated Greek indices. The constant coefficient $\alpha = m_p / \tau = 6\pi\mu\alpha$ is introduced to simplify the expressions. α is defined as the ratio between the particle mass and the particle response time and is thus expressed in kg/sec. In a given case \dot{W}^P is only dependent on the particle velocity and the slip velocity between particle and local fluid. The simple quadrant analysis distinguishes between negative and positive power as below:

$$\begin{aligned} 1. & \begin{cases} (u_\beta - v_\beta) > 0 \\ v_\beta > 0 \end{cases} \rightarrow \dot{W}_\beta^P > 0. \\ 2. & \begin{cases} (u_\beta - v_\beta) > 0 \\ v_\beta < 0 \end{cases} \rightarrow \dot{W}_\beta^P < 0. \\ 3. & \begin{cases} (u_\beta - v_\beta) < 0 \\ v_\beta < 0 \end{cases} \rightarrow \dot{W}_\beta^P > 0. \\ 4. & \begin{cases} (u_\beta - v_\beta) < 0 \\ v_\beta > 0 \end{cases} \rightarrow \dot{W}_\beta^P < 0. \end{aligned} \quad (3.3)$$

Positive power \dot{W}^P means that the local fluid exerts work on the particle, whereas $\dot{W}^P < 0$ implies that the work performed by the fluid on the particles is negative. This scheme will be used to explore the exchange of mechanical energy between the particle phase and the fluid phase.

Similarly, the work W^f done by a particle to move the local fluid a distance $\vec{L}^f = \vec{u}dt$ during one time step is:

$$W^f = -\vec{F}(\vec{x}_p) \cdot \vec{L}^f = -\vec{F}_i(\vec{x}_p) \cdot \vec{u}(\vec{x}_p, t)dt = -6\pi\mu\alpha[\vec{u}(\vec{x}_p, t) - \vec{v}] \cdot \vec{u}(\vec{x}_p, t)dt \quad (3.4)$$

The associated power $\dot{W}^f = W^f / dt$ becomes:

$$\dot{W}_\beta^f = -6\pi\mu\alpha[u_\beta - v_\beta]u_\beta = -\alpha[u_\beta - v_\beta]u_\beta. \quad (3.5)$$

Once again, we can distinguish between motions that give rise to positive and negative power supply:

$$\begin{aligned} 1. & \begin{cases} (v_\beta - u_\beta) > 0 \\ u_\beta > 0 \end{cases} \rightarrow \dot{W}_\beta^f > 0. \\ 2. & \begin{cases} (v_\beta - u_\beta) > 0 \\ u_\beta < 0 \end{cases} \rightarrow \dot{W}_\beta^f < 0. \\ 3. & \begin{cases} (v_\beta - u_\beta) < 0 \\ u_\beta < 0 \end{cases} \rightarrow \dot{W}_\beta^f > 0. \\ 4. & \begin{cases} (v_\beta - u_\beta) < 0 \\ u_\beta > 0 \end{cases} \rightarrow \dot{W}_\beta^f < 0. \end{aligned} \quad (3.6)$$

The sum of \dot{W}^f and \dot{W}^P represents the net loss or gain of mechanical energy per unit time. By summing up the over all three coordinate directions, we obtain:

$$\dot{W}^f + \dot{W}^P = -\alpha(\vec{u} - \vec{v}) \cdot (\vec{u} - \vec{v}) \equiv -\varepsilon^P \leq 0. \quad (3.7)$$

The sum is always negative which implies that mechanical energy is continuously drained from the fluid-particle suspension due to fluid-particle interactions. The drainage of mechanical energy, or more specifically the loss of kinetic energy, can be interpreted as *particle dissipation* ε^P . The particle dissipation is unconditionally positive, irrespective of whether mechanical energy is transferred from the particles to the fluid or vice versa. This extra dissipation plays an important role in turbulence modulations and can possibly lead to a reduction of the turbulent kinetic energy of the carrier fluid in the spanwise and wall-normal directions and an attenuation of particle fluctuation in streamwise direction, as will be shown in next section.

To facilitate the further analysis, the Reynolds decomposition is introduced. The instantaneous fluid and particle velocity components are decomposed in mean (\bar{u}, \bar{v})

and fluctuating (\tilde{u}, \tilde{v}) parts. Let us first introduce this decomposition in eq. (3.2) for power transferred to the particles. After averaging (denoted by an overbar), we obtain:

$$\begin{aligned} \overline{\dot{W}_\beta^P} &= \alpha \overline{[(U_\beta + \tilde{u}_\beta) - (V_\beta + \tilde{v}_\beta)](V_\beta + \tilde{v}_\beta)} \\ &= \alpha \left[\underbrace{(U_\beta - V_\beta)V_\beta}_I + \underbrace{(U_\beta - V_\beta)\tilde{v}_\beta + (\tilde{u}_\beta - \tilde{v}_\beta)V_\beta}_{=0} + \underbrace{(\tilde{u}_\beta - \tilde{v}_\beta)\tilde{v}_\beta}_{II} \right] \end{aligned} \quad (3.8)$$

Here, the first term (I) results from work performed by the mean Stokes force on the particles whereas the last term (II) stems from work done by the fluctuating part of the Stokes force. If $\overline{\dot{W}}_\beta^P$ is computed directly in the course of a simulation, term (II) can be obtained by subtraction of term (I). In a fully developed plane channel flow where the flow field and the particle concentration have reached a statistically steady state, the first term makes a contribution only in the streamwise direction. In the wall-normal and spanwise directions, only term (II) is responsible for the power transfer.

When the same decomposition is introduced into the expression (3.5) for the power supplied to the fluid by a particle, we obtain:

$$\begin{aligned}\overline{\dot{W}}_\beta^f &= -\alpha \overline{[(U_\beta + \tilde{u}_\beta) - (V_\beta + \tilde{v}_\beta)](U_\beta + \tilde{u}_\beta)} \\ &= -\alpha \left[\underbrace{(U_\beta - V_\beta)U_\beta}_I + \underbrace{(U_\beta - V_\beta)\tilde{u}_\beta + (\tilde{u}_\beta - \tilde{v}_\beta)U_\beta}_{=0} + \underbrace{(\tilde{u}_\beta - \tilde{v}_\beta)\tilde{u}_\beta}_{II} \right]\end{aligned}\quad (3.9)$$

This expression can be interpreted in the same manner as eq. (3.8).

The Reynolds-averaged particle-induced dissipation can now be obtained either by introduction of the Reynolds decomposition in eq. (3.7) or simply by adding $\overline{\dot{W}}_\beta^f$ and $\overline{\dot{W}}_\beta^P$. In any case we find that

$$\overline{\varepsilon}_\beta^P = -\left(\overline{\dot{W}}_\beta^f + \overline{\dot{W}}_\beta^P\right) = \alpha \left[\underbrace{(U_\beta - V_\beta)(U_\beta - V_\beta)}_I + \underbrace{(\tilde{u}_\beta - \tilde{v}_\beta)(\tilde{u}_\beta - \tilde{v}_\beta)}_{II} \right] \geq 0. \quad (3.10)$$

This expression shows that both the mean and fluctuating parts of the slip velocity contributes to the energy dissipation. Moreover, the slip velocity in all three coordinate directions contributes to the total mean dissipation, i.e.

$$\overline{\varepsilon}^P = \overline{\varepsilon}_x^P + \overline{\varepsilon}_y^P + \overline{\varepsilon}_z^P = \alpha \left[\underbrace{(\vec{U} - \vec{V}) \cdot (\vec{U} - \vec{V})}_I + \underbrace{(\vec{\tilde{u}} - \vec{\tilde{v}}) \cdot (\vec{\tilde{u}} - \vec{\tilde{v}})}_{II} \right] \quad (3.11)$$

The results derived in this Section will be used to analyze the statistics which results from the computer simulations. Although the preceding considerations were made only for a single particle, for which the coefficient α is given, the expressions above are valid for any finite number of particles provided that α is multiplied by the local number of particles.

4. Results

Table 1. Particle properties in the five different simulations all with $Re^* = 360$. N_p is the particle number; ϕ_p is the volume fraction and the superscript + refers to normalization with viscous units. Some primary statistics deduced from Case C were presented by Zhao et al. (2010).

Case	N_p	ϕ_p	τ^+	D	a^+
A	10^5	$2.9 \cdot 10^{-5}$	30	1041	0.36
B	10^6	$2.9 \cdot 10^{-4}$	30	1041	0.36
C	$4 \cdot 10^6$	$1.16 \cdot 10^{-3}$	30	1041	0.36
D	$5 \cdot 10^6$	$0.93 \cdot 10^{-3}$	5	174	0.36
E	$5 \cdot 10^6$	$1.16 \cdot 10^{-3}$	50	1736	0.36

Five sets of particles (see Table 1) were simulated with various particle numbers and different particle response times in a fully developed channel flow at a friction Reynolds number $Re^* = 360$ based on the distance h between the parallel walls. The size of the computational domain is $6h$ and $3h$ in the streamwise x -direction and spanwise z -direction, respectively. The particle-laden Navier-Stokes equation (2.1) was discretized on 128^3 grid nodes. Periodic boundary conditions were imposed in the homogeneous directions and no-slip and impermeability boundary conditions were enforced at the solid walls ($y = 0$ and $y = h$).

Statistical results from Cases A, B and C, i.e. with three different particle loadings, will be compared in order to demonstrate the importance of the loading on turbulent modulations. Furthermore, Cases C, D and E with different particle response times but similar volume fractions were designed to investigate how the particle response time influences the turbulent flow. These parameter studies are presented in Sec. 3.1.

To obtain further details concerning fluid-particle interactions, the typical case C is focused on to explain the mechanisms of turbulence modifications by analyzing the kinetic energy transfer between fluid and particles in Sec. 3.2. Finally, scatter plots are introduced in Section 3.3 as a novel means of inspecting the influence of the slip flow on the kinetic energy transfer and energy dissipation.

4.1 The effect of particle volume fraction and particle response time

Firstly, it is immediately observed that the fluid flow field and the turbulence statistics are practically unaffected by the presence of the solid particles in Case A with modest particle loading. The data is almost indistinguishable from the results in the unladen channel flow simulation. This is consistent with earlier observations by Picciotto *et al.* (2006) from a simulation with the same number of particles. Secondly, in Case B and C with substantially higher loadings of the same particles, the mean velocity have increased at the constant driving pressure gradient. This is in accordance with the laboratory measurements by Rossetti & Pfeffer (1972) and the computer experiments by Zhao *et al.* (2010). The turbulence field has also been severely affected. The streamwise turbulence intensity is augmented whereas the velocity fluctuations in the spanwise and wall-normal directions have been damped, along with a substantial attenuation of the Reynolds shear stress in Fig. 1(f). It is noteworthy that only modest changes are observed when the number of particles is increased from 0.1 to 1.0 millions, whereas major changes occur when the N_P is further increased to $4 \cdot 10^6$.

The effect of the particle response time τ^+ is shown in Figure 2. Results from the three particle sets of Case C, D and E with different τ^+ -values are compared with statistics from an unladen channel flow. Firstly, an interesting finding here is that the modulations of the turbulence field by the particles are selectively depending on the response time. In Case D with modest response time $\tau^+=5$ no noticeable changes are observed in the mean streamwise velocity profile and streamwise turbulence intensity, even though the particle volume fraction is almost as high as in Cases C and E. Nevertheless, the velocity fluctuations in the spanwise and wall-normal directions are attenuated and so is the Reynolds shear stress. Secondly, the other two sets of particles with larger inertia, i.e. Cases C and E, exhibit a substantial impact on the mean velocity profile as well as on the turbulence intensities and the Reynolds stress. These effects are most pronounced in Case E with the most inertial particles.

In one-way coupled simulations by Zhao & Andersson (2012) the particles fluctuated less vigorously than the fluid in the spanwise and wall-normal direction, whereas the streamwise agitation of the particles exceeded the streamwise turbulence intensity. With inclusion of particle-turbulence interactions in the two-way coupled simulations presented herein, the particles tend to enhance the streamwise fluid velocity fluctuations and correspondingly reduce the spanwise and wall-normal fluctuations. In Case D, the modulations of flow field occurred only in the spanwise and wall-normal directions whereas the streamwise fluctuations were left unaffected. This is because two independent mechanisms of particle-fluid interactions exist, which apparently plays different roles in different directions. These two mechanisms of turbulence attenuation or augmentation will be explored in terms of transfer of kinetic energy between the particle and fluid phases and the extra energy dissipation in the following Sections. At this stage we can conclude that the modulation on turbulence is largely dependent on the particle inertia and caused by two different mechanisms.

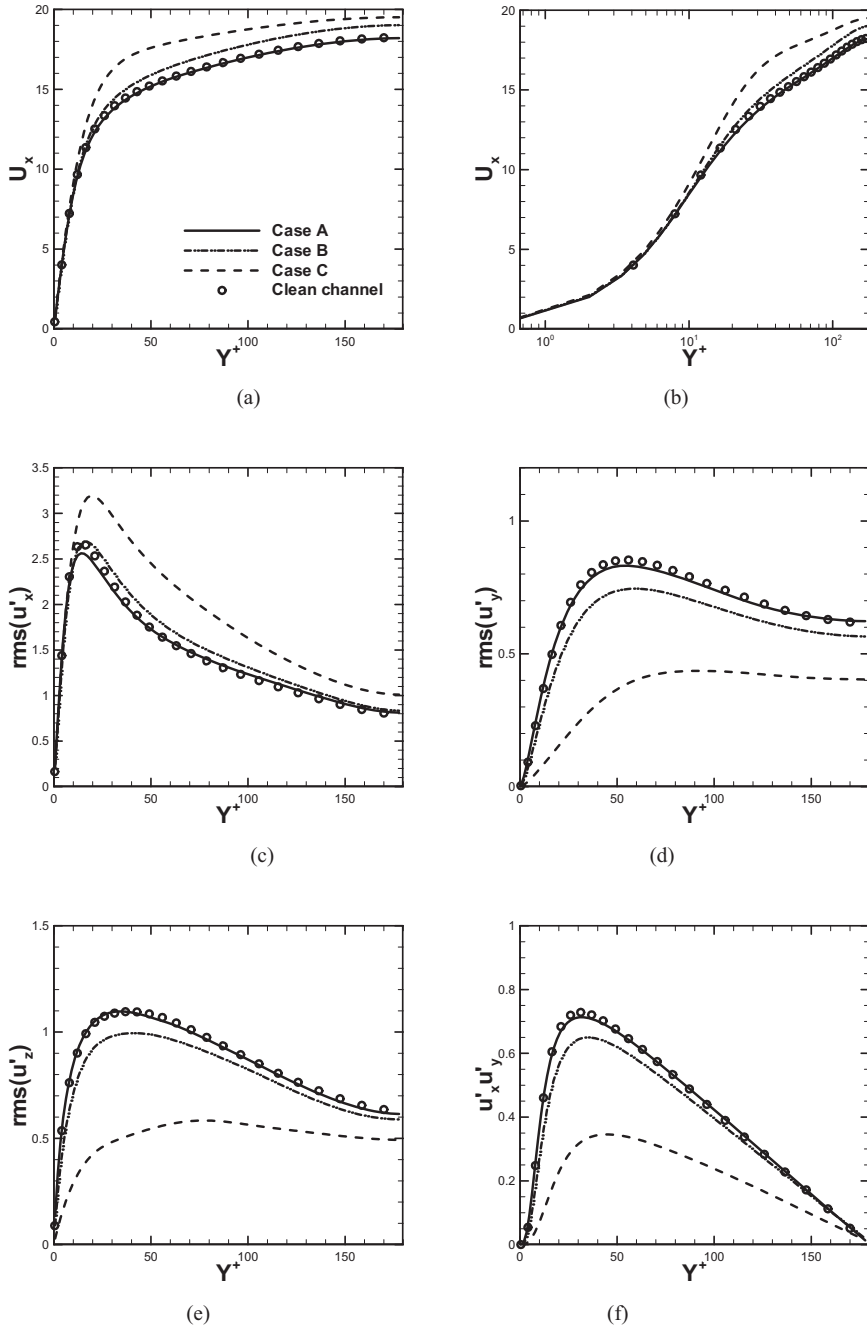


Figure 1 Primary fluid velocity statistics for Case A, B and C. Comparison between particle-free flow (symbols) and particle-laden flows (lines). (a) (b) Mean velocity in the streamwise direction with linear and semi-logarithmic scaling; (c) Velocity fluctuations in streamwise direction; (d) Velocity fluctuations in wall-normal direction; (e) Velocity fluctuations in spanwise direction; (f) Reynolds shear-stress.

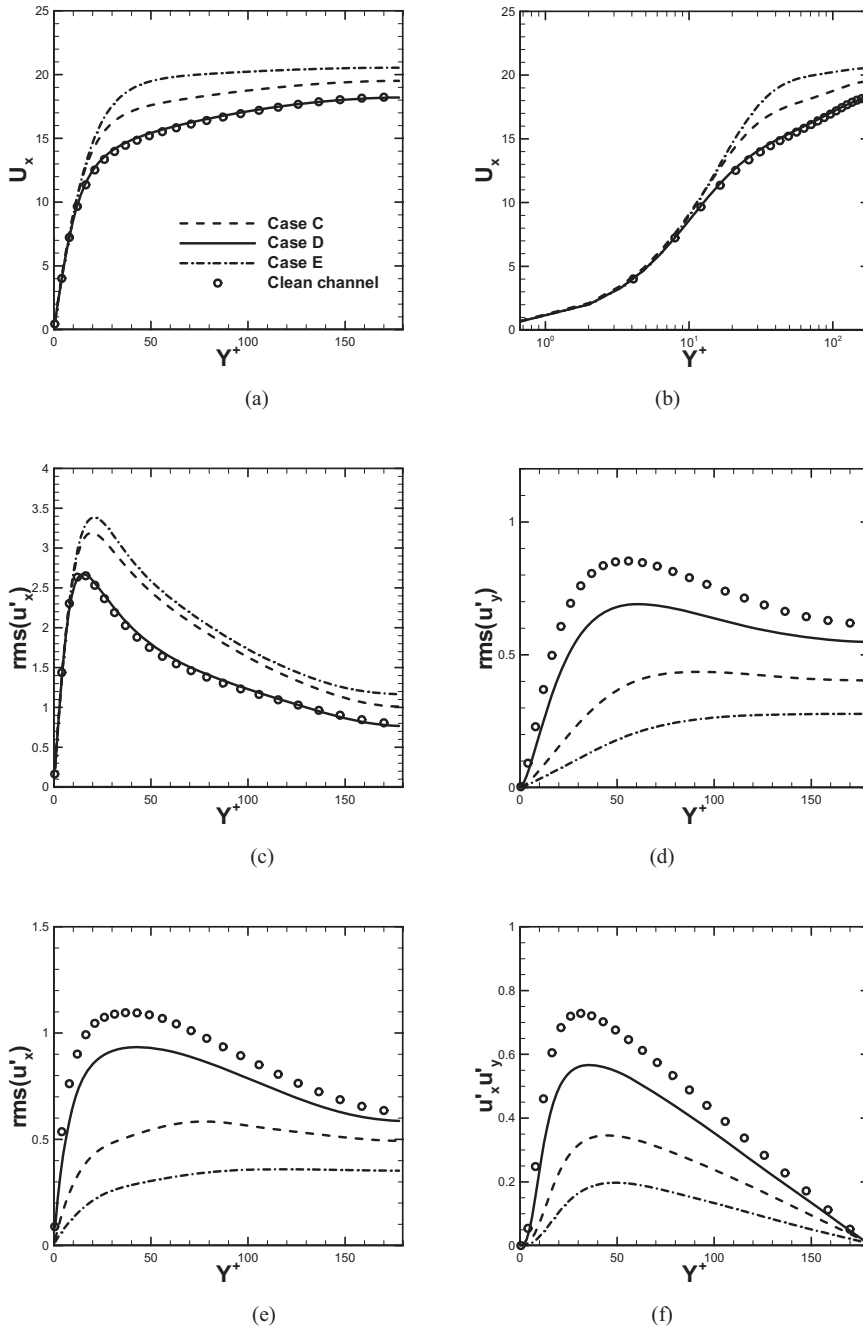


Figure 2 Primary fluid velocity statistics for Case C, D, and E. Comparison between particle-free flow (symbols) and particle-laden flows (lines). (a, b) Mean streamwise velocity in the streamwise direction; (c) Velocity fluctuations in streamwise direction; (d) Velocity fluctuations in wall-normal direction; (e) Velocity fluctuations in spanwise direction; (f) Reynolds shear stress.

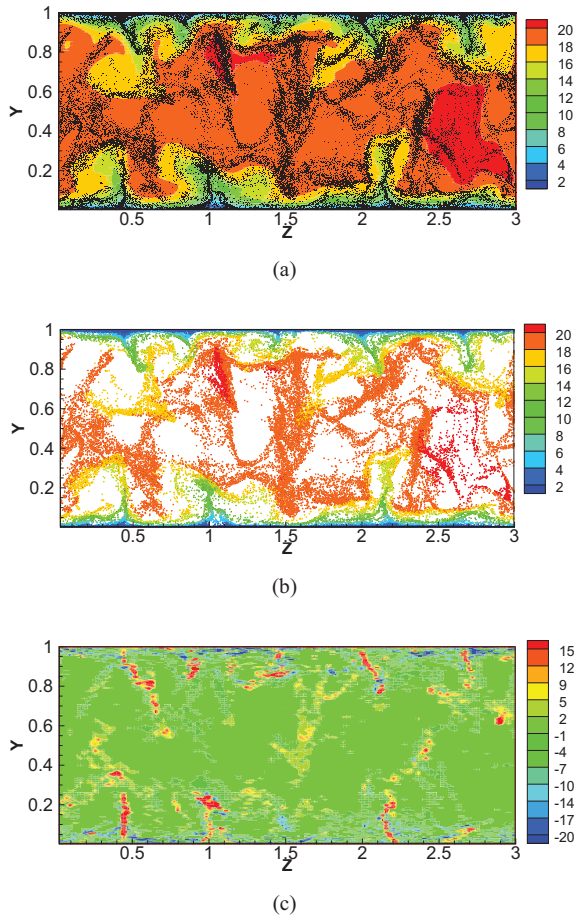


Figure 3. Instantaneous flow contours in a cross-sectional (y, z)-plane. (a) Streamwise fluid velocity u_x (colour-contours) and point-particle distribution (black dots); (b) streamwise particle velocity v_x ; (c) streamwise component of the drag force $-f_x^p$ from the fluid on the particles.

4.2 Modulations on flow structure and kinetic energy transport

Primary statistics which revealed the influence of particle loading and particle response time on the turbulence modulation were presented in the preceding Section 3.1. To explore this phenomenon in greater detail, the particle-turbulence interactions for one typical case (Case C) will be considered here with the view to explain the two different mechanisms involved, i.e. kinetic energy transfer between the two phases and the extra energy dissipation.

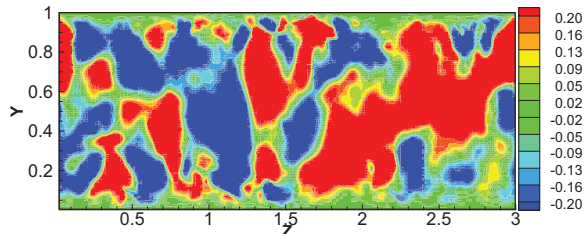
First of all, to obtain a direct impression of the particle-laden flow some contour plots are shown in Fig. 3. A snapshot of the modulated turbulence field, as reported by Zhao *et al.* (2010), is depicted in Fig. 3(a). The typical smaller scale-eddies close to

the walls have been damped and point particles are clustering in preferred regions while other zones are void.

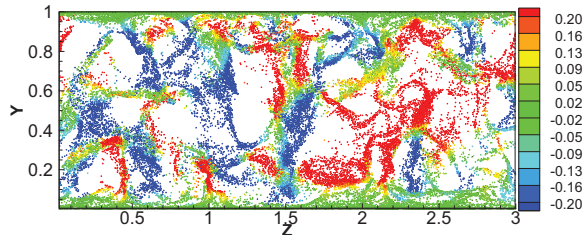
It is immediately observed that both the fluid and particle streamwise velocities, i.e. u_x and v_x , are positive throughout the entire cross-section in Fig. 3(a) and 3(b), respectively. From the quadrant analysis in eq. (3.3), we can infer that the fluid exerts work on the particles when the Stokes force is positive, i.e. in the red zones in Fig. 3(c), and $\dot{W}_x^P < 0$ in the blue zones. Negative values of the Stokes force occur almost only in the close vicinity of the channel walls, whereas contours of positive drag force can be observed far away from the wall and even in the channel centre. We therefore believe that the point-particles absorb kinetic energy from the large-scale eddies in the core region of the channel and transfer the energy back to the smaller-scale eddies adjacent to the walls. This interpretation is consistent with the force statistics to be presented in Figure 5 and 6.

Another noteworthy observation that can be made from Figure 3 is that particularly high positive values of $-f_x^P$ are associated with strong ejections of low-speed fluid away from the walls. Strong ejections from the lower wall are seen at $Z \approx 0.45, 1.0$ and 2.2 and from the upper wall at $Z \approx 0.4, 2.1$ and 2.7 . According to eq. (3.7) the particle dissipation ε_p is proportional to the square of the magnitude of the Stokes force. High energy dissipation rates are therefore associated with the ejection events. In this regard, one should recall that Rashidi *et al.* (1990) observed experimentally that the number of ejections was reduced in the presence of small polystyrene particles additives as compared with the unladen flow. The turbulence intensities and the Reynolds shear stress were correspondingly damped. The particularly high energy dissipation rate associated with the ejections might explain why the number of ejections is reduced.

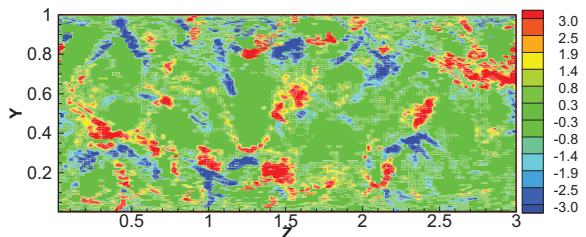
In wall-bounded turbulence particles are carried towards the wall during sweeping events and lifted away from the wall by the ejections. The contour plots in Fig. 4 show the fluid and particle velocities and the Stokes drag force in wall-normal direction at exactly the same instant of time as for the contour plots in Figure 3. Figure 4(b) confirms that $v_y > 0$ around the ejections from the lower wall observed in Figure 3(b) whereas v_y attains negative values near the locations where fluid is ejected away (i.e. downwards) from the upper wall. However, the direction of the wall-normal drag force displayed in Fig. 4(c) is not uniquely related to the direction of the local flow. The particle motion away from the walls along with the ejection events is apparently driven by Stokes drag in most cases. However, such a covariance between the direction of the Stokes force and the particle motion is not observed around the distinct ejection event close to $Z = 1$ at the lower wall. We are therefore not yet able to judge to what extent the particle drift is associated with the wall-normal component of the Stokes drag force.



(a)



(b)



(c)

Figure 4. Instantaneous flow contours in a cross-sectional (y, z)-plane at the same time instant as in Figure 3. (a) Wall-normal fluid velocity u_y , (colour-contours); (b) wall-normal particle velocity v_y ; (c) wall-normal component of the drag force $-f_y^P$ from the fluid on the particles.

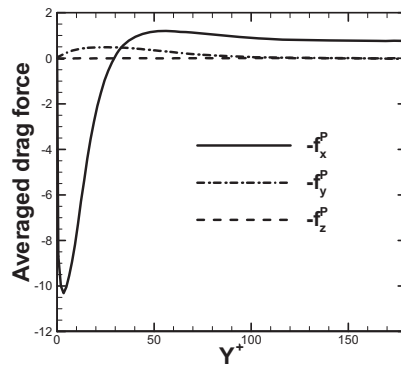


Figure 5 Profiles of the directional components of the averaged drag force $-\overline{f_i^P}$.

The mean values of the drag force acting from the fluid on the particles are shown in Fig. 5. The Stokes drag force F_i on individual point-particles given in eq. (2.2) is first summed up for all particles in a given grid cell as in eq. (2.4) and thereafter averaged in time and in the two homogeneous coordinate direction. The streamwise component $-\overline{f_x^P}$ is positive and fairly uniform from $Y^+ > 50$ and all the way to the channel center. This is consistent with the contour plot in Fig. 3(c) where significant negative force values are observed only in the vicinity of the walls. Indeed, the $-\overline{f_x^P}$ -profile in Fig. 5 changes sign at $Y^+ \approx 36$ and attains large negative values in the buffer layer and the viscous sub-layer with a distinct negative peak at about $Y^+ \approx 4$. The pronounced negative values of the mean Stokes force show that the mean particle velocity $\overline{V_x}$ exceeds the mean fluid velocity $\overline{U_x}$ seen by the particles, i.e. the conditionally-averaged fluid velocity at the particle positions. One should recall, however, that the fluid velocity seen by the particles are lower than the Reynolds-averaged fluid velocity since the inertial particles tend to concentrate in regions with locally low fluid velocity in the streamwise direction. Due to the particle inertia, the particles do not adjust to local flow conditions but retain their higher streamwise momentum. In the logarithmic layer and further out, however, the particles lag the local fluid velocity, as observed for instance in the experiments by Rashidi *et al.* (1990).

The wall-normal component $-\overline{f_y^P}$ appears to be modestly positive in the near-wall region and vanishingly small in the core of the channel. The mean Stokes force is therefore directed away from the lower wall and thus opposes the slow drift of particles towards the wall. This so-called turbophoresis is known to be responsible for the tendency of inertial particles to accumulate in the near-wall region. According to the $-\overline{f_y^P}$ profile in Fig. 5, the turbophoresis effect is not caused by the Stokes drag in the wall-normal direction. Rather contrary we believe that $-\overline{f_y^P} > 0$ tends to reduce the number of particle collisions with the wall. It should be pointed out that $-\overline{f_y^P}$ exhibits an anti-symmetric variation across the channel, i.e. the wall-normal Stokes drag is directed away from the wall on both sides of the channel. The mean Stokes drag in the spanwise direction, on the other hand, turns out to be vanishingly small in Figure 5. This is due to the symmetry properties of the present flow problem and $-\overline{f_z^P} \approx 0$ signifies the adequacy of the present sampling.

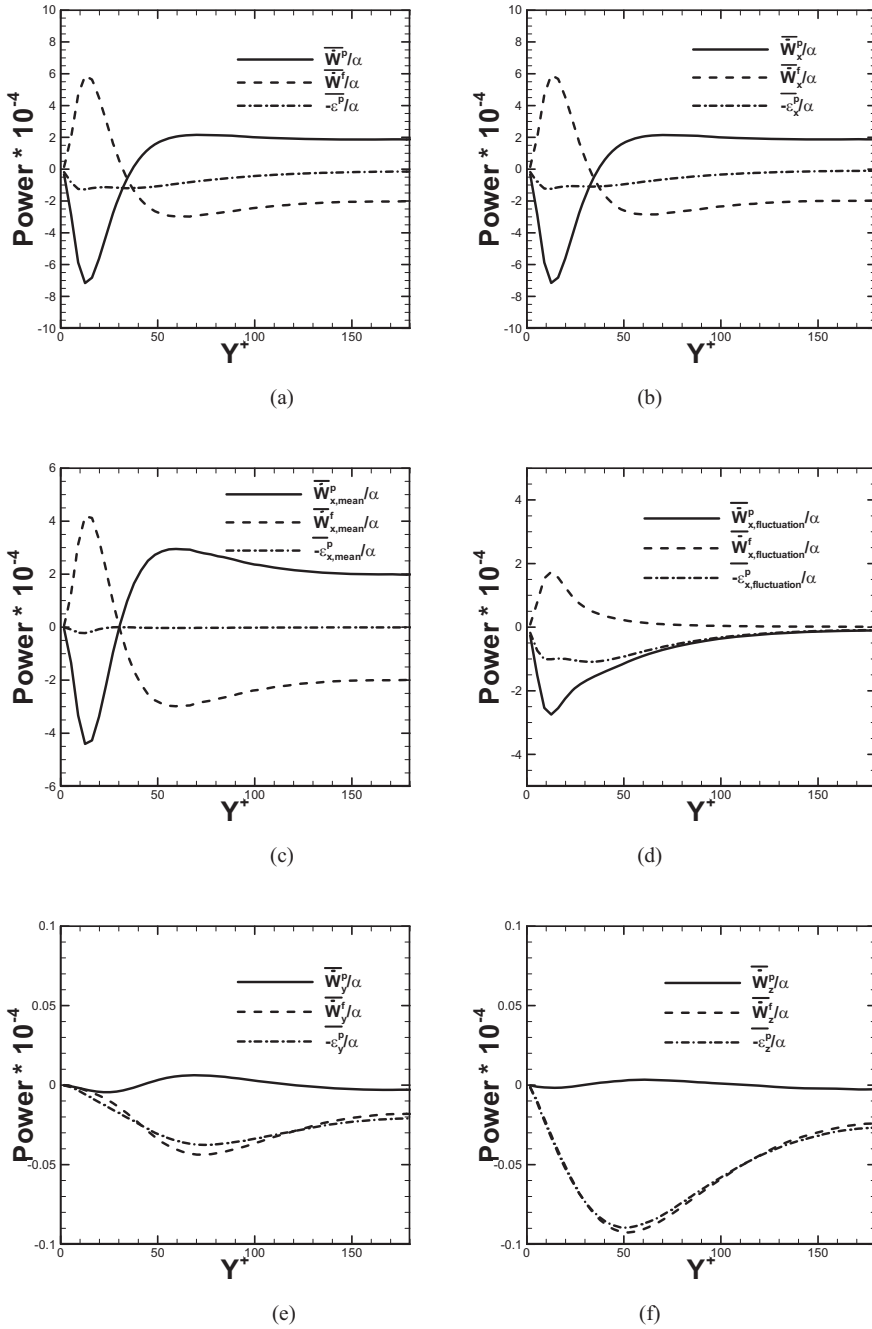


Figure 6 Profiles of the mean power transferred from the fluid to the particles \overline{W}^P , from the particles to the fluid \overline{W}^F and the particle dissipation $\overline{\varepsilon}^P$. (a) Accumulated results; (b) overall data in the streamwise direction; (c) contributions from the mean velocities in the streamwise direction; (d) contributions from the velocity fluctuations in the streamwise direction; (e) contributions from the velocity fluctuations in the wall-normal direction; (f) contributions from the velocity fluctuations in the spanwise direction.

The only linkage between the point-particles and the fluid motion is through the instantaneous reaction force \overrightarrow{f}^P in eq. (2.1). The same force is also crucially involved in the exchange of mechanical energy between the fluid and particles in equations (3.2) and (3.5) and in the particle-induced energy dissipation in eq. (3.7). The energy transfer and dissipation are shown in Fig. 6(a) with the directional contributions detailed in the subsequent panels in order to give us further insight in the transfer processes.

The overall energy transfer rates are evidenced by the profiles in Fig. 6 (a). Roughly opposite trends are observed for $\overline{\dot{W}}^P$ and $\overline{\dot{W}}^f$. The particles exert work on the local fluid in the buffer layer and viscous layer ($\overline{\dot{W}}^P < 0$ and $\overline{\dot{W}}^f > 0$) whereas the particles receive energy from the fluid ($\overline{\dot{W}}^P > 0$ and $\overline{\dot{W}}^f < 0$) beyond $Y^+ \approx 36$. In view of the modest drift of particles towards the wall, one may argue that the particles represent a vehicle for energy transport away from the core region. On the average, the particles receive energy from the fluid in the center region, drift towards the wall, and ultimately return most of the energy back to the fluid.

A particularly noteworthy observation which can be made from Fig. 6(a) is that $\overline{\dot{W}}^P$ and $\overline{\dot{W}}^f$ do not add up to zero but to a non-zero $-\overline{\varepsilon}^P$. The imbalance between the power transferred from the fluid to the particles ($\overline{\dot{W}}^P$) and the power received by the fluid from the particles ($\overline{\dot{W}}^f$) is a measure of the extra energy dissipation caused by the point-particles. The particle dissipation is most pronounced in the near-wall region but retain an appreciable level also in the inner part of the logarithmic layer. $\overline{\varepsilon}^P$ can thus be considered as a scalar measure of the particle-turbulence interactions, which indeed are most profound in the vicinity of the wall where also the highest particle density is found.

In order to explain the modulations of the turbulence field observed in Fig. 1 and 2, the Reynolds decomposition is introduced into \dot{W}_β^P and \dot{W}_β^f defined in eq. (3.2) and (3.5), respectively. We then arrive at (3.8) and (3.9) which show that both the mean velocities and the velocity fluctuations contribute to the energy exchange process. Furthermore care is taken to distinguish between the contributions from different directional components of the velocity vectors.

Firstly, the total power associated with the streamwise motions is shown in Fig. 6(b). The profiles in this panel are almost indistinguishable from the corresponding distributions in Fig. 6(a). It is therefore tempting to conjecture that almost all the energy exchange between the two phases is associated with the streamwise motions. Let us therefore proceed to see if the mean motion or the velocity fluctuations are dominant. Examination of the contributions from the mean in panel (c) and from the fluctuations in panel (d) reveals a number of important findings. The profiles in Fig. 6(c) are surprisingly similar to the profiles in Fig. 6(b), although the characteristic near-wall peak values are about 50% higher in Fig. 6(b) than in Fig. 6(c). The profiles shown in Fig. 6(d) confirm that this excess power exchange in the near-wall region is contributed by the velocity fluctuations. However, the substantial contributions from the streamwise fluctuations decay monotonically towards the channel center where almost all the energy exchange stems from the mean velocities. It is noteworthy that the contributions from the fluctuating velocity field give rise to a consistently negative $\overline{\dot{W}_x^P}$ and $\overline{\dot{W}_x^f} > 0$ all the way from the wall to the channel center. The average energy transfer caused by the streamwise velocity fluctuations are thus from the particles to the fluid, irrespective of the distance from the wall. This explains the enhancement of the fluid turbulence intensity observed in Figure 1(c).

Although the energy exchange between the two phases due to the mean motion exceeds the exchange caused by the velocity fluctuations, the particle dissipation $\overline{\varepsilon^P}$ associated with the latter is at least five times greater than the dissipation caused by the mean motions. This somewhat surprising observation is a direct consequence of the recent finding by Zhao *et al.* (2012) that the fluctuating part of the slip velocity vector is more energetic than the corresponding mean slip velocity. Thus, the energy associated with the particle fluctuations is partly given away to the fluid and partly being dissipated.

In order to complete the detailed exploration of the energy transfer and dissipation mechanisms, the contributions associated with wall-normal and spanwise velocity fluctuations are shown in Fig. 6 (e) and (f), respectively. In both panels, the power received by the fluid from the particles dominates and reaches a maximum value around $Z^+ \approx 50 - 60$. Since the energy transfer from the fluid to the particles is of marginal importance we obtain from eq. (3.10) that $\overline{\varepsilon_y^P} \approx -\overline{\dot{W}_y^f}$ and $\overline{\varepsilon_z^P} \approx -\overline{\dot{W}_z^f}$.

This leads to the conclusion that, as far as motions in the cross-section plane are concerned, energy is drained from the fluid motion and dissipated rather than transferred to the particle motions.

The fluid motions in the (y, z) -plane appear to be unable to exert work on the particles. According to eq. (3.2), this implies that the covariance of the particle and fluid

velocity fluctuations is almost equal to the particle intensity in that direction. This does not necessarily imply that the covariance also equals the fluid intensity. Indeed, we just observed that $\overline{\dot{W}_y^f}$ attains an appreciable level although $\overline{\dot{W}_y^p} \approx 0$. This observation is an outcome of particle inertia. The particles are unable to follow the eddy motion in the cross-sectional plane and the unresponsive particles give rise to extra dissipation which in turn plays a crucial role in the attenuation of the wall-normal and spanwise turbulence intensities shown in Figure 1(d) and 1(e).

Let us finally emphasize that the contributions to the energy exchange and dissipation from the streamwise motions dominate over the contributions from the motions in the cross-sectional plane. The latter is, however, by no means negligible and tends to explain the observed modulations of the turbulence field in Figure 1. In particular, the enhancement of the streamwise fluctuations in the near-wall region arises partly due to work associated with the mean motion and partly due work related with the velocity fluctuations. The attenuation of the spanwise and wall-normal motion is on the other hand caused by particle-induced energy dissipation.

The statistical results presented in Figures 5 and 6 were obtained by conditional sampling rather than by conventional Reynolds-averaging. Conditional sampling has been used for instance by Squires & Eaton (1990) and Mortensen *et al.* (2007). The fluid velocity of concern is that at the particle positions since only that velocity is involved in the Stokes drag force in eq. (2.2). Inertial particles tend to concentrate in preferred areas where the local fluid velocity differs from the Reynolds-averaged fluid velocity and conditional sampling is therefore crucially important. This is illustrated by the primary velocity statistics shown in Figure 7. The mean streamwise fluid velocity in Fig. 7(a) is strikingly different from the Reynolds-averaged mean velocity. While the particle mean velocity is consistently lower than the Reynolds-averaged fluid velocity, the particle velocity exceeds the conditionally-averaged fluid velocity in the buffer region and lags the fluid velocity seen by the particles in the core region. As far as the rms-values of the velocity fluctuations are concerned, i.e. the directional intensities, the particle intensities are substantially closer to the conditionally-averaged fluid intensities than to the fluid intensities obtained by conventional Reynolds-averaging.

The directional energy spectra shown in Figure 8 aim to reveal if the effect of the particle additives is concentrated at particular length scales. As far as the motion in the cross-sectional plane is concerned, the damping of the fluid motion prevails across the entire range of scales. The streamwise fluctuations, which are enhanced by the inertial particles, appear to be damped at smaller scales and only the largest eddies become more energetic. In spite of the particles being point-particles, even the large-eddy motion is severely affected by the presence of the particles.

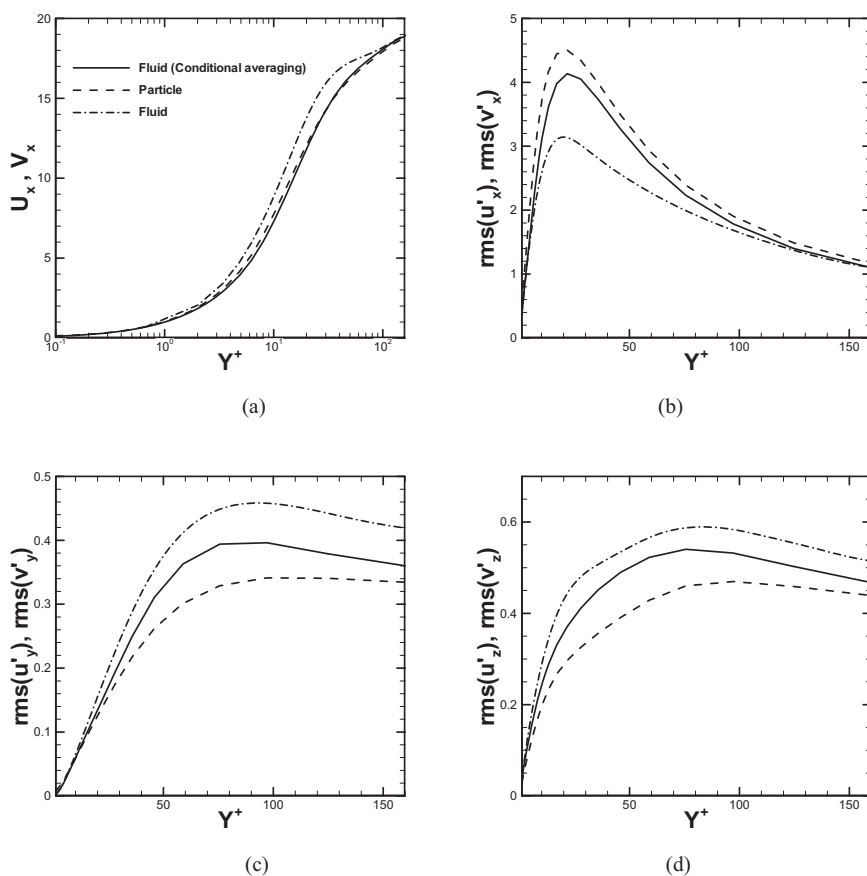


Figure 7. Comparison between traditionally sampled fluid statistics and conditionally-sampled results on the particle positions. (a) Streamwise mean velocity; (b) streamwise velocity fluctuations; (c) wall-normal velocity fluctuations; (d) spanwise velocity fluctuations.

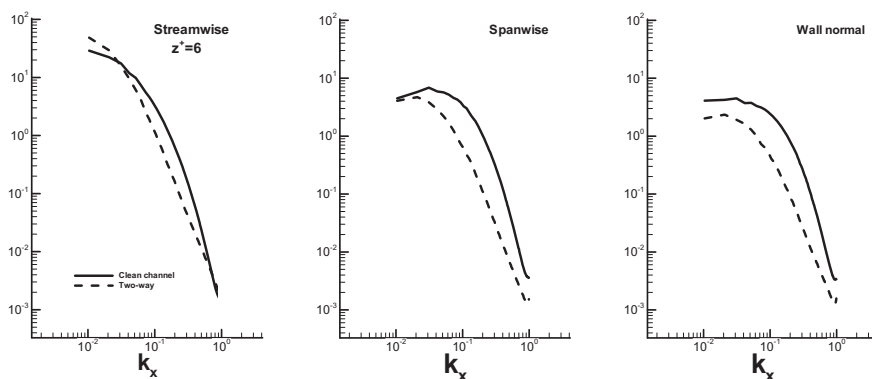


Figure 8 One-dimensional spectra of the fluid kinetic energy in the viscous sublayer at $Y^+ \approx 6$ (a) Streamwise direction; (b) spanwise direction; (c) wall-normal direction.

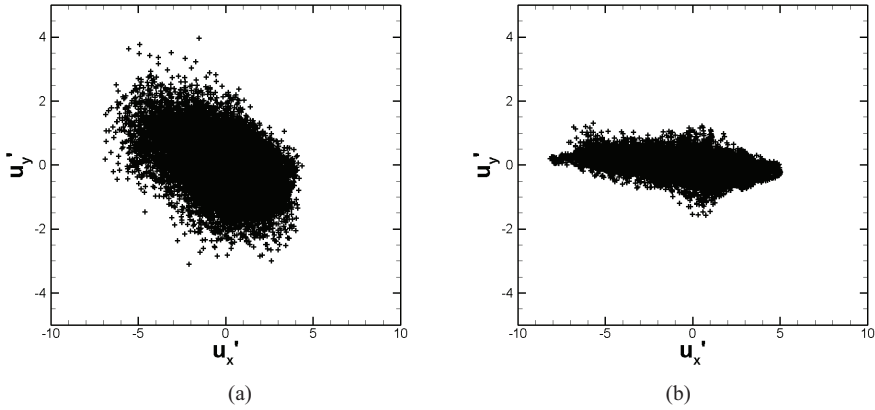


Figure 9. Scatter plot of the instantaneous velocity fluctuations in the wall-normal versus the streamwise direction at $Y^+ \approx 38$. (a) Unladen channel flow; (b) particle-laden channel flow.

Last but not least, the present study shows that particle additives may lead to drag reduction even though the additives are tiny spherical particles and not elongated fiber-like particles or elastic polymers for which drag reduction is a well-established phenomenon (e.g. Gillissen *et al.* 2008). It should be recalled that the present flow was driven by a given streamwise mean pressure gradient and we could observe from Fig. 1(a) that the bulk flow increased when the particles were added to the flow. The increased bulk flow at a given pressure gradient is deemed as equivalent of drag reduction or pressure-loss reduction if the bulk flow is given. The drag reduction for Case C particles has been reported in a Letter by Zhao *et al.* (2010). We intentionally simplified our approach by neglecting other forces than Stokes drag in order to focus on the particle-fluid interaction in two-way coupled simulations. Neglecting gravity makes it difficult to compare the results of the present study with experimental measurements for instance in horizontal channel flows where gravity inevitably comes into play. Only a modest number of papers have convincingly reported observations of drag reduction achieved by means of spherical particles. Rossetti & Pfeffer (1972) performed measurements in vertical and horizontal channel flows of dilute suspensions of glass beads and reported drag reduction at Reynolds numbers in the range from 10000 to 25000 with different mass loadings. Yamamoto (2001) and Li *et al.* (2001) performed large-eddy and direct numerical simulations of particle-laden flow in a vertical channel with gravity included in order to compare their results with the experimental measurements by Kulick *et al.* (1994). They both observed an increase of the mean streamwise velocity for mass loadings 1 and 0.4. The modulations they reported of the turbulence field are in qualitative accordance with the present results. Yamamoto (2001), however, argued that the drag reduction observed could be ascribed to the presence of the gravity force which tends to accelerate the local fluid. In the present study, on the other hand, gravity has been ignored and an increased bulk flow is nevertheless observed. It can therefore be concluded that gravity is not the only means by which drag reduction can be achieved

and other mechanisms do exist. The present investigation may serve the purpose to elucidate these mechanisms.

The present channel flow laden with spherical particles shows striking similarities with characteristics of fiber-laden or polymer-laden drag-reduced flow, e.g. the primary flow statistics in Figure 1. The scatter plots in Figure 9 show how the joint probability density function is affected by the particle additives (right) as compared with the unladen channel flow (left). The substantially different scattering reduces the covariance between streamwise and wall-normal fluctuations and gives rise to the rather dramatic reduction of the Reynolds shear stress shown in Fig. 1(f). The scatter plot in Fig. 9(b) exhibits the same features as the corresponding plot deduced by Gampert & Yong (1990) for a polymer-laden flow. It can be concluded that the spherical point particles have a surprisingly similar influence on turbulent flow field as elongated particles.

Frohnafel *et al.* (2007) pointed out that drag reduction in turbulent channel flow is associated with an increased anisotropy of the turbulence close to the walls where a highly anisotropic state of turbulence is commonly found. The damping of the velocity fluctuations in the wall-normal and spanwise directions and the augmentation of streamwise velocity fluctuations as observed in Fig. 1 do indeed reflect an increased anisotropy caused by the particles. L'vov *et al.* (2004) ascribed the drag reduction mechanism by means of polymers in wall-bounded turbulence to the polymer stretching which tended to suppress the momentum flux towards the walls. In the present study the Reynolds shear stress is damped along with the reduction of the momentum flux to wall. Gillissen *et al.* (2008), studied drag reduction achieved by means of rigid fibers and deduced the fiber stress and the fiber viscosity in drag-reduced flows. He observed that the fiber viscosity increased with the distance from the wall. This is somewhat consistent with Balachandar & Eaton (2010) who claimed that the turbulence attenuation may result from the enhanced effective viscosity caused by the presence of tiny particles.

In this sub-section, the attenuation of the turbulence field by the presence of tiny spherical particles has been analyzed by means of the work performed by the Stokes drag force. A slip velocity between a particle and the local fluid arises due to the particle inertia. This slip velocity creates an imbalance between the work performed by the particles on the fluid and the work exerted by the fluid on the particles. The local fluid exerts work on the particles in the core region of the channel whereas the particles perform work on the fluid in the buffer layer and the viscous sub-layer. Anyhow, as a result of this imbalance, kinetic energy is drained from the fluid-particle suspension by means of particle dissipation. The particles play two important and independent roles in a wall-bounded shear flow. One is as a vehicle to transport turbulent kinetic energy from the core region and into the near-wall layers, and the other is to cause extra energy dissipation. The enhancement of the streamwise

turbulence intensity is due to the former, whereas the latter mechanism is responsible for the attenuation of velocity fluctuations in the cross-sectional plane. The ultimate implication of these two different mechanisms is therefore to increase the anisotropy of the turbulence.

4.3 Analysis of kinetic energy transfer by scatter plots

In two-way coupled simulations of particle-laden flows, mechanical energy is continuously exchanged between the fluid and particle phase. Moreover, a fraction of the mechanical energy is lost during the exchange process and gives rise to what we call particle dissipation. According to the analysis in Section 3, the inter-phasic energy exchange depends on the covariance between the slip velocity and the particle or fluid velocities, as shown in eq. (3.2) and (3.5), respectively. In this sub-section a novel approach to analyze these energy exchange processes is illustrated. Instead of the traditional scatter plots shown in Fig. 9, a scatter plot between a given fluid or particle velocity component and the slip velocity component in the same direction is provided.

Instantaneous values of the streamwise fluid velocity u_x are plotted against the streamwise component of the slip velocity vector $v_x - u_x$ in Fig. 10(a). Similarly, the streamwise particle velocity v_x is shown against $u_x - v_x$ in Fig. 10(b). The plots are arranged such that contributions to positive power supply $\overline{\dot{W}}_x^f$ and $\overline{\dot{W}}_x^p$ are to the right as long as u_x and v_x never attains negative values. The colour-coding represents the density of events, i.e. the joint probability density function (pdf). The pdf exhibits two different peaks, both close to $u_x - v_x = 0$. Notice that the contour lines representing the very highest densities are omitted to facilitate the interpretation of the plots. One peak in Fig. 10(a) is around $u_x \approx 3$, i.e. in the viscous sublayer, and the other peak is slightly below $u_x = 20$ in the channel center. The high probability of $v_x - u_x \approx 0$ in the core region shows that the inertial particles are more able to follow the fluid motion in the region where the time scale of the prevailing large-eddy motion is relatively large. The pdf is severely skewed towards the right ($v_x - u_x > 0$) around the lower peak and towards the left ($v_x - u_x < 0$) around the higher peak. On the average the work on the fluid by the particles gives rise to $\overline{\dot{W}}_x^f > 0$ in the viscous sublayer whereas $\overline{\dot{W}}_x^f$ becomes negative in the core region of the channel. These findings are fully consistent with the cross-sectional snapshot in Figure 3(c) and the statistics shown in Figure 6(b). The asymmetry of the scatter plot in Fig. 10(b) is qualitatively different and less pronounced than in Fig. 10(a). The straight line is the demarcation line between positive and negative values of u_x and no events with $u_x < 0$ (i.e. below the line) are observed. The scatter plot is skewed towards the left for lower values of v_x and the covariance between v_x and $(u_x - v_x)$ becomes negative in the near-wall region. The power $\overline{\dot{W}}_x^p$ which stems from work done by the fluid on the particles is therefore negative in the buffer layer and viscous sublayer in keeping with Fig. 6(b).

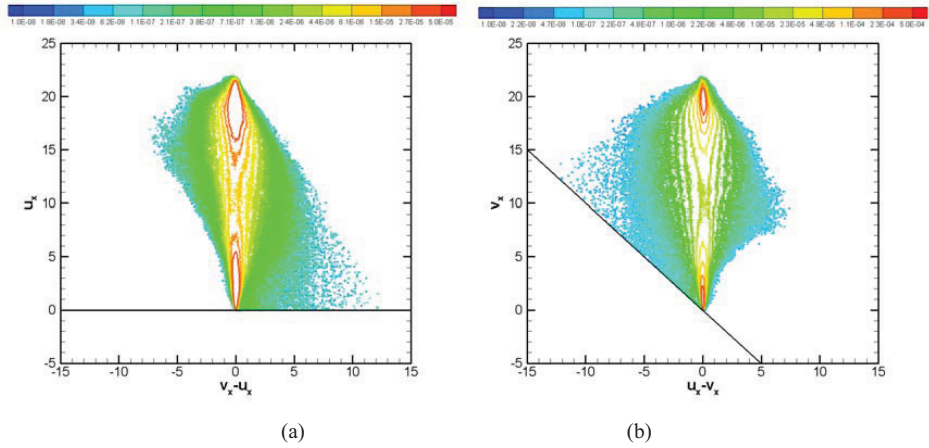


Figure 10. Scatter plot of streamwise velocity components. (a) Fluid velocity versus slip velocity; (b) particle velocity versus slip velocity. The straight lines in panels (a) and (b) are $u_x = 0$ and $v_x = -(u_x - v_x)$, respectively.

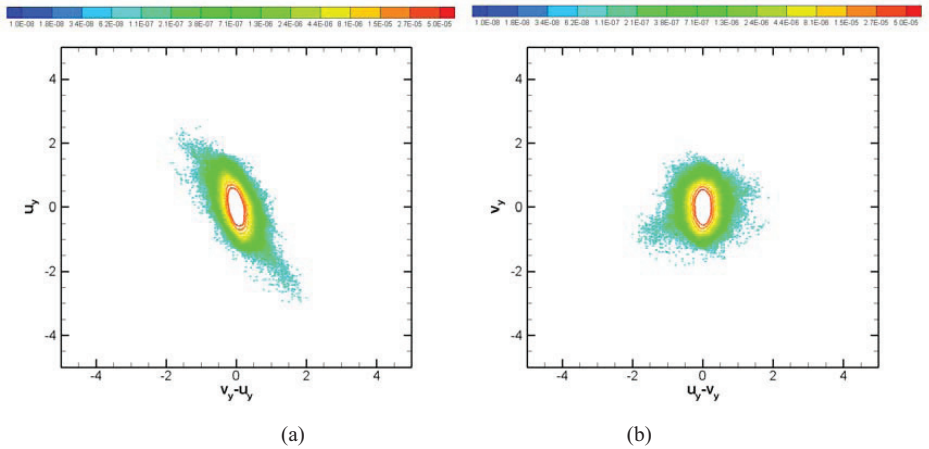


Figure 11. Scatter plot of wall-normal velocity components. (a) Fluid velocity versus slip velocity; (b) particle velocity versus slip velocity.

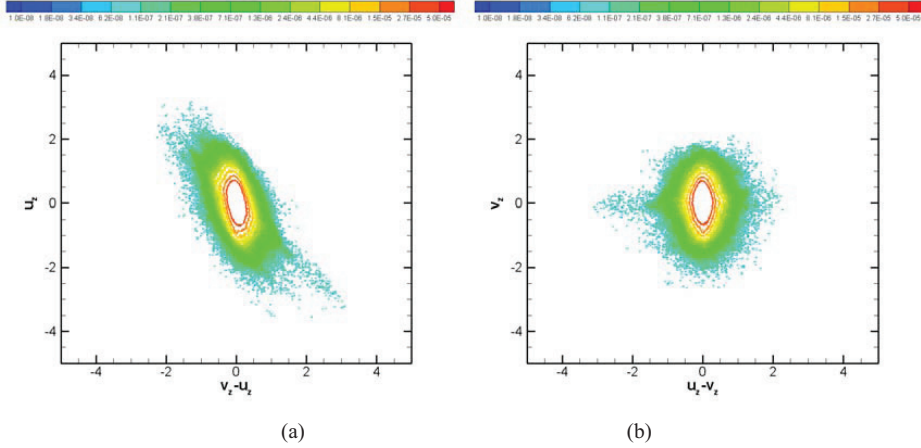


Figure 12. Scatter plot of spanwise velocity components. (a) Fluid velocity versus slip velocity; (b) particle velocity versus slip velocity.

Scatter plots corresponding to those in Fig. 10 are shown in Fig. 11 and Fig. 12 in terms of the wall-normal and spanwise velocity components, respectively. The covariances between the fluid velocity u_y and the slip velocity $v_y - u_y$ in Fig. 11(a) and between u_z and $v_z - u_z$ in Fig. 12(a) both exhibit distinct asymmetries with dominance from events in the second and fourth quadrants. These asymmetries make $\overline{\dot{W}_y^f}$ and $\overline{\dot{W}_z^f}$ negative, as already shown by statistical results in Fig. 6(e) and 6(f). However, the loss of fluid kinetic energy due to the particle-fluid interactions is not transferred to particles. The vanishingly small levels of $\overline{\dot{W}_y^p}$ and $\overline{\dot{W}_z^p}$ in Fig. 6 are fully consistent with the associated scatter plots in Fig. 11(b) and Fig. 12(b). The former plot exhibits symmetries about both the v_y -axis and the $v_y - u_y$ -axis and the covariance between v_y and $v_y - u_y$ becomes negligibly small. The same arguments apply for the scatter plot in Fig. 12(b). The power transferred from the fluid to the particles by means of cross-sectional motions is therefore negligible and the loss of fluid kinetic energy is lost due to particle dissipation rather than being transferred to particle kinetic energy.

Let us finally consider the covariance between the power \dot{W}^f resulting from work by the particles on the fluid versus the power \dot{W}^p resulting from work by the fluid on the particles in Figure 13. The straight line $\dot{W}^f = -\dot{W}^p$ in Fig. 13(a) corresponds to $\varepsilon^p = 0$ according to eq. (3.7). All events are below this line and therefore give rise to particle dissipation. The distance from the line to a point in the scatter plot is a measure of the contribution of that event to the particle dissipation and thereby to the drainage of mechanical energy from the fluid-particle suspension. The particle dissipation is a

result of an imbalance in the power exchange between the particles and the fluid, i.e. when $\dot{W}^f \neq -\dot{W}^p$. For a modest power exchange, i.e. events close to the origin in Fig. 13(a), the imbalance is also fairly small and so is the particle dissipation. The largest imbalance and thus the greatest particle dissipation are associated with events with a substantial power exchange.

The scatter plot of \dot{W}_x^f versus \dot{W}_x^p in Fig. 13(b) is indistinguishable from the plot in Fig. 13(a). We can therefore conclude that the streamwise motions are responsible for almost all of the energy exchange between the particles and the fluid. This is indeed confirmed by the scatter plots of the power exchanges caused by cross-sectional motions in Fig. 13(c) and 13(d) when the different scaling on the axes is recognized. The vast majority of events in these two scatter plots are below $\dot{W}_y^f = 0$ and $\dot{W}_z^f = 0$ and the power transferred from the particles to the fluid becomes distinctly negative, as seen in Fig. 6(e) and 6(f). However, as already noticed, the energy exchange associated with the cross-sectional motions is only a small fraction of the energy exchange caused by the streamwise velocity; see e.g. Fig. 13(b).

5. Concluding remarks

In the present work two-way coupled DNSs with an Eulerian-Lagrangian point-particle approach have been performed. Five cases were designed to study the influences of the particle response time and particle loadings on the modulations of the turbulent flow field in a fully-developed channel flow. Statistical results showed an attenuation of the Reynolds shear stress and the velocity fluctuations in the wall-normal and spanwise directions, whereas an augmentation of the velocity fluctuations in the streamwise direction was observed. These turbulence modulations have been explained in terms of the directional components of the Stokes force, the kinetic energy transfer between the carrier fluid and inertial particles, as well as the extra energy dissipation induced by the particles. The results revealed that the work done by local fluid on the particles is anisotropic and heterogeneous, i.e. in the streamwise direction the local fluid exerted work on the particles in the channel center but the particles exerted work on the local fluid in the buffer layer and viscous sub-layer. In the two other directions, i.e. the spanwise and wall-normal directions, the local fluid exerted work on the particles all across the channel cross-section.

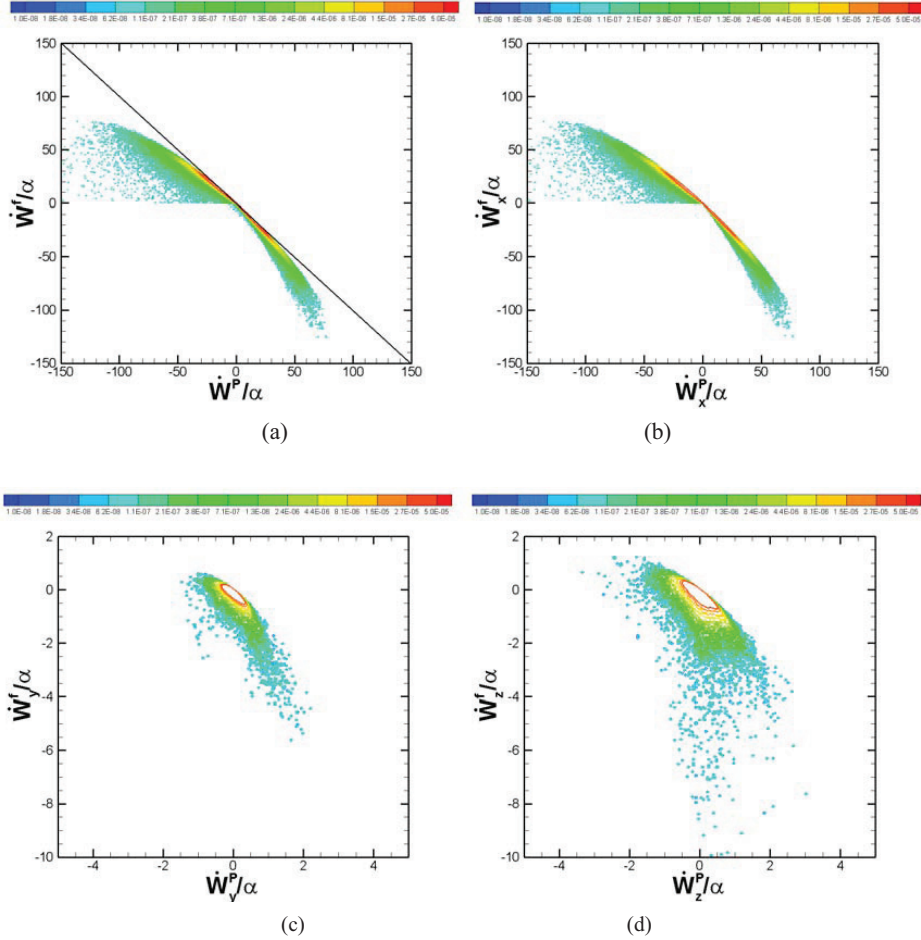


Figure 13. Scatter plots of the power resulting from work by the particles on the fluid \dot{W}^f versus power resulting from work by the fluid on the particles \dot{W}^P . (a) Total powers. Events on the straight line $\dot{W}^f = -\dot{W}^P$ corresponds to $\varepsilon_P = 0$. (b) Power exchange due to streamwise motions; (c) power exchange due to wall-normal motions; (d) power exchange due to spanwise motions. Notice the different scaling in the two lower panels.

By decomposing the turbulent velocity field into mean and fluctuating parts, we found that the enhancement of streamwise turbulence was caused by the work done by particles on the local fluid. The extra energy dissipation, which is due to the particle-fluid interactions, was not sufficient to prevent the streamwise intensity to increase. The velocity fluctuations in the cross-sectional plane, however, were substantially damped. By means of the present statistics of the power exchange between the two phases, we can also conclude that the particles play two distinctly different roles in the flow. One is to redistribute the kinetic energy in the flow and the other one is to provide an extra drain of energy from the suspension by means of particle dissipation. The physical mechanisms responsible for the turbulence

modulations caused by the presence of tiny point-particles have been fully explained by means of the present analysis in which statistical data were further supported by instantaneous scatter plots of the fluctuating fluid or particle velocity versus the fluctuation slip velocity.

Acknowledgements

This work has been supported by A/S Norske Shell through a research fellowship (contract no. 4610020178/C08156) and by The Research Council of Norway (Programme for Supercomputing) through a grant of computing time.

References

- Balachandar, S. & Eaton, J. K. 2010 Turbulent dispersed multiphase flow. *Annu. Rev. Fluid Mech.* **42**, 111–33.
- Bari, H.A.A. & Yunus, R.B.M. 2009 Drag reduction improvement in two phase flow system using traces of SLES surfactant. *Asian J. Ind. Eng.* **1**, 1–11.
- Bijlard, M. J., Oliemans, R. V. A., Portela, L. M., & Ooms, G. 2010 Direct numerical simulation analysis of local flow topology in a particle-laden turbulent channel flow. *J. Fluid Mech.* **653**, 35–56.
- Dritselis, C.D. & Vlachos, N.S. 2008 Numerical study of educed coherent structures in the near-wall region of a particle-laden channel flow. *Phys. Fluids* **20**, 055103.
- Dritselis, C.D. & Vlachos, N.S. 2011 Numerical investigation of momentum exchange between particles and coherent structures in low Re turbulent channel flow. *Phys. Fluids* **23**, 025103.
- Elghobashi, S. & Truesdell, G. C. 1993 On the two-way interaction between homogeneous turbulence and dispersed solid particles. I: Turbulence modification. *Phys. Fluids A* **5**, 1790-1801.
- Frohnepfel, B., Lammers, P. & Jovanović, J. 2007 Interpretation of the mechanism associated with turbulent drag reduction in terms of anisotropy invariants. *J. Fluid Mech.* **577**, 457–466.
- Gampert, B. & Yong C.K., 1990 The influence of polymer additives on the coherent structure of turbulent channel flow. In: Gyr, A. (Editor) *Structure of Turbulence and Drag Reduction*. Springer, Berlin Heidelberg, 223–232
- Gillissen, J.J.J., Boersma, B.J., Mortensen, P.H. & Andersson, H.I. 2008 Fibre-induced drag reduction. *J. Fluid Mech.* **602**, 209–218.

- Gore, R. A. & Crowe, C. T. 1989 The effect of particle size on modulating turbulent intensity. *Int. J. Multiphase Flow* **15**, 279–285.
- Hussainov, M., Kartushinsky, A., Rudi, Shcheglov, I., Kohnen, G., & Sommerfeld, M., 2000 Experimental investigation of turbulence modulation by solid particles in a grid-generated vertical flow. *Int. J. Heat Fluid Flow* **21**, 365-373.
- Kulick, J. D., Fessler, J. R. & Eaton, J. K. 1994 Particle response and turbulence modification in fully developed channel flow. *J. Fluid Mech.* **277**, 109-134.
- Li, Y., McLaughlin, J. B., Kontomaris, K. & Portela, L. 2001 Numerical simulation of particle-laden turbulent channel flow. *Phys. Fluids* **13**, 2957
- Mortensen, P.H., Andersson, H.I., Gillissen, J.J.J. & Boersma, B.J. 2007 Particle spin in a turbulent shear flow. *Phys. Fluids* **19**, 078109.
- Pan, Y. & Banerjee, S. 1996 Numerical simulation of particle interactions with wall turbulence. *Phys. Fluids* **8**, 2733–2755.
- Picciotto, M., Giusti, A., Marchioli, C. & Soldati, A. 2006 Turbulence modulation by micro-particles in boundary layers. *IUTAM Symposium on Computational Approaches to Multiphase Flow*, edited by S. Balachandar & A. Prosperetti (Springer), 53–62.
- Radin, I., Zakin, J.L. & Patterson G.K. 1975 Drag reduction in solid-fluid systems. *AICHE J.* **21**, 358–371.
- Rani, S. L., Winkler, C. M. & Vanka, S. P. 2004 Numerical simulations of turbulence modulation by dense particles in a fully developed pipe flow. *Powder Tech.* **141**, 80–99.
- Rashidi, M., Hetsroni, G. & Banerjee, S. 1990 Particle-turbulence interaction in a boundary layer. *Int. J. Multiphase Flow* **16**, 935–949.
- Rosetti, S. J. & Pfeffer, R. 1972 Drag reduction in dilute flowing gas-solid suspensions. *A.I.Ch.E. J.* **18**, 31-39.
- Squires, K. D., & Eaton, J. K. 1990 Particle response and turbulence modification in isotropic turbulence. *Phys. Fluids A* **2**, 1191–1203.
- Tanaka, T. & Eaton, J. K. 2008 Classification of turbulence modification by dispersed spheres using a novel dimensionless number. *Phys. Rev. Lett.* **101**, 114502.
- Truesdell, G. C. & Elghobashi, S. 1994 On the two-way interaction between homogeneous turbulence and dispersed solid particles. II. Particle dispersion. *Phys. Fluids* **6**, 1405–1407.

Sato, Y. & Hishida, K. 1996 Transport process of turbulence energy in particle-laden turbulent flow. *Int. J. Heat Fluid Flow* **17**, 202–210.

Vreman, A. W. 2007 Turbulence characteristics of particle-laden pipe flow. *J. Fluid Mech.* **584**, 235–279

Yamamoto, Y., Potthoff, M., Tanaka, T., Kajishima, T. & Tsuji, Y. 2001 Large-eddy simulation of turbulence gas-particle flow in a vertical channel: effect of considering inter-particle collisions. *J. Fluid Mech.* **442**, 303–334.

Zhao, L.H., Andersson, H. I. & Gillissen, J. J. J. 2010 Turbulence modulation and drag reduction by spherical particles. *Phys. Fluids* **22**, 081702.

Zhao, L.H. & Andersson, H. I. 2011 On particle spin in two-way coupled turbulent channel flow simulations. *Phys. Fluids* **22**, 081702.

Zhao, L.H. & Andersson, H. I. 2012 Statistics of particle suspensions in turbulent channel flow. *Commun. Comput. Phys.* **11**, 1311-1322.

Zhao, L.H., Marchioli, C. & Andersson, H.I. 2012 Stokes number effects on particle slip velocity in wall-bounded turbulence and implications for dispersion models. *Phys. Fluids*, revised version submitted.

Part 2.3

One-way coupled simulations of prolate spheroid suspensions

Article 9

DNS of non-spherical particles in turbulent flows

H.I. ANDERSSON & LIHAO ZHAO

ERCOFTAC bulletin , **84**, 4-8, 2010.

Is not included due to copyright

Article 10

Comparison of Lagrangian approach and statistical approach in simulation of fiber suspension turbulent channel flow.

LIHAO ZHAO, H.I. ANDERSSON & J.J.J. GILLISSEN

Manuscript, 2011.

Is not included due to copyright

Part 2.4

Two-way coupled simulations of prolate spheroid suspensions

Article 11

Torque-coupling and fiber-turbulence interactions

H.I. ANDERSSON, LIHAO ZHAO & M. BARRI

Journal of Fluid Mechanics, accepted for publication, 2012.

Torque-coupling and particle-turbulence interactions

HELGE I. ANDERSSON, LIHAO ZHAO
AND MUSTAFA BARRI

Department of Energy and Process Engineering, The Norwegian University of Science and Technology, NO-7491 Trondheim, Norway

(Received 04.11.2011 and in revised form ??)

A novel scheme for strong coupling between inertial Lagrangian point-particles and a continuous Eulerian fluid phase has been developed. A full mechanical coupling can only be achieved if torque-coupling is applied along with the more conventional force-coupling. The torque vector acting from the particles on the fluid is expressed in terms of a new anti-symmetric particle stress tensor which adds to the Stokes stress tensor.

A strongly-coupled simulation of a turbulent channel flow laden with prolate spheroidal particles with aspect ratio 5:1 demonstrated that the inclusion of torque-coupling reduced the modulation of the turbulent flow field observed in a two-way force-coupled simulation. The spin and orientation of the spheroids were significantly affected.

Key Words: Particle suspensions, torque-coupling, turbulence modulations, DNS

1. Introduction

The motion of small heavy particles embedded in a turbulent carrier fluid is of vital importance in industrial and environmental fluid mechanics. The dynamics of inertial particles suspended in a fluid flow constitute a many-body dynamical problem intricately coupled with a continuum flow problem. A viable approach would therefore be to represent both the fluid flow and the particle motion in accordance with the basic laws of mechanics, i.e. so-called 'first principles'. The flow field is thus obtained directly from the Navier-Stokes equations in a direct numerical simulation (DNS) while the particle dynamics is governed by equations of translational and rotational motion for each and every particle.

The Lagrangian *point-particle approach* has been used extensively in turbulent dispersed multiphase flow computations. For several decades such *one-way* coupled simulations have been performed with the view to study particle dispersion, transport and deposition; see e.g. the recent review by Balachandar & Eaton(2010). In certain parameter ranges, however, the presence of solid particles in the fluid may alter the flow field and *two-way* coupled simulations (Eaton 2009) are required in order to investigate the turbulence modulation caused by inertial particles. Such simulations became feasible about two decades ago (e.g. Squires & Eaton 1990) and are today performed with several million spherical point-particles (Zhao *et al.* 2010 ; Zhao & Andersson 2011).

The point-particle approach is based on the assumption that the particle diameter d is smaller than the Kolmogorov length scale η and the particle Reynolds number $Re_p < 1$. For finite-size particles, i.e. $d > \eta$, the flow field in the vicinity of the each particle has to

be resolved numerically. Uhlmann (2008) and Lucci et al. (2010) used an immersed boundary method (IBM) to achieve this goal for as many as 4096 and 6400 finite-size freely moving spherical particles, respectively. In such fully-resolved approaches, the boundary conditions imposed on each individual particle surface automatically assure both force- and torque-coupling between the particles and the fluid.

Both the point-particle and the fully-resolved approaches are applicable also to non-spherical particles. Here, we are concerned with the former, which was extended to ellipsoidal particles by Zhang et al. (2001). This study, as well as the subsequent investigations by Mortensen et al. (2008) and Marchioli et al. (2010) were confined only to one-way coupling. If, on the other hand, the feedback from the suspended particles is of concern, one may conjecture that not only force-coupling but also torque-coupling might be important. To the authors' knowledge, no such scheme is available for point-particles.

In the present paper a novel scheme for torque-coupling is presented which enables for the first time a strong mechanical coupling between inertial point-particles and the Newtonian carrier fluid. To this end a particle stress tensor is introduced into the particle-laden Navier-Stokes equations which, analogous to the stress tensor for micropolar fluids (Eringen 1966), is proportional to the rotational slip velocity. Results from a strongly-coupled simulation of elongated particles are presented with the view to illustrate the significance of the new scheme.

2. A novel scheme for strong two-way coupling

Dilute suspensions of solid point-particles in a viscous (Newtonian) fluid is routinely treated in a mixed Lagrangian-Eulerian approach in which the particle motion is modeled in a Lagrangian way and the fluid flow is formulated in an Eulerian framework, e.g. by means of DNS. Two-way coupled simulations imply that the fluid motion is affected by forces from the point-particles (Eaton 2009), but the fluid is unaffected by the particle torques. To this end a new scheme aimed to allow also for torque-coupling between the inertial particles and the flow field is devised. Prolate spheroids are used as a prototype of elongated fiber-like particles to demonstrate the performance of the scheme. Effects of gravity on the particle dynamics and the fluid motion are neglected.

2.1. Particle dynamics

Let us consider the motion of ellipsoidal particles in a Newtonian fluid with density ρ and dynamic coefficient of viscosity μ . More specifically, the particles are prolate spheroids with mass m and aspect ratio $\lambda = b/a$ where a and b are the semi-minor and semi-major axes, respectively. The mathematical modeling of the ellipsoidal point-particles follows the methodology outlined by Zhang et al. (2001) and subsequently adopted by Mortensen et al. (2008) and Marchioli et al. (2010). The translational and rotational motion of one single particle is governed by:

$$m \frac{dv_i}{dt} = F_i, \quad I'_{ij} \frac{d\omega'_j}{dt} + \epsilon_{ijk} \omega'_j I'_{kl} \omega'_l = N'_i \quad (2.1)$$

respectively, where ϵ_{ijk} is the Levi-Civita alternating or permutation tensor. Two different Cartesian frames of reference are used. Newton's 2^d law of motion (2.1a) is expressed in an *inertial frame* $x_i = \langle x_1, x_2, x_3 \rangle$ and Euler's equation (2.1b) is formulated in the *particle frame* $x'_i = \langle x'_1, x'_2, x'_3 \rangle$ with its origin at the particle mass center and the coordinate axes aligned with the principal directions of inertia. Thus, $v_i = dx_i/dt$ denotes the translational particle velocity in the inertial frame whereas ω'_i is the angular

velocity of the particle in the particle frame and I'_{ij} is the moment of inertia tensor for the non-spherical particles.

If the particles are sufficiently small so that the neighboring flow can be considered as Stokesian, the force F_i acting on a particle from the surrounding fluid can be expressed as:

$$F_i = D_{ij}(u_j - v_j) + \frac{Re_\kappa^{1/2}}{\mu a} D_{ij} L_{jk} D_{kl}(u_l - v_l), \quad D_{ij} = \pi \mu a K_{ij} \quad (2.2)$$

where u_i is the fluid velocity at the particle position and $Re_\kappa = \rho \kappa a^2 / \mu$ is a shear Reynolds number based on the modulus κ of the velocity gradient tensor. Here, L_{ij} is the lift tensor and the resistance tensor K_{ij} in the inertial frame is related to the resistance tensor K'_{ij} in the particle frame as $K_{ij} = A_{ik}^t K'_{kl} A_{lj}$ where A_{ij} denotes the orthogonal transformation matrix which relates the same vector in the two different frames through the linear transformation $x_i = A_{ij} x'_j$. The expressions for the hydrodynamic drag and lift forces on a non-spherical particle were derived by Brenner (1964) and Harper & Chang (1968), respectively. According to eq. (2.2), which is valid only when the particle Reynolds number is low, the force acting on the particle is therefore linearly dependent on the difference in translational velocity between the fluid and the particle.

Similarly, the torque N'_i is linearly dependent on the difference in angular velocity between the fluid and the particle, i.e.

$$\begin{aligned} N'_1 &= \frac{16\pi\mu a^3\lambda}{3(\beta_0 + \lambda^2\gamma_0)} [(1 - \lambda^2)S'_{23} + (1 + \lambda^2)(\Omega'_1 - \omega'_1)] \\ N'_2 &= \frac{16\pi\mu a^3\lambda}{3(\alpha_0 + \lambda^2\gamma_0)} [(\lambda^2 - 1)S'_{13} + (1 + \lambda^2)(\Omega'_2 - \omega'_2)] \\ N'_3 &= \frac{32\pi\mu a^3\lambda}{3(\alpha_0 + \beta_0)} (\Omega'_3 - \omega'_3). \end{aligned} \quad (2.3)$$

The parameters α_0 , β_0 and γ_0 depend on the particle aspect ratio λ . These expressions were first derived by Jeffery (1922) for an ellipsoidal particle in creeping motion, i.e. $Re_p < 1$. Here, S'_{ij} and Ω'_i denote the fluid rate-of-strain tensor and rate-of-rotation vector, respectively. The vorticity of the fluid flow field is thus $2\Omega'_i$.

The shape of a prolate spheroid is characterized by the particle aspect ratio λ , whereas the ability of the particle to adjust to the ambient flow field can be estimated in terms of the particle response time:

$$\tau = \frac{2\lambda\rho_p a^2 \ln(\lambda + \sqrt{\lambda^2 - 1})}{9\mu \sqrt{\lambda^2 - 1}} \quad (2.4)$$

where ρ_p is the particle density. τ was introduced by Zhang et al. (2001) as a time scale of the translational motion. The rotational relaxation time for spherical particles is $3\tau/10$ (Zhao & Andersson 2011), but no such scalar time scale seem to exist for non-spherical particles (Mortensen et al. 2008).

2.2. Strong two-way coupling

Cauchy's equation of motion, i.e. the principle of conservation of linear momentum, can be expressed in Cartesian tensor notation as:

$$\rho \frac{Du_i}{Dt} = \frac{\partial T_{ji}}{\partial x_j} + \rho f_i \quad (2.5)$$

where T_{ji} is a stress tensor and f_i is a body force. For a Newtonian fluid the stress tensor is:

$$T_{ji} = T_{ij} = -p\delta_{ij} + \mu\left(\frac{\partial u_i}{\partial x_j} + \frac{\partial u_j}{\partial x_i}\right) \quad (2.6)$$

and when this symmetric stress tensor is inserted in the Cauchy equation (2.5) we arrive at the celebrated Navier-Stokes equations.

The force from an individual particle on the fluid is equal to $-F_i$ according to Newton's 3rd law '*actio equals reactio*'. The feedback from n_p particles within a given volume Δ (e.g. a grid cell) adds up to:

$$f_i^P = -\frac{1}{\Delta} \sum_{l=1}^{n_p} F_i \quad (2.7)$$

where F_i is given by eq. (2.2). This force per unit volume can be included in the linear momentum equation (2.5) to account for the effect of the solid particles on the fluid motion. This is known as the *point-force approximation* to two-way coupling; see e.g. Balachandar & Eaton (2010). This approach was probably first introduced by Squires & Eaton (1990) in order to study the modulation of isotropic turbulence by spherical particles.

Similarly, the torque from a single particle on the fluid is $-N_i$ where N_i is given in equation (2.3). It is known from tensor analysis that to any vector $-N_i$ corresponds an anti-symmetric tensor of 2^{nd} -order that contains the same information as the vector; see e.g. Irgens (2008). The torque vector $-N_i$ can thus be obtained from a *particle stress tensor* T_{ij}^P according to:

$$-N_m = -\frac{1}{2}\epsilon_{mij}T_{ij}^P \Delta \quad (2.8)$$

In practice, the torque should be the sum of torques over all particles inside the grid cell under consideration. We furthermore assume that $T_{ij}^P = -T_{ji}^P$, i.e. we impose an anti-symmetry on T_{ij}^P . From (2.8) we thus arrive at the following expression for the anti-symmetric particle stress tensor:

$$T_{ij}^P = \frac{1}{\Delta} \sum_{l=1}^{n_p} \epsilon_{mij} N_m = \frac{1}{\Delta} \sum_{l=1}^{n_p} \begin{bmatrix} 0 & +N_3 & -N_2 \\ -N_3 & 0 & +N_1 \\ +N_2 & -N_1 & 0 \end{bmatrix} \quad (2.9)$$

where the summation is carried out over all particles in the volume Δ .

When the new stress tensor (2.9) is introduced in the Cauchy equation (2.5) together with the familiar Stokes stress tensor (2.6), the torques exerted by the particles on the fluid give rise to the additional term:

$$\frac{\partial T_{ji}^P}{\partial x_j} = -\frac{\partial T_{ij}^P}{\partial x_j} = -\frac{1}{\Delta} \epsilon_{mij} \frac{\partial}{\partial x_j} \sum_{l=1}^{n_p} N_m \quad (2.10)$$

to be added to the x_i -component of the Navier-Stokes equation. If Δ is the volume of a computational grid cell, this accounts for the feedback on the fluid of the total torque from the n_p particles inside the cell. This is a *point-torque approximation* analogous to the point-force approximation (2.7) commonly employed in two-way coupled simulations.

2.3. Analogy with micropolar fluids

For micropolar fluids Eringen (1966) suggested that Stokes' stress tensor (2.6) should be replaced by:

$$T_{ij} = -p\delta_{ij} + \mu\left(\frac{\partial u_i}{\partial x_j} + \frac{\partial u_j}{\partial x_i}\right) + \mu_r\left(\frac{\partial u_j}{\partial x_i} - \frac{\partial u_i}{\partial x_j}\right) - 2\mu_r\epsilon_{mij}\omega_m \quad (2.11)$$

The positive constant μ_r is called the dynamic *microrotation viscosity* and this new viscosity coefficient is understood to be a fluid property which is characteristic for the fluid-particle suspension. A comprehensive account of the theory of micropolar fluids has been provided by Lukaszewicz (1999).

The expression within the second parenthesis in (2.11) is directly related to the angular velocity of the fluid as:

$$\left(\frac{\partial u_j}{\partial x_i} - \frac{\partial u_i}{\partial x_j}\right) = 2\Omega_m\epsilon_{mij} \quad (2.12)$$

since components of the fluid angular velocity vector can be written as $\Omega_m = (1/2)\epsilon_{mji}\partial u_i/\partial x_j$ and use has been made of the identity $\epsilon_{ijk}\epsilon_{rsk} = \delta_{ir}\delta_{js} - \delta_{is}\delta_{jr}$. Eringen's expression (2.11) for the stress tensor in a micropolar fluid can now be rewritten as:

$$T_{ij} = -p\delta_{ij} + \mu\left(\frac{\partial u_i}{\partial x_j} + \frac{\partial u_j}{\partial x_i}\right) + \underbrace{2\mu_r\epsilon_{mij}(\Omega_m - \omega_m)}_{T_{ij}^P} \quad (2.13)$$

where the last term is considered to represent the effect of the particles on the motion of the fluid-particle mixture. The vector field ω_i is called the field of *microrotation* and represents the angular velocity of the solid particles. In the theory for micropolar fluids ω_i is obtained from a transport equation for angular momentum; see Eringen (1966) and Lukaszewicz (1999). In the present context, however, the expression (2.9) replaces the modelling of T_{ij}^P (2.13) used in the continuum mechanics approach by Eringen (1966). The concept of microrotation viscosity μ_r is therefore avoided since the particle stress tensor is computed directly from the individual point particles inside a fluid volume (or grid cell) in accordance with (2.9).

3. Particle-laden channel flow simulation with force- and torque-coupling

A particle-laden fully-developed turbulent channel flow at Reynolds number $Re = 360$ based on the channel height h and the wall-friction velocity u_* is now considered. The Eulerian flow field u_i of the carrier phase is obtained by means of DNS, i.e. by solving the Cauchy equation (2.5) in time and three-dimensional space. The DNS-solver is the same as that used by Mortensen et al. (2008) for one-way coupled simulations, but now with the point-force and the point-torque approximations in eqs (2.7) and (2.10) implemented. Zhang et al. (2001) assumed that an ellipsoidal particle deposits on the wall if the particle touches the surface. In the presents study, however, we follow Mortensen et al. (2008) and assume that a particle which hits the wall bounces elastically back into the flow while retaining its translational velocity in the homogeneous directions as well as its spin. The computational domain is $6h$ and $3h$ in the streamwise and spanwise directions, respectively, and the computational mesh consisted of 128^3 grid points.

Two and a half million mono-sized non-spherical particles are released randomly into an already developed turbulent flow field. The particles are prolate spheroids with aspect ratio $\lambda = 5$ and particle response time τ^+ equal to 30. The superscript $+$ indicates that

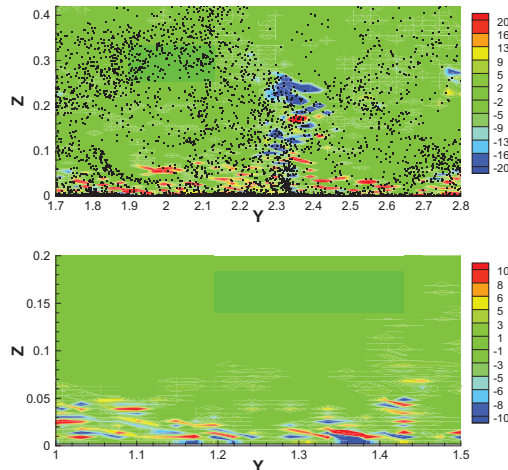


FIGURE 1. Instantaneous feedback in the streamwise direction from the spheroidal particles on the flow field. Near-wall contour plots in the cross-sectional plane of (a) particle-force f_x^P ; and (b) the torque-force $\partial T_{jx}^P / \partial x_j$. The coordinates Y and Z in the spanwise and wall-normal directions, respectively, are scaled with h and $Z = 0.1$ corresponds to $z^+ = 36$.

τ in eq. (2.4) is normalized with the viscous time scale ν/u_*^2 . The temporal sampling interval Δt^+ is 3600 and statistics averaged also in the two homogeneous directions are denoted by angular brackets.

To enable an investigation of the influence of torque-coupling in addition to force-coupling alone, we also performed another simulation with the same spheroidal particles in the same channel but only with the point-force approximation (2.7) activated. To the best of our knowledge, no such two-way coupled simulations with non-spherical point-particles have been performed. We are thus in the position to compare results from a *strongly-coupled* (i.e. force- and torque-coupling) with a *weakly-coupled* (only force-coupling) simulation.

It is well known that inertial particles concentrate preferentially in a turbulent flow field; see e.g. Balachandar & Eaton (2010). This is reflected in figure 1 which shows the cross-sectional distribution of the instantaneous feedback from the inertial point-particles on the fluid. It is readily seen that the streamwise component f_x^P attains appreciable values not only in the immediate vicinity of the wall but also out in the logarithmic wall-layer, i.e. beyond $z^+ = 30$. On the contrary, the streamwise component of $\partial T_{jx}^P / \partial x_j$ makes a significant contribution only for $Z < 0.05$, i.e. in the viscous-dominated sublayer. Besides the spotty appearance of the particle-force and the torque-force, it is noteworthy that the latter attains locally high values which are comparable in magnitude with the local particle-force values.

The primary fluid statistics are presented in figure 2. The two-way force-coupling gives rise to a substantially increased mean velocity $\langle u_x \rangle$ and streamwise turbulence intensity $rms(u'_x)$ while the two other turbulence intensities and the Reynolds shear stress $\langle u'_x u'_z \rangle$ are damped as compared with the one-way coupled channel flow. Exactly the same effects were reported from our recent study on spherical particles (Zhao et al. 2010). The tendencies observed with force-coupling alone are reduced in the force- and torque-

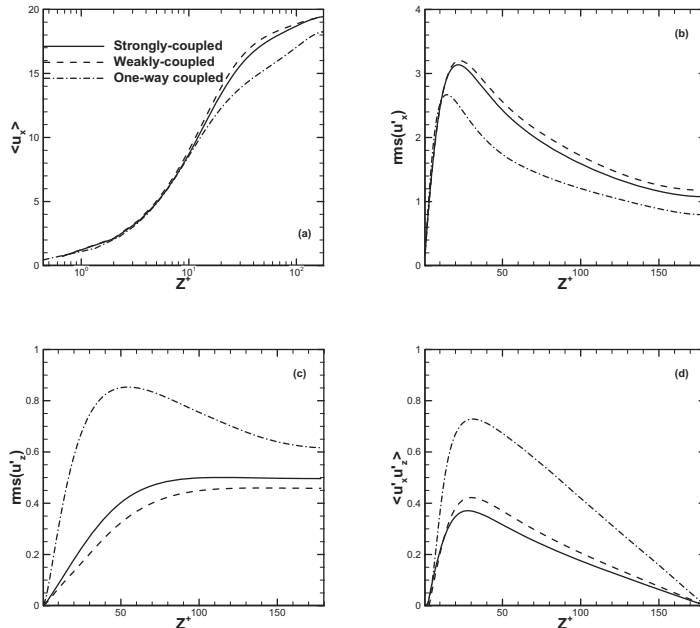


FIGURE 2. Flow-field statistics from the strongly-coupled simulation (solid lines) compared with results from the weakly-coupled simulation (broken lines). Results from a one-way coupled simulation (dash-dotted lines) are included for comparative purposes. (a) Mean streamwise velocity $\langle u_x \rangle$; (b) streamwise turbulence intensity $rms(u'_x)$; (c) wall-normal turbulence intensity $rms(u'_z)$; (d) Reynolds shear stress $\langle u'_x u'_z \rangle$.

coupled simulation, besides that the shear stress $\langle u'_x u'_z \rangle$ is further damped by the inclusion of torque-coupling.

The orientation of non-spherical particles is determined by the turbulence of the carrier fluid and will thus be affected by the modulation of the flow field caused by the feedback from the particles onto the fluid. The instantaneous orientation of the semi-major axis of a given spheroid relative to the coordinate axes $x_i = \langle x, y, z \rangle$ of the inertial frame is defined by means of the direction angles $\theta_i = \langle \theta_x, \theta_y, \theta_z \rangle$. Mean values of the direction cosines $|\cos\theta_i|$ are presented in figure 3. The variation of the direction cosines in the one-way coupled case exhibits the same trends as reported by Mortensen et al. (2008) for ellipsoidal particles with somewhat different aspect ratios but the same response time $\tau^+ = 30$. However, the tendency of the elongated particles to align themselves in the mean flow direction is more pronounced in the two-way coupled simulations. Mortensen et al. (2008) speculated that the preferential orientation in the streamwise direction was caused by the intense fluctuations of the streamwise fluid velocity. According to the data in figure 2(b), a major effect of the feedback from the point-particles on the fluid is a further increase of streamwise fluctuations. Indeed, the $|\cos\theta_x|$ -profile in figure 3(a) exhibits a distinct peak around $z^+ \approx 30$, i.e. fairly close to where the streamwise velocity fluctuations are most intense. The partial alignment of the particles with the x-direction becomes somewhat reduced when also torque-coupling is included together with force-coupling and this is thus consistent with the slightly reduced turbulence intensity

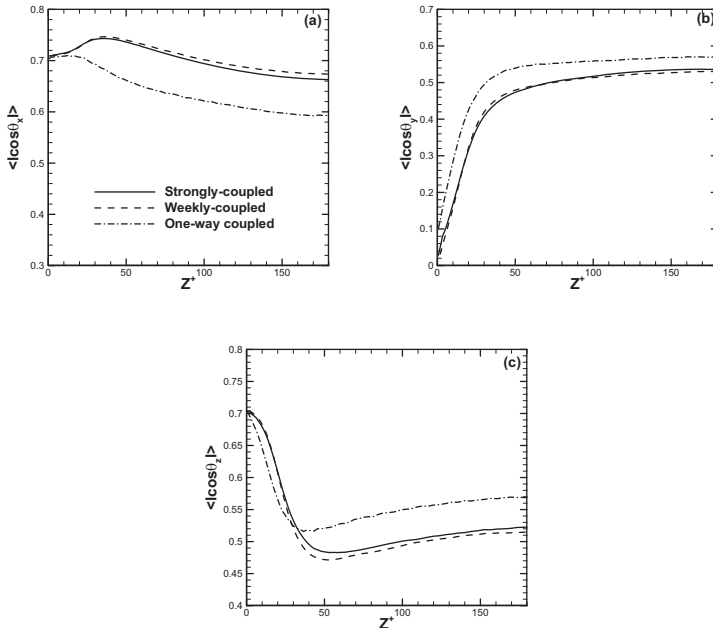


FIGURE 3. Mean particle orientation in the weakly- and strongly-coupled simulations. (a) Streamwise direction cosine $|\cos\theta_x|$; (b) spanwise direction cosine $|\cos\theta_y|$; (c) wall-normal direction cosine $|\cos\theta_z|$. Legend as in figure 2.

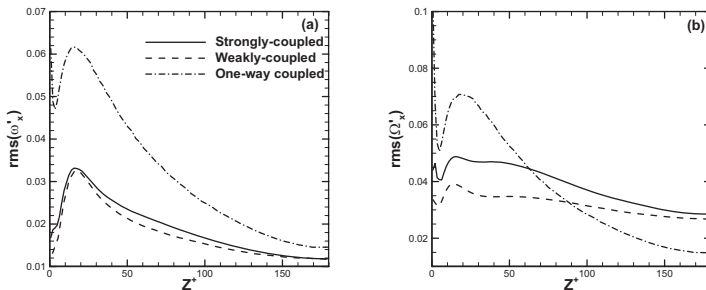


FIGURE 4. The streamwise component of the fluctuating spin vector. (a) Particle spin $rms(\omega'_x)$; (b) Fluid spin $rms(\Omega'_x)$. Legend as in figure 2.

$rms(u'_x)$. According to the data in figure 2, the point-particles impart a larger anisotropy on the fluid velocity fluctuations than that observed in the one-way coupled case. This explains why the almost isotropic particle orientation in the channel center becomes distinctly anisotropic in the weakly- and strongly-coupled simulations.

The fluctuating part of the streamwise angular velocity of the fluid and particles is shown in figure 4. In the one-way coupled simulation the fluctuating particle spin $rms(\omega'_x)$ exhibits almost exactly the same variation across the channel as the fluid spin $rms(\Omega'_x)$

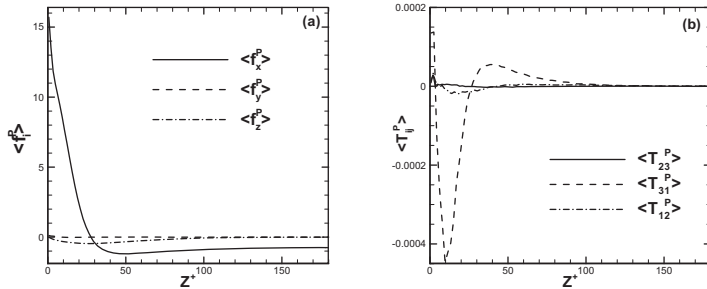


FIGURE 5. Mean values of the particle force (2.7) and the particle stress (2.9). (a) Mean particle force $\langle f_i^P \rangle$; (b) Mean particle stress $\langle T_{ij}^P \rangle$.

where the local maximum around $z^+=20$ is a signature of the coherent vortices which represent a dominating agent in near-wall turbulence. The streamwise fluid vorticity is substantially reduced in the near-wall region and increased in the core region in the two-way coupled simulations, whereas the corresponding particle spin is damped all across the channel. It is noteworthy that inclusion of torque-coupling in addition to force-coupling has an almost negligible effect on the particle spin intensity in figure 4(a), whereas torque-coupling tends to oppose the tendency of two-way force-coupling to damp the coherent vortices (Zhao et al. 2010). The distinctly higher fluid spin intensity in figure 4(b) than particle spin intensity in fig. 4(a) suggests that the inertial particles are either unable to adjust to the local fluid rotation or tend to avoid regions with locally high streamwise vorticity.

The three components of the mean particle force f_j^P defined in eq. (2.7) and the non-zero elements of the mean particle stress tensor T_{ij}^P defined in eq. (2.9) are shown in figure 5. The spanwise component of the former and $\langle T_{23}^P \rangle$ are practically zero. This is in accordance with the symmetries of the present flow and therefore reflects the adequacy of the sampling time. The mean value of the streamwise force $\langle f_x^P \rangle$ in the particle-laden momentum eq. (2.5) is positive in the near-wall region and becomes negative throughout the logarithmic region and all the way to the channel center. It is readily seen from figure 1(a) that the positive contributions to $\langle f_x^P \rangle$ are confined to $z^+ < 20$ and are moreover evenly distributed in the spanwise direction, whereas the negative contributions, i.e. regions where the fluid moves faster than the particles, stem from certain localized areas, e.g. around $Y = 2.3$ in fig. 1(a). The non-zero elements of the mean particle stress tensor T_{ij}^P are shown in figure 5(b). The only significant element is $T_{31}^P = -T_{13}^P = \frac{1}{\Delta} \sum_{l=1}^{n_p} N_2$ which exhibits an abrupt variation in the viscous-affected near-wall region. After time-averaging this gives rise to the new term $d \langle T_{31}^P \rangle / dx_3$ in the Reynolds-averaged Cauchy equation (2.5), which inevitably changes sign where $\langle T_{31}^P \rangle$ attains its minimum value close to $z^+ = 10$. The distribution of $\langle T_{31}^P \rangle$ suggests that the torque-coupling is influential only in the viscous sublayer and the buffer region.

4. Concluding remarks

We have devised a torque-coupling scheme for point-particles which enables a stronger mechanical coupling between the Lagrangian particulate phase and the Eulerian fluid phase than a standard two-way coupling scheme. A particle stress tensor expressed in

terms of the relative angular velocity, i.e. the spin-slip, was included in the Cauchy equation which governed the carrier-phase turbulence. The inclusion of torque-coupling in addition to force-coupling represents a refinement of earlier two-way coupled simulations.

A strongly-coupled simulation with 2.5 million spheroidal particles with aspect ratio 5 was performed to demonstrate the impact of strong coupling between the particles and the fluid. The results obtained with both force- and torque-coupling (i.e. strong coupling) were compared with data from a two-way coupled simulation, i.e. only force-coupled and thus weak coupling. Force-coupling alone has a major effect on the flow field and the observed modulations of the turbulence resemble those observed for spherical particles by Zhao et al.(2010). Inclusion of torque-coupling tends to oppose the effect of force-coupling. Although the resulting torque-force in the Cauchy equation attains appreciable values only in the viscous and buffer sub-layers, the flow field and the particle orientations are affected all the way to the channel center.

This work has been supported by The Research Council of Norway (project no 191210/V30) and A/S Norske Shell (contract no. 4610020178/C08156) through research fellowships to MB and LZ and by The Research Council of Norway (Programme for Supercomputing) through a grant of computing time.

REFERENCES

- Balachandar, S. & Eaton, J.K. 2010 Turbulent dispersed multiphase flow. *Annu. Rev. Fluid Mech.* **42**, 111-133.
- Brenner, H. 1964 The Stokes resistance of an arbitrary particle IV. Arbitrary fields of flow. *Chem. Engng Sci.* **19**, 703-727.
- Eaton, J.K. 2009 Two-way coupled turbulence simulations of gas-particle flows using point-particle tracking. *Int. J. Multiphase Flow* **35**, 792-800.
- Eringen, A.C. 1966 Theory of micropolar fluids. *J. Math. Mech.* **16**, 1-18.
- Harper, E.Y. & Chang, I.-D. 1968 Maximum dissipation resulting from lift in a slow viscous shear flow. *J. Fluid Mech.* **33**, 209-225.
- Irgens, F. 2008. Continuum Mechanics, *Springer Verlag*.
- Jeffery, G.B. 1922 The motion of ellipsoidal particles immersed in a viscous fluid. *Proc. Roy. Soc. A* **102**, 161-179.
- Lucci, F., Ferrante, A. & Elghobashi, S. 2010 Modulation of isotropic turbulence by particles of Taylor-length scale size. *J. Fluid Mech.* **650**, 5-55.
- Lukaszewicz, G. 1999 Micropolar Fluids - Theory and Applications, *Birkhäuser Verlag*.
- Marchioli, C., Fantoni, M. & Soldati, A. 2010 Orientation, distribution, and deposition of elongated, inertial fibers in turbulent channel flow. *Phys. Fluids* **22**, 033301.
- Mortensen, P.H., Andersson, H.I., Gillissen, J.J.J. & Boersma, B.J. 2008 Dynamics of prolate ellipsoidal particles in a turbulent channel flow. *Phys. Fluids* **20**, 093302.
- Squires, K.D. & Eaton, J.K. 1990 Particle response and turbulence modification in isotropic turbulence. *Phys. Fluids A* **2**, 1191-1203.
- Uhlmann, M. 2008 Interface-resolved direct numerical simulation of vertical particulate channel flow in the turbulent regime. *Phys. Fluids* **20**, 053305.
- Zhang, H., Ahmadi, G., Fan, F. G. & McLaughlin, J. B. 2001 Ellipsoidal particles transport and deposition in turbulent channel flows. *Int. J. Multiphase Flow* **27**, 971-1009.
- Zhao, L.H., Andersson, H.I. & Gillissen, J.J.J. 2010 Turbulence modulation and drag reduction by spherical particles. *Phys. Fluids* **22**, 081702.
- Zhao, L.H., & Andersson, H.I. 2011 On particle spin in two-way coupled turbulent channel flow simulations. *Phys. Fluids* **23**, 093302.

Part 2.5

Appendix

Appendix 1

**Modulations on turbulence with the presence of
particle $St=200$**

LIHAO ZHAO

2011.

In current appendix, the main objective is to verify present code² in the two-way coupled simulation of spherical particle suspensions with the published data by Dritselis and Vlachos (2008)¹.

In both work the pseudo-spectral direct numerical simulation is used to solve the turbulent Poiseuille flow (incompressible and Newtonian) in a channel at a frictional Reynolds number, which is defined as $Re_\tau = u_\tau h/\nu$, where $u_\tau = \sqrt{\tau_w/\rho}$ is the friction velocity with τ_w the wall shear stress and ρ the fluid density, ν is the kinematic fluid viscosity and h is the channel half-height. The reference geometry consists of two infinite flat parallel walls with periodic boundary conditions in the streamwise (x) and spanwise (z) directions and no-slip conditions in the wall-normal direction (y).

Each individual particle is treated as pointwise, rigid, elastically-rebounding spheres with Stokes number $St = \tau_p/\tau_f = 200$, which is defined as the ratio between the particle response time τ_p and the viscous time scale of the flow τ_f . Here, $\tau_p = \rho_p d_p^2/18\mu$ is the particle characteristic time scale, with ρ_p and d_p the particle density and diameter respectively, and $\tau_f = \nu/u_\tau^2$ is the viscous time scale of the flow. In both work, gravity is ignored to isolate effects due solely to turbulence, and the Lagrangian equation of particle motion includes only inertia and Schiller-Naumann corrected Stokes drag. In vector form: $d\mathbf{u}_p/dt = (\Delta u/\tau_p)[1 + 0.15(|\Delta \mathbf{u}| d_p/\nu)^{0.687}]$.

The detailed simulation conditions are listed in Table 1 and Table 2 for present work and the work done by Dritselis and Vlachos¹ respectively. Since the volume fraction is low in both simulations, the effect of four-way coupling used by Dritselis and Vlachos¹ is expected to be negligible. In Fig.1 and Fig.2 the both results are identical that with the presence of particles the mean fluid velocity is augmented while the turbulence intensities are damped compared with the particle free flow. The comparison demonstrates the reliability of current code in two-way coupled simulation.

Re_τ	Computation domain	Mesh	Coupling	N_p	Φ_p
180	$12h \times 2h \times 6h$ ($x \times y \times z$)	$128 \times 128 \times 128$	2-way	350000	6.8×10^{-5}

TABLE I. Computation conditions in present simulation. (N_p : number of particles; Φ_p : particle volume fraction.

Re_τ	Computation domain	Mesh	Coupling	N_p	Φ_p
170	$2\pi h \times 2h \times \pi h$ ($x \times y \times z$)	$128 \times 129 \times 128$	4-way	87500	6.8×10^{-5}

TABLE II. Computation conditions in Dritselis and Vlachos¹. (N_p : number of particles; Φ_p : particle volume fraction.

REFERENCES

¹C.D. Dritselis and N.S. Vlachos, “Numerical study of educed coherent structures in the near-wall region of a particle-laden channel flow,” *Phys. Fluids*, **20**, 055103 (2008).

²L.H. Zhao, H.I. Andersson, and J.J.J. Gillissen, “Turbulence modulation and drag reduction by spherical particles,” *Phys. Fluids*, **22**, 081702 (2010).

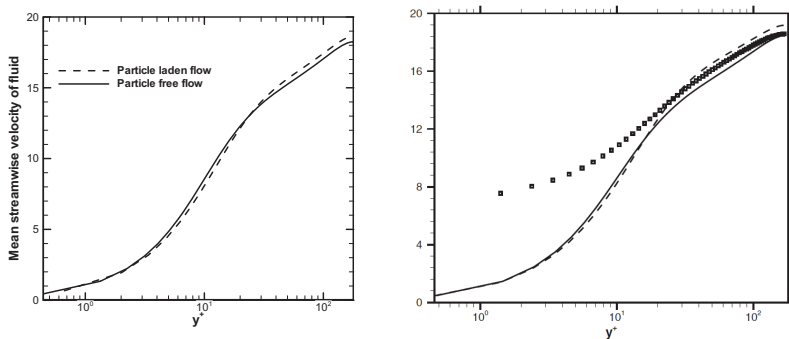


FIG. 1. Left: mean streamwise velocity of the fluid in present simulation. Right: mean streamwise velocity of the fluid in Dritselis and Vlachos¹. Continuous line: fluid velocity of particle-free flow; dashed line: fluid velocity of particle-laden flow; symbols: particle velocity.

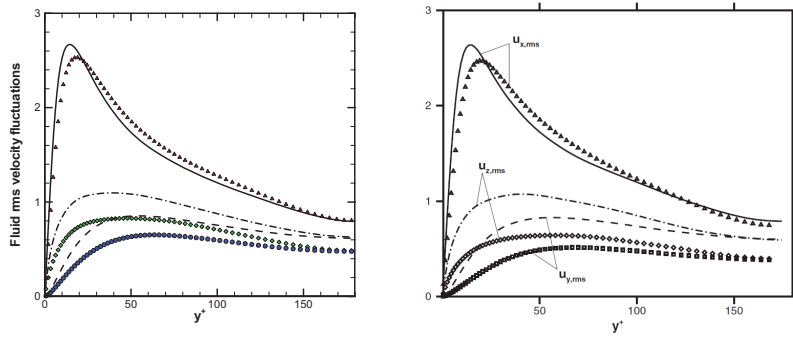


FIG. 2. Left: turbulence intensities of the fluid in present simulation. Right: turbulence intensities of the fluid in Dritselis and Vlachos¹. Lines: particle-free flow; symbols: particle-laden flow.

Appendix 2

**Two-way coupled simulation of particle laden
channel flow at $Re_\tau = 790$**

LIHAO ZHAO

2011.

Is not included due to copyright

Appendix 3

Two-way coupled simulation of fiber suspension turbulent channel flow

LIHAO ZHAO

2011.

Is not included due to copyright

